Modeling the Hydraulic Characteristics of Fully Developed Flow in Corrugated Steel Pipe Culverts

by

Jonathan Scott Toews

A Thesis submitted to the Faculty of Graduate Studies of

The University of Manitoba

in partial fulfilment of the requirements of the degree of

Master of Science

Department of Civil Engineering

University of Manitoba

Winnipeg, Manitoba, Canada

Abstract

The process of fish migration within rivers and streams is important, especially during the spawning season which often coincides with peak spring discharges in Manitoba. Current environmental regulations for fish passage through culverts require that the average velocity be limited to the prolonged swimming speed of the fish species present. In order to examine the validity of this approach, physical model results were used to calibrate and test a commercially available Computational Fluid Dynamics (CFD) model.

Detailed analysis showed that CFD models and the empirical equations used were both able to give a better representation of the flow field than the average velocity. However, the empirical equations were able to provide a more accurate velocity distribution within the fully developed region. A relationship was then developed, to estimate the cumulative percent area less than a threshold velocity within CSP culverts, to be used as a guideline during the design phase.

Acknowledgements

I would like to thank everyone that I have had the opportunity to meet and work with along the way to completing this thesis. I am grateful for the support and assistance of many organizations that have been instrumental throughout this process. Thank you to my thesis advisor, Dr. Shawn Clark, for his guidance and mentorship and for giving me the opportunity to continue my education and develop as an engineer in an enjoyable environment as a student.

Many thanks go to the University of Manitoba Graduate Fellowship for generously granting me a research scholarship that has allowed me time to dedicate to my research. As well, thanks for the funding provided by the Province of Manitoba for supplementing this scholarship with the Manitoba Graduate Scholarship. I'd like to also thank Manitoba Hydro, particularly my line advocate Rob Tkach, for funding the current research. Additionally, thanks to Dave Penny from the Corrugated Steel Pipe Institute, and Ninel Gonzalez from Manitoba Infrastructure and Transportation for their generous funding during the physical model development phase of this research.

I would like to acknowledge everyone I have had the opportunity to work with, and advice given by, during this project including Dr. Mark Tachie, Nicholas Kehler, Martin Hunt, and Mitchel Peters. Lastly, I'd like to thank my family and friends for supporting me and encouraging me throughout my time as a student.

Table of Contents

List of Figures

List of Tables

Nomenclature

Symbol	Units	Description
A	[m^2]	Flow cross-sectional area
A_o	[-]	Log-law constant (= 5.0)
A_x	[m^2]	Fractional area open to flow in the streamwise direction
A_y	[m^2]	Fractional area open to flow in the vertical direction
A_z	[m^2]	Fractional area open to flow in the spanwise direction
d_{50}	[m]	Grain size diameter with 50% non exceedence probability
d_e	[m]	Infill depth
d_p	[m]	Distance along wetted perimeter for Clark and Kehler (2011) empirical equations
D	[m]	Culvert diameter
F	[-]	Froude number
g	[m/s^2]	Acceleration of gravity
h	[m]	Water depth
k	[m]	Roughness
k_n	[$ft^{1/3}/m^{1/3}$]	Unit conversion factor for Manning's equation (1.00 for SI, 1.486 for imperial)
k_s	[m]	Equivalent sand grain roughness
k_v	[-]	Von Karman constant (= 0.41)
n	[$s/m^{1/3}$]	Manning's roughness coefficient

n_c	[s/m$^{1/3}$]	Composite Manning's roughness coefficient
P	[m]	Flow wetted perimeter
Q	[m^3/s]	Discharge
r	[m]	Dimensional parameter for Clark and Kehler (2011) empirical equations
R	[m]	Hydraulic radius
R_{con}	[-]	Conversion parameter in Flow3D
R_{DIF}	[kg/(m s)]	Turbulent diffusion
R_{SOR}	[kg/(m s)]	Mass source
RR	[m/m]	Relative roughness
S	[m/m]	Channel slope
t	[m]	Dimensional parameter for Clark and Kehler (2011) empirical equations
T	[m]	Dimensional parameter for Clark and Kehler (2011) empirical equations
U	[m/s]	Average streamwise velocity at a point
U_{*av}	[m/s]	Average shear velocity
U_{*dp}	[m/s]	Local shear velocity
U_{av}	[m/s]	Bulk average streamwise velocity ($= Q/A$)
U_{ck}	[m/s]	Streamwise velocity as predicted by Clark and Kehler's (2011) developed empirical equations at a point
U_{meas}	[m/s]	Measured streamwise velocity at a point

U_{mod}	[m/s]	Streamwise velocity as predicted by the CFD model at a point
V	[m/s]	Velocity in vertical direction at a point
V_f	[-]	Fractional volume open to flow
W	[m/s]	Velocity in spanwise direction at a point
Y_v	[%]	Cumulative percent area with velocity below threshold velocity
β_1	[-]	Empirical velocity distribution coefficient
v	[m^2/s]	Kinematic viscosity
ρ	[kg/m^3]	Fluid density
θ	[rads]	Geometric property of partially-filled circular channel, dependent on water depth

Chapter 1: Introduction

1.1 Background

There are a great deal of small rivers and stream crossings within the Province of Manitoba. In order to facilitate these crossings, corrugated steel pipe (CSP) culverts are often used because they are cost-effective and hydraulically efficient. It is important while designing these stream crossings to provide a safe design without compromising the needs of the local fish species within the channel. In Canada, legislation requires fish passage to be available to all fish species (R. S., 1985, c. F-14). Legislation states that an efficient fishway shall be provided by the owner or occupier where it is necessary for the public's interest. This fishway must be maintained in an effective condition by the owner or occupier, in such a manner that, in the opinion of the Minister, it satisfactorily permits the free passage of fish through it.

This makes fish passage through culverts an important design consideration when dealing with stream crossings on fish-bearing streams. This is especially true during high flows due to snowmelt, which often coincide with the fish spawning season in Manitoba. These fish passage regulations have created new design considerations for designers of hydraulic structures: to provide an environmentally responsible option, while providing a safe and economical design. When designing a fish crossing, according to the Manitoba Stream Crossing Guidelines for the Protection of Fish and Fish Habitat (Department of Fisheries and Oceans, 1996), culverts under 25 m long must have an

average velocity less than 1 m/s, while culverts over 25 m must have an average velocity under 0.8 m/s. These restrictions may be more stringent depending on the type of fish species within the waterway, for example Northern Pike have a limit velocity of 0.6 m/s. These regulations are set to ensure that excessive water velocities will not occur, because fish may potentially fail to navigate the full length of the culvert if the flow characteristics exceed the swimming ability of the fish (Behlke et al., 1991).

The Manitoba Stream Crossing Guidelines for the Protection of Fish and Fish Habitat (Department of Fisheries and Oceans, 1996) also states that culverts must be designed such that fish do not experience a delay greater than seven consecutive days once in each 50 year period. The Transportation Association of Canada's Guide to Bridge Hydraulics lists a delay greater than 3 days as acceptable with a frequency of once in ten years (Katopodis, 1992; Neill, 2001).

Round culverts are often chosen despite the fact that they are the least desirable from a fish passage perspective because they have considerable economic and constructability advantages over the alternatives, such as bridges and stream bed simulation culverts. Round culverts may be seen as undesirable for fish passage, because circular culverts concentrate the flow into a smaller cross-section. This can cause loss of fish habitat and natural substrate as well as potentially removing irregularities that create zones of quiescent flow where fish can rest. Compounding this problem of balancing economic and environmental designs is that the hydraulic regime of CSP culverts is very complex

and poorly understood. The current research will use Computational Fluid Dynamics (CFD) in conjunction with experimental data from previous and current research performed at the Hydraulics Research & Testing Facility (HRTF) at the University of Manitoba to provide a better understanding of culvert hydraulics and determine if CFD is a viable option for culvert design.

Current models for fish passage are one-dimensional, such as HEC-RAS, using the average velocity as an indication of the velocity against which a fish will have to swim (Katopodis, 1992). Physical modeling has confirmed that the flow velocity decreases towards the boundary layer (Kehler, 2009; Knight & Sterling, 2000). Due to their natural instincts, fish are unlikely to swim against water flowing at velocities higher than the average velocity within the cross-sectional area and rather choose a location for swimming with velocities that are within the capabilities of the fish species (Behlke et al., 1991). With the use of CFD modeling for flow through culverts, three-dimensional velocity distributions can provide a better understanding of the hydraulics within culverts for fish passage.

1.2 Objective

The main objective of this thesis is to provide a greater understanding of the hydraulic regime in CSP culverts by investigating the applicability of Computational Fluid Dynamics (CFD) to predict flow conditions in a culvert and verifying these results using experimental data. The study will focus on CSP culverts with and without gravel infill. Additionally, the study will focus on situations which are particularly relevant to culvert installations within the Prairies. This will be accomplished by using small (to horizontal) slopes as well as culverts operating under tailwater control.

The specific technical objectives of this report are to:

- Examine the change in roughness characteristics with changing water levels (h/D) at each slope
- Examine the hydraulic regime of culverts: calibrate the CFD model using data that was acquired at the HRTF
- Verify the CFD model using data collected to further complement existing data
- Compare equations developed by Clark and Kehler (2011) against CFD results
- Expand/modify the empirical equations developed by Clark and Kehler (2011), if this is determined to be significant
- Determine the effects of lining the culvert bottom with gravel
- Determine the length required to obtain uniform flow for different hydraulic conditions, and

- Develop a methodology for determining the cross-sectional area within a culvert where the velocity is below any specified value within the fully developed region

1.3 Overview

The background and objectives for this research are detailed in Chapter 1. Chapter 2 is a literature review which will cover the current state of culvert modeling and equations. This review will include composite roughness methods, development length, as well as one and two-dimensional models for culvert hydraulics. The use and acceptability of CFD modeling will also be discussed by using cases with different model types that were compared against physical data, and finally a detailed description of Flow3D. Chapter 3 the testing procedure will be described in detail for both the physical modeling and the numerical modeling portion of the current research. Chapter 4 consists of the detailed analysis and comparison between the physical model, numerical model and empirical equations. Finally, Chapters 5 will summarize the contributions of this research, and state the conclusions and recommendations for future work.

Chapter 2: Literature Review

This section will review the most recent fish passage research, culvert research as well as successful applications of CFD models.

2.1 Fish Swimming Location Preference

Behlke et al. (1991) completed a report on the fundamentals of culvert design for the passage of weak-swimming fish. It was found from observation that the easiest location for fish to swim was at the edges of the culvert cross-section with their bodies normal to the sloping culvert wall. It was then hypothesised that fish would swim in these locations for three reasons: (1) protection from predators; (2) a preference to swim with their bodies oriented with the water velocity gradient; or (3) to orient themselves normal to their substrate.

Cotel et al. (2006) studied Brown trout for the purpose of determining their preferred habitat within a stream. From observation it was found that the Brown trout were usually found in the lower 5 cm (h/D ~ 10-20%) of the stream due to the velocity gradients found in this region. This suggests that this is their preferred location within a stream profile.

Kane et al. (2000) found that juvenile fish are motivated to move upstream if a food source is available. This was achieved by placing salmon eggs at the upstream end of a

culvert. Video footage was used to supplement visual observations for this research, and it was found that fish would use large corrugations to their advantage when ascending a culvert. In general, fish were found to swim close to the culvert wall and channel bottom of the culvert. However for cases with high discharges, fish would swim near the surface and close to the sidewall where the velocities are reduced within the cross-section.

These studies demonstrate that fish will choose regions within a culvert or stream that have lower velocities. Therefore, having a better understanding of culvert hydraulics and having the ability to model the entire culvert cross-section accurately (as opposed to using the average velocity) is important to provide a better representation of what may become a barrier to fish.

2.2 Culvert Hydraulics

Culverts are governed by either inlet or outlet control. The control type experienced will determine the performance of the culvert and thus the design discharge, which is often limited due to fish-passage regulations. Inlet-controlled culverts are only dependent on the inlet geometry of the culvert, while outlet-controlled culverts are also dependent on the barrel roughness, area, shape, length, slope and tailwater elevation (Sturm, 2010). Thus, outlet control calculations are generally more complex than inlet control. The control type that is most often experienced within Manitoba is outlet control. This is a result of the low surface gradients which allow for higher tailwater elevations, thus

forcing the tailwater conditions to dominate the hydraulic regime of the culvert. Outlet control under uniform flow conditions will be studied for this reason.

2.2.1 Development Length

There is a multitude of literature on pipe development lengths that have been conducted using a variety of instrumentation for full pipe flow. Hinze (1975) and Yen (2001) both provide detailed discussions on the importance of allowing and selecting the appropriate entry length for experimental procedures. Hinze (1975) recommended an upstream development length of 160 times the hydraulic radius, R, to be used as a guideline in an experimental setup, which was determined experimentally by Nikuradse (1932). Yen (2001) showed that to achieve uniform flow, there are more requirements than having a uniform depth along the length of a channel. A sufficiently long channel must be used to ensure that the cross-sectional velocity, pressure, and turbulence characteristics do not change with further horizontal distance (x) for flow to become uniform. Within laboratory setups $100R$ is often used, while $50R$ is recommended to reduce downstream effects. However, others have found that this length is insufficient. Rouse (1946) recommended that $x/R = 200$ be the minimum entry length for turbulent flow. Therefore it is important to demonstrate for each experimental setup that fully developed flow has in fact occurred where measurements are being taken.

2.2.2 One Dimensional Velocity Prediction Models

Manning's equation continues to be one of the most commonly used tools to determine the fluid depth and average velocity under uniform flow conditions. The concept of Manning's equation was developed from the Chezy formula for uniform flow, which has been revised over an extended period of time by Manning, Flamant, and King (Williams, 1970). The form of the equation used today contains a term denoted as Manning's n which represents the lumped resistance to flow. The final form of Manning's equation is written as

$$U_{av} = \frac{k_n}{n} R^{2/3} S^{1/2} \qquad [2.1]$$

Where U_{av} is the average streamwise velocity, R is the hydraulic radius, and S is the channel slope. The k_n term is a constant that depends on the chosen system of units ($k_n = 1.00$ for SI and 1.486 for imperial). The discharge can be determined by multiplying equation 2.1 by the flow area of the channel, resulting in

$$Q = AU_{av} = \frac{k_n}{n} AR^{2/3} S^{1/2} \qquad [2.2]$$

where Q is the discharge, and A is the flow area. Conversely, for a known Q, n, channel geometry, and slope one can use equation 2.2 to determine the normal depth in the channel. Some sort of iterative technique is required.

The following geometric relationships between water depth, h, and other geometric properties greatly facilitates the solution of equation 2.2 for a partially-filled circular channel.

$$\theta = 2\cos^{-1}(1 - 2h/D) \qquad [2.3]$$

$$A = (\theta - \sin\theta)D^2/8 \qquad [2.4]$$

$$P = \theta D/2 \qquad [2.5]$$

There are several different methods which may be used to determine the channel roughness based on the surface properties. Tables have been made available by the CSP culvert industry (Corrugated Steel Pipe Institue, 2007) to estimate n for a CSP culvert. However, there are several more sophisticated methods to determine the roughness of the rock-filled portion of a culvert when infill is present. The simplest method, for channels with bed material, is the Strickler equation (Sturm, 2010)

$$n = 0.041{d_{50}}^{1/6} \qquad [2.6]$$

where d_{50} is the diameter of the grain size in meters with a 50% non-exceedance probability.

Once the individual roughness of both the culvert and bed material has been determined, a composite roughness must be determined. Again, there are a variety of methods to complete this task using weighted average techniques. Chow (1959) presented a few methods which include the Horton method, Einstein and Banks method, Lotter's formula, and finally the Krishnamurthy and Christensen formula for computing the composite Manning's n. Lotter's formula, equation 2.7, assumes the total discharge is the sum of the discharges of the subsections and provided the lowest mean error when applied to 36 stream cross-sectional data (Motayed & Krishnamurthy, 1980).

$$n_c = \frac{PR^{5/3}}{\sum_{i=1}^{N} \frac{P_i R_i^{5/3}}{n_i}} \qquad [2.7]$$

The resulting n_c represents the Manning's roughness of the composite channel. The other methods used to determine the composite roughness use either the assumption that the total resisting force is equal to the sum of the resisting forces over each segment of the wetted perimeter, or that each section of the channel can be well represented by the average velocity (Sturm, 2010).

Straub & Morris (1950) carried out hydraulic testing on CSP culverts with diameters of 0.46, 0.61, and 0.91 m. The corrugation size used for these tests was 13 x 68 mm, with a slope of 0.20% and a length of 58.83 m. A total of 36 tests were conducted for all three diameters for partially full flow with uniform depth measured through the length of the culvert using a series of manometer tubes. The main purpose of their research was to determine the entrance losses for different inlet configurations. The range of relative depths (h/D) observed for their set of tests was between 0.30 and 0.90. Very little variation in Manning's n was noticed over this range of relative depths.

A report produced by the Kansas Department of Transportation (McEnroe & Malone, 2008) completed research on helical CSP culverts with a corrugation of 13 x 68 mm for three diameters of 0.46, 0.38 and 0.30 m. These culverts were each tested at a single slope which was 0.39, 0.85 and 0.68% respectively for each diameter. Normal depth was set throughout the length of the culvert using a flap gate to

adjust the tailwater level, and measured using a series of manometer tubes along the length of the culvert. The range of h/D observed within this study was 0.29 to 0.90. Their findings indicate that the Manning's n value is not consistent for different discharges, and tends to increase as the discharge decreases.

Additionally, Mangin completed research at Youngstown State University in 2010 compiling a series of data sets to determine a relationship that could accurately predict h/D that is a function of Q, D, S and roughness, k. The purpose of this research was to eliminate the need to estimate a channel's roughness or Manning's n value. An equation was developed by compiling a comprehensive data set using dimensional analysis with four pi groups, which are: $\pi_1 = h \cdot D^{-1}$; $\pi_2 = Q \cdot g^{-0.5} D^{-2.5}$; $\pi_3 = S$; $\pi_4 = k \cdot D^{-1}$ where h is the water depth, D is the diameter of the culvert, g is gravity, and k is the corrugation height of the culvert. Pi group 1, π_1, was then set to be a function of π_2, π_3 and π_4 as shown by

$$\pi_1 = a[{\pi_2}^b {\pi_3}^c {\pi_4}^e + j] \qquad [2.8]$$

Through detailed analysis Mangin's final equation becomes

$$h/D = 0.32\left[\left(\frac{Q}{\sqrt{gD^5}}\right)\left(\frac{k}{D}\right)^{1/6}/\sqrt{S} + 0.64\right] \qquad [2.9]$$

However, this equation was developed using relative depths greater than 0.2. The lack of data below $h/D = 0.2$ leads to a deviation from the observed flow depth at low discharges.

2.2.3 Previous Culvert Velocity Distribution Research

Knight and Sterling (2000) completed their research in a smooth pipe with an internal diameter of 0.24 m that was 21.26 m long. The piping was in a tilting flume, with an adjustable bed slope. Streamwise velocity, and boundary shear stress distribution measurements were taken at normal depth (h) for multiple infill depths (d_e), discharges and slopes. Measurements were taken using a pitot-static tube and a Preston tube, which allowed the boundary shear stress to be measured with an accuracy of 0.2-4%.

The findings showed that there was a sharp gradient of low to high velocities near the boundary walls. Additionally, there was still a significant portion of the flow which had a measured streamwise velocity that was less than the average cross-sectional velocity. Another key characteristic was that the maximum velocity tended to dip below the water surface, which was attributed to secondary circulations. However, precise measurements of these secondary circulations were not taken. A three-dimensional laser Doppler anemometer was recommended for this purpose. Additionally, the maximum velocity was found to be forced towards the water surface as h decreased. Each of the tests showed a relatively flat boundary shear stress distribution near the centreline of the channel bottom for channels without infill ($d_p/P \leq 0.2$, d_p as defined in Figure 1 later in this chapter). The local boundary shear stresses tended to be higher for the bed portion than for the channel walls and were extremely sensitive to the geometry for the cases where the pipe had infill (Knight & Sterling, 2000).

The work completed by Ead et al. (2000) consisted of tests in an 8 m long, 0.62 m diameter, annular CSP culvert with 13 x 68 mm corrugations. Fourteen pressure taps were utilized to measure the water surface profile along the centreline. Three slopes were utilized (0.55, 1.14, and 2.55%), with several discharges for each slope. The water surface profiles were found to characteristically have a dip at the entrance, eventually becoming parallel to the bed slope at normal depth after some horizontal distance (x). Ead et al. (2000) completed a second set of experiments, where a Prandtl tube was used to measure the streamwise velocity at the 14 stations. During these experiments it was observed that the flow became fully developed at a distance of $x/D = 2$. Findings included that fish could pass through the channel near the culvert walls due to the relatively lower streamwise velocity. The velocity profile was found to be well represented by the Prandtl equation for rough turbulent flow, and the equivalent sand grain roughness was approximated by the amplitude of the corrugation.

House et al. (2005) completed work on streambed simulation culverts used for fish-passage. Detailed measurements of the velocity profile were generally taken at the middle and at the outlet of the study culverts. Velocity measurements were taken with a Marsh-McBirney Flowmate model 2000 current meter and a Global Flow Probe model 101 current meter. Velocity measurements were averaged over a 20 second period, and were found to be accurate to the nearest 0.03 m/s. A relationship was developed to predict the percentage of the flow area below a threshold velocity as follows

$$logit\ Y_v = ln\left[\frac{Y_v}{100-Y_v}\right] = \beta_1(U - U_{av}) \qquad [2.10]$$

where Y_v is the cumulative percentage of the cross-section below a given velocity, U is a specified velocity, U_{av} is the average channel velocity, and β_1 is a velocity distribution coefficient defined by

$$\beta_1 = 14.11 - 5.26A_{total} + 3.67Q - 16.56F + 2.29RR \qquad [2.11]$$

Where A is the total cross-sectional flow area (m^2), Q is the discharge (m^3/s), F is the Froude number, and RR is the relative roughness (m). When the $logit$ percent area is back transformed using the following equation to calculate the percent area below a threshold velocity, the percent area then becomes

$$Predicted\ \%\ Area = \frac{100 * e^{logit\ Y_v}}{1 + e^{logit\ Y_v}} \qquad [2.12]$$

The accuracy of the above equation was observed to be acceptable, but it was recommended that a more robust regression should be completed on a wider range of stream crossings. Additionally the above equation was suggested to be used as a guide in the development of future research aimed at improving the understanding of the details of fish movements in streambed simulation culverts (House et al, 2005).

Abbs et al. (2007) completed work on culverts to determine the backwater effects on the velocity distribution. Several hydraulic conditions were tested by changing the discharge and backwater condition at a slope of 0.72% in a 0.50 m diameter and 8.00 m long culvert. Velocity distributions were measured using an Acoustic Doppler Velocimeter (ADV) within the CSP culvert at several locations along the length. The findings indicated that a significant portion of the flow area was in fact below that of the average velocity. Additionally, it was found that as the backwater effect was increased,

the percentage of flow area less than the average velocity for the normal depth increased significantly (Abbs et al., 2007). Since backwater or tailwater controlled culverts are common within Manitoba, it is important to be able to adequately predict the area of flow below the mean velocity and the development length under these backwater conditions.

Magura (2007) completed work on a 0.62 m diameter, 14.28 m long CSP culvert with 10% gravel infill and a projected inlet with several slopes (0.0, 0.5, and 1.0%), subcritical flow and a discharge ranging from 64 to 254 L/s. Velocity measurements were recorded using an Acoustic Doppler Velocimeter, revealing regions with significantly lower velocities near the gravel bed and surface suggesting strong secondary circulations. The log-law region of the velocity profiles were examined, which were found to be consistent with the Nikuradse equivalent sand grain roughness and shear velocity around the wetted perimeter (Magura, 2007).

Kehler (2009) ensured that uniform flow conditions occurred within the CSP culvert by taking a series of centreline velocity profiles along the length of the culvert, x. At a location that the profile was independent of x, additional profiles were taken to ensure that uniform flow occurred for an adequate section of the culvert over all test conditions. It was found that for tests without gravel infill the development length ranged between 5.95-12.11 diameters, while tests with gravel infill had a development

length that ranged between 15.14-17.16 diameters. Subsequently, two-dimensional velocity profiles were taken at 20 diameters downstream of the culvert inlet.

A series of five experimental tests were completed in a CSP culvert with a diameter of 0.8 m and a length of 21 m. The tests were performed at three slopes (0.028, 0.110, and 0.270%) and two discharges (0.086 and 0.176 m^3). Acoustic Doppler velocimeters (up, down, and side-looking) were used to measure the velocity field over half of the culvert cross-section. It was found that a significant portion of the streamwise velocity was below that of the average streamwise velocity. Additionally, a modified version of the log-law was proposed to estimate water velocities within the fully developed region:

$$U^+ = \frac{1}{k}\ln(t^+) + A_o - \Delta B \quad \text{for} \quad \mathrm{t} < 0.36T \qquad [2.13]$$

$$U^+ = \frac{1}{k}\ln(t^+) + A_o - \Delta B - 3.70\left(1 - 2\frac{d_p}{P}\right)\left[\frac{\left(t^+ - 0.36T^+\right)}{0.64T^+}\right]^{1.38} \quad \text{for} \quad \mathrm{t} \geq 0.36\mathrm{T} \qquad [2.14]$$

where A_o equals 5.00, k is the von Karman constant of 0.41, and ΔB is the roughness shift which is given by

$$\Delta B = \frac{1}{k}\ln\left(\frac{k_s\sqrt{gRS}}{v}\right) \qquad [2.15]$$

where k_s is the equivalent sand grain roughness, t^+ and T^+ are normalized by v/U_{*dp}, and U^+ is normalized by the local shear stress, U_{*dp}, based on a best fit line to the measured data which is given by

$$U_{*dp} = \sqrt{gRS}\left[1.1 - 1.39\left(\frac{d_p}{p}\right)^2\right] \qquad [2.16]$$

and all geometric dimensions are defined in the following figure after Clark and Kehler, 2011.

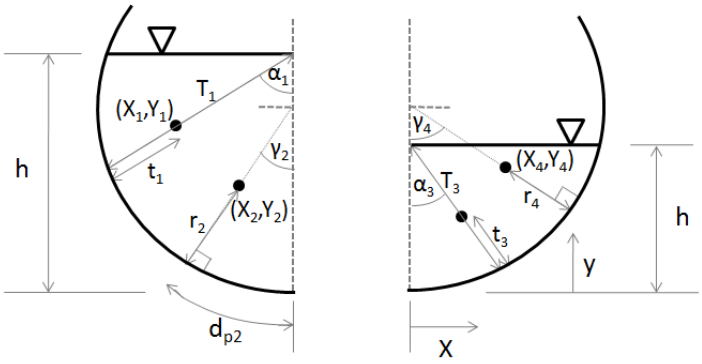

Figure 1: Dimension definitions after Clark & Kehler, 2011

Overall, there are a wide range of developed relationships to determine the velocity distribution within a culvert in the developed region. However, the ability to predict flow characteristics along the entire length of a culvert is also important. By calibrating a CFD model within the developed region, the CFD model may be used in a predictive manner across the entire domain, which is a significant advantage over the previously mentioned models.

2.3 Computational Fluid Dynamics

Computational fluid dynamics (CFD), as defined by the McGraw-Hill Concise Encyclopedia of Physics, is the numerical approximation to the solution of mathematical models for fluid flow and heat transfer. Research using CFD is important, because through its application and verification to physical models it can be used to model the flow at a potentially lower cost compared to physical modeling. Since little research has been done on the application of modeling culverts using CFD software, the literature

presented below are successful applications of CFD. These examples demonstrate that if CFD is used effectively it is a viable option when modeling a flow field.

2.3.1 Application of CFD Theory

Reece (1977) completed research on the theory of turbulence modeling using the Navier-Stokes equations (a modified version is given in subsection 2.2.3), using the exact equations for the Reynolds stresses, as opposed to using a turbulence model. Reece (1977) stated that the equations are impossible to solve analytically. However, in the general case, solutions can be inferred from two facts: (1) the equations govern a physical flow; and (2) the flow is well-defined and appears to yield consistent measurements. It is important to acknowledge the fact that the solutions which are obtained are approximations of a set of discretized algebraic equations. Referring to the discretization process, Reece quotes Kwak et al. (1975) as saying "that the mesh-size must be smaller than the Kolmogorov microscale to resolve the smallest scales of turbulence". To solve the Navier-Stokes equations it is necessary to eliminate appropriate effects that are of no significance and to select those terms in the equations which may be represented in a simpler form. This process of eliminating the Navier-Stokes equations of their physically insignificant terms will always be useful as there will always be an optimum balance between the desired accuracy and speed of calculation for any given problem. Reece then went on to develop a generalized Reynolds-stress model for turbulence of the third order that was applied to two and three dimensional problems. The models were then applied to open channel cases, however, it is

important to note that a special set of boundary conditions were used at the free surface. The free surface was treated as a symmetry boundary, with the exception of the interface, which acts as a wall on the Reynolds stresses. The model was found to generally show good agreement with the measured data. The prediction of three-dimensional flows were much more accurate over the entrance region than those generated by lower-order models, however the modeled results were deficient in the respect that they over predicted the secondary circulations in some circumstances. One of Reece's final assessments states that "The predictions obtained justify the use of the model. However, we must concede that the model requires, in its three-dimensional form, slightly over 150% more computer time than, say, a k-ϵ model".

Nezu and Nakagawa (1993) state that the k-ϵ model has a much wider applicability than the Prandtl mixing-length model and can simulate fully developed channel flows quite well, while calculating the velocity distribution and turbulence quantities. They continue by stating that the k-ϵ model, along with a damping modification of the dissipation term for the free surface boundary condition and a general symmetry boundary performs well for open channels.

Leschziner and Rodi (1979) completed calculations on strongly curved open channel flow using a k-ϵ turbulence model. The model was set up in cylindrical coordinates to take into account the curvature of the channel. Boundary conditions for the inlet plane, walls, free surface, and outlet were all considered within the model. Through data

analysis two effects were found to be unique to strongly curved channels: (1) the transverse surface slope develops before the bend inlet and extends beyond the bend outlet; and (2) continuous buildup or decay of the transverse slope occurs so that there is no distinct region where axial symmetry exists. The results of the model were judged to be sufficient to be tested against more complex geometries. This further demonstrates the wide applicability of the k-ϵ model to complex problems.

Naot and Rodi (1982) developed a model that was able to properly predict the secondary currents in channel flow without solving the full stress equation model (similar to that presented by Reece, 1977). This model required that the free surface be taken into account in two ways. Firstly, damping of the vertical velocity fluctuations was required, thus increasing the horizontal velocity fluctuations due to continuity. Secondly, the turbulent length scale was reduced due to geometrical restrictions at the surface. The basic k-ϵ model was utilized, while the free surface was treated like a plane of symmetry for all variables except for the dissipation rate, ϵ. This rate was taken into account by allowing the surface dissipation rate to have a virtual origin above the water surface and be proportional to the distance from this origin. Another key characteristic of the model was the wall treatment. A wall-function was used to set the boundary conditions along the wall. This in effect meant that the boundary condition was not set at the wall, but at the first grid point outside of the viscous sub-layer in a region where the logarithmic law of the wall was valid and turbulence was nearly in local isotropy. The model was then applied to two, and three-dimensional square duct problems. It was

shown with comparison to experimental data that the secondary velocity fields were simulated quite well, and were in only slightly poorer agreement with the measurements than were Reece's 1977 predictions which were based on a full stress equation model.

Demuren and Rodi (1986) completed work on the dispersion of pollutants in meandering channels, comparing experimental and predicted flow conditions. The turbulence model used was a version of the k-ϵ model that was modified to take into account the streamline curvature effects on turbulence by the transformation of the model equations from Cartesian to polar coordinates. In gentle curves a higher order model was recommended to properly take into account the extra curvature effects. However, with strongly curved channels the pressure gradients were in most cases considerably higher than the gradients of the Reynolds stresses so the refined modeling was not required. With detailed comparisons between experimental and predicted flow data of the velocity and concentration field, it was shown that a good correlation existed.

2.3.2 CFD Modeling with Commercially Available Software

The previous section demonstrated that CFD can be used successfully in a wide variety of situations, many of the researchers presented had extensive theoretical backgrounds and often wrote their own CFD code. The average hydraulic engineer responsible for a culvert design or a fisheries engineer responsible for regulatory approval might not have

the same background. Furthermore, they would not have the time available to develop their own code. However, they may be able to receive the training and have sufficient time available to use a commercially available CFD software program to model culvert hydraulics. As this has yet to be done extensively, this section will focus on outlining successful applications of CFD software in other fields.

Yeung (2001) developed a model using the commercial software CFX version 4.1 to predict flow distributions and water residence time through rectangular service reservoirs. By using CFD software, information was available at every cell within the model domain. Yeung (2001) stated that this feature is extremely useful, as opposed to only having data at specific measurement locations. The flow conditions within the CFD software were estimated using the k-ε turbulence model. Since the developed model was used to predict the water residence time; the CFD software had a distinct advantage over that of the physical models by discretizing the data over the entire model domain. As well, in addition to the aforementioned benefits, the CFD modeling was found to remove the subjectivities of data analysis by providing a standard method of data extraction (Yeung, 2001).

Khan et al. (2006) applied a three-dimensional CFD model to a contact tank. Khan used the commercially available software STAR-CD. This model solves the fundamental flow equations such as continuity and conservation of mass and momentum, and uses the k-ε turbulence model to calculate the eddy viscosity and mixing coefficients. The model was

compared against three-dimensional velocities from a 1:8 scale physical model. The objective of their research was to show that CFD models can simulate three-dimensional velocity fields accurately. Simultaneous validation of velocities and flow through curve (FTC) data was completed to ascertain the predictive capabilities of CFD models. Through analysis of the test results, it was concluded that CFD can generally reproduce the velocity field and the FTC in a contact tank well.

Chanel and Doering (2008) presented their results of a comparison between a physical model and a commercially available CFD model (Flow3D). Their objective was to verify that CFD models are cost-effective alternatives to scaled physical models. From the results it was determined that CFD models and physical measurements matched reasonably well. They went on to further conclude that commercially available software, such as Flow3D, has the ability to model various spillway geometries and configurations when applied appropriately (Chanel and Doering, 2008).

Kopeinig (2004) developed a CFD model for a CSP culvert. The model was developed within Flow3D, and was verified for a single test case using measured field data. They then developed a series of numerical models that were used in a predictive manner to determine the best configuration of baffle blocks for fish passage. These results were used to develop a set of tables to help during the culvert design phase for fish passage (Kopeinig, 2004). Additional work was suggested by Kopeinig to further verify and

include different variations of the slope and discharge in order to compliment the model's validity.

2.3.3 Flow3D Theory Overview

Flow3D has a multitude of physics model options, making it applicable to a wide range of fluid flow problems. Due to Flow3D's general use, and application by several major water resources groups within Manitoba, it was selected to be used to determine the applicability of applying a commercially available CFD model to CSP culvert problems.

Flow3D is a general purpose CFD model used to calculate two or three-dimensional flow problems. There are a multitude of flow options (physically and numerically based) within Flow3D. However, for the purpose of this research, the free surface turbulence model component was investigated. The equations of fluid motion are described by non-linear, second-order differential equations. Numerical solutions often require approximations of various terms to reduce computational time. These approximations come in the form of different turbulence models available within Flow3D. Because of this, the results obtained using these approximated terms yielded an approximate solution to the desired problem.

The general form of the mass continuity equation is as follows

$$V_F \frac{\partial \rho}{\partial t} + \frac{\partial}{\partial x}(\rho U A_x) + R\frac{\partial}{\partial y}\left(\rho V A_y\right) + \frac{\partial}{\partial z}(\rho W A_z) + \xi \frac{\rho u A_x}{x} = R_{DIF} + R_{SOR} \quad [2.17]$$

where V_F is the fractional volume open to flow, ρ is the fluid density, R_{DIF} is a turbulent diffusion term, and R_{SOR} is a mass source. The velocity components (U, V, W) are in the coordinate directions (x, y, z). The fractional area open to flow in the x-direction is represented by A_x; similarly the area fractions open to the flow in the y and z-directions are represented by A_y and A_z. The coefficient R is a conversion parameter from Cartesian coordinates depending on the coordinate system used within the model.

The general form of the Navier-Stokes equations shown in Cartesian coordinates are as follows

$$\frac{\partial U}{\partial t} + \frac{1}{V_F}\left\{UA_x\frac{\partial U}{\partial x} + VA_y\frac{\partial U}{\partial y} + WA_z\frac{\partial U}{\partial z}\right\} - \xi\frac{A_yV^2}{xV_F} = -\frac{1}{\rho}\frac{\partial p}{\partial x} + G_x + f_x - b_x - \frac{R_{SOR}}{\rho V_F}(U - u_w - \delta u_s) \quad [2.18]$$

$$\frac{\partial V}{\partial t} + \frac{1}{V_F}\left\{UA_x\frac{\partial V}{\partial x} + VA_y\frac{\partial V}{\partial y} + WA_z\frac{\partial V}{\partial z}\right\} + \xi\frac{A_yUV}{xV_F} = -\frac{1}{\rho}\left(R\frac{\partial p}{\partial y}\right) + G_y + f_y - b_y - \frac{R_{SOR}}{\rho V_F}(V - v_w - \delta v_s) \quad [2.19]$$

$$\frac{\partial W}{\partial t} + \frac{1}{V_F}\left\{UA_x\frac{\partial W}{\partial x} + VA_y\frac{\partial W}{\partial y} + WA_z\frac{\partial W}{\partial z}\right\} = -\frac{1}{\rho}\frac{\partial p}{\partial z} + G_z + f_z - b_z - \frac{R_{SOR}}{\rho V_F}(W - w_w - \delta w_s) \quad [2.20]$$

In these equations, (G_x, G_y, G_z) are body accelerations, (f_x, f_y, f_z) are viscous accelerations, (b_x, b_y, b_z) are flow losses in porous media or across porous baffle plates, and the final terms account for the injection of mass at a source represented by a geometry component. The term $U_w = (u_w, v_w, w_w)$ in the above equations is the velocity of the source component. The term $U_s = (u_s, v_s, w_s)$ is the velocity of the fluid at the surface of the source relative to the source itself.

Numerical modeling starts with the physical geometry of the desired model, and a computational mesh is used to capture this geometry. The computational mesh consists of a number of interconnected cells, which divide the physical space into small volumes with nodes associated with each volume. The data computed (pressure, temperature, and velocity) at each nodal location is stored at each time-step. Flow3D uses a rectangular grid system, which is the most basic of grid types. This method of grid development effectively makes the equations used for solving the fluid motion equations much simpler to solve, and the governing equations were originally developed on a rectangular grid.

All fluid parameters are stored at these representative nodal locations, and represent the flow field throughout the discretized model space. Since the physical characteristics vary continuously in space, in theory a finer mesh will provide a better representation of reality than a coarser mesh. In practice, there is a threshold where the increase in accuracy is not sufficient to warrant an increased mesh density. Combined with the fact that time can become a limiting factor, refining the mesh for the same physical space will consequently increase the computational time and may not provide a better solution than a coarser mesh. Therefore a balance between a better representation throughout the entire flow field and computation time must be made for engineering purposes.

Flow3D uses rectangular grids because they are very simple to create and store due to their structured nature. These grids are numbered using three indices: i in the x-direction, j in the y-direction and k in the z-direction. From this numbering system each cell can be identified by a unique address (i, j, k) similar to the physical space. Another benefit of using structured grids is that they are generally more accurate and have better stability within numerical models than using unstructured grids, where grid cells may be curvilinear. This is because some of the oldest numerical schemes are based on the finite difference and finite volume methods that have been developed using a rectangular mesh. As a result, finding numerical solutions using rectangular grids are generally more efficient.

Since this research focuses on free surface flow, it is important to note that many different simulation types exist within Flow3D. There is an added difficulty when modeling any free surface environment because flow parameters and materials experience a discontinuity at the surface. In Flow3D, the gas next to the water surface is replaced by an empty space which has a uniform pressure and temperature while the inertia of the air is ignored. These assumptions are generally valid, since the flow details of the gas typically have little effect on the general flow characteristics of the heavier fluid. By modeling with one fluid, the free surface then becomes a boundary of its own. It is important to be able to define the free surface boundary condition properly to accurately model the free surface dynamics.

Flow3D uses the Volume of Fluid (VOF) method to model the free surface. It consists of three main parts: the first being the definition VOF function, second is a method to solve the VOF equations, and finally setting the boundary conditions. Along this boundary all velocity gradients and the shear stress are set to zero. This in turn reduces the turbulence production (k) at the free surface (Flow-Science, 2009). Auxiliary models are also available to the user depending on the type of model being set up. The auxiliary models which were used within the model set up were the gravity and viscosity models, which will be discussed in more detail within Section 3.2.

Chapter 3: Testing Procedure

Chapter 3 outlines the physical model apparatus, experimental plan and Flow3D model development.

3.1 Physical Model

A scaled CSP culvert model was constructed at the University of Manitoba's Hydraulic Research & Testing Facility (HRTF). Only a brief description of the equipment and procedures will be given below, as a detailed description was given by Kehler (2009). The project area consisted of a space approximately 3.65 m wide, 27 m long, and 2.5 m in height. This model space provided sufficient room to allow for a headwater box, CSP culvert, and tailwater box with a return channel.

The headwater box was developed to have a sufficient length and width to model natural incoming stream conditions. The headwater box had an internal width of 2.73 m and a total internal length of 4.56 m. The inlet of the CSP culvert projected 1.22m into the headwater box. This allowed for different inlet configurations to be built within the headwater box if they were required. However, for this research all physical modeling was done with a projecting inlet. Flow straighteners, composed of a series of 0.3 m long PVC tubing oriented in the preferential flow direction, were located approximately 2.20 m upstream of the inlet of the CSP culvert. Additionally, a horse hair filter was attached to the flow straighteners to drag along the water surface to reduce any surface

disturbances. Finally, the inlet pipe discharged straight down and was forced towards the back wall to dissipate energy before going through the flow straighteners.

A 0.80 m diameter CSP culvert with annular corrugations of 13 mm in amplitude and 68 mm in wavelength was used. The culvert consisted of five 4.27 m sections for a total culvert length of 21.35 m. Each section was connected together using culvert couplers, creating a sufficiently stable connection. Significant work was done to reduce leakage throughout the culvert due to rivets and seams. An industrial polyurethane waterproofing sealant was used along these areas to eliminate leakage during testing along the length of the culvert. A series of 18 saddle yokes were utilized to support the culvert along its length. By supporting the culvert in this fashion, the culvert was able to have an adjustable slope that ranged between horizontal and 1.5%.

The tailwater box was constructed in the same fashion as the headwater box, with a return channel and a method to control the water level. Due to the location of the water collection channel, the return channel required the flow to be 180 degrees from the exit of the culvert. This was done by providing a sufficiently long outlet channel, which was 3.34 m long and 1.75m wide with well rounded corners to direct the flow into the return channel. The return channel was 0.91 m wide, which allowed the flow to return to the laboratory flow system. A radial tailwater gate was used to control the tailwater level within the culvert to ensure that normal depth had been reached.

Gravel with a d_{50} of 2.76 cm and a reasonably uniform gradation was used within the culvert for the gravel infill tests. The gravel was distributed and leveled by hand initially. A survey was then conducted to ensure that the gravel infill had a consistent depth over the length of the culvert. In the case of the additional tests that were performed after 2009, baffles at the desired gravel depth were installed approximately every $2D$ along the length of the culvert to reduce interflow through the gravel infill.

Discharge measurements were taken using a MSR Magnum Standard Magmeter. The Magmeter was connected to a computer equipped with Labview software used to average 250 readings for each measurement. A series of 28 manometer tubes were used along the length of the culvert to ensure that uniform depth was reached over the entire culvert length. Once uniform depth was achieved throughout the culvert, velocity measurements were taken to capture the two-dimensional velocity profile within the fully developed region. These measurements were taken 16 m ($20D$) downstream from the culvert inlet, which was found to be well within the fully developed region by Kehler (2009). Velocity measurements were taken using three different Acoustic Doppler velocimeters (ADV's). The ADV's used were an upward and downward looking SonTek 16 MHz MicroADV, as well as a side looking Sontek 10 MHz ADV.

The physical modeling plan was developed to utilize previous data collected at the University of Manitoba (Kehler, 2009), and to provide a broader range of velocity profiles at similar slopes. Data from Kehler (2009) was used as the first eight test

conditions, while the remaining tests seen in Table 1 were completed to complement Kehler's (2009) data.

Table 1: Physical model tests

Test	Discharge [m^3/s]	Slope [%]	Rock Infill [%]	h [m]
1	0.086	0.028	0.00	0.49
2	0.086	0.110	0.00	0.35
3	0.176	0.110	0.00	0.52
4	0.085	0.270	0.00	0.27
5	0.176	0.270	0.00	0.40
6	0.075	0.270	9.71	0.24
7	0.075	0.270	18.38	0.22
8	0.075	0.270	27.85	0.20
9	0.123	0.042	0.00	0.51
10	0.125	0.124	0.00	0.40
11	0.217	0.124	0.00	0.54
12	0.125	0.249	0.00	0.31
13	0.225	0.249	0.00	0.44
14	0.250	0.249	0.00	0.48
15	0.200	0.504	0.00	0.35
16	0.089	0.295	10.00	0.23
17	0.260	0.295	10.00	0.36

A key difference to note is that for tests 6-8 the integrated discharge, rather than the discharge measured by the Magmeter, was used. There was a significant difference between these two numbers because of the amount of interflow within the clean gravel. The choice to use the integrated discharge was made because in field conditions a culvert with rock infill would retain silt within the voids in the gravel layer. However, baffles were installed approximately every 1.6 m to limit the amount of interflow that occurred, and to take this assumption into account for tests 16 and 17.

3.1.1 Data Collection

A traversing mechanism was utilized to facilitate accurate geometrical positioning of the ADV's within the culvert cross-section 20 diameters downstream from the culvert inlet. The predicted water depth from Manning's equation, using the published value of Manning's n (0.024) for the CSP culvert (Corrugated Steel Pipe Institue, 2007), was used to set the upper limit of the expected flow field. A gridded profile was then developed, using this upper limit and the culvert wall, within an Excel file. These point locations were then converted to the number of required counts, used by the traversing mechanisms to accurately position and record the ADV's location, within the same Excel file. In the previous research completed (Kehler, 2009), 12,000 samples were deemed to be an appropriate number of samples to provide results that were within 2% of the measured long term turbulence characteristics. However, for the purpose of this research the measured streamwise velocity will be compared against the modeled streamwise component of the flow field and turbulence quantities were not as important. Therefore, 12,000 samples were collected at two points to determine how many samples were required to accurately measure the streamwise velocity. It was determined that it was sufficient to measure 6,000 samples to be within the error of the ADV's (1% of the measured velocity or 0.25 cm/s (SonTek, 2001)) as seen in Figure 2 and Figure 3, where the dashed lines denote the error of the ADV's long term measurement.

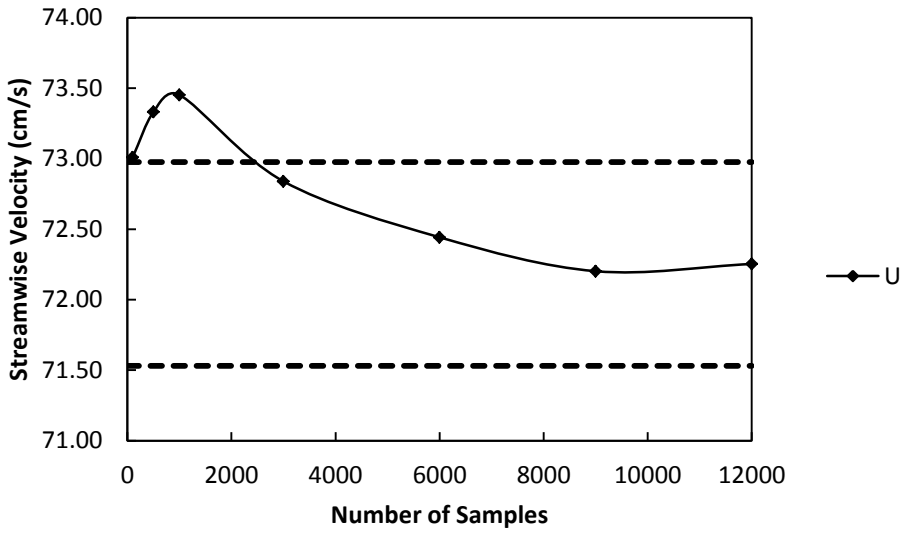

Figure 2: Data point analysis for point #1

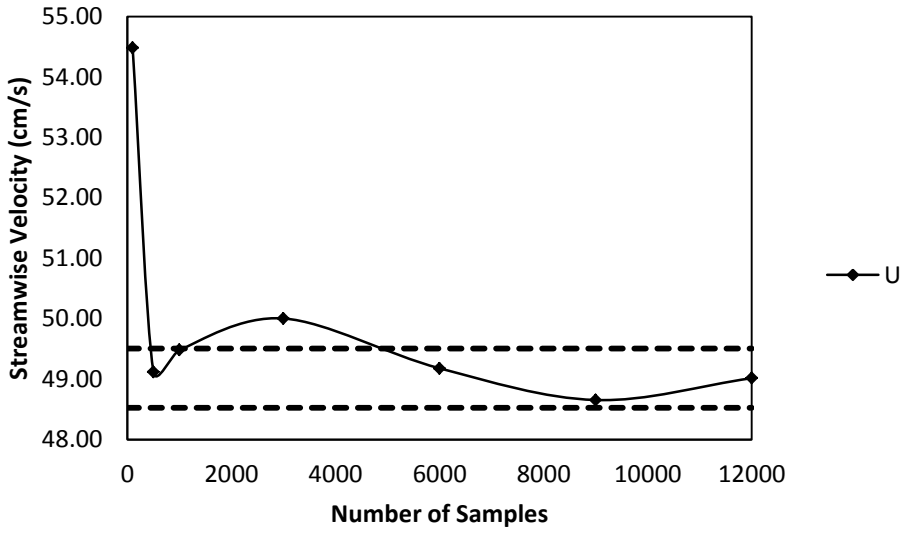

Figure 3: Data point analysis for point #2

3.2 Flow3D Model Development

This section will be broken down into the same categories that Flow3D uses to set up a model. These sections include the general model assumptions, physics models, fluids, meshing and geometry, boundary conditions, initial conditions, desired output, and numerical operation methods.

3.2.1 General

The threshold for steady-state was set to occur when the change in total mass, total fluid energy, total solid energy, average mean kinetic energy, average mean turbulent energy and average mean turbulence reached values of less than 1.0%. Simulations were run either to steady-state or for 700 seconds of simulation time, whichever came first. If the model stopped after 700 s it was found to be in a quasi-steady state condition, wherein the streamwise velocity distribution changed slightly, but consistently between time steps.

The interface tracking was set to be a free surface or sharp interface. These methods were described earlier within section 2.2.2, which use the VOF method. The flow mode within the model was assumed to be incompressible; this was done to allow Flow3D to utilize this assumption to simplify the governing equations of fluid flow. The general form of the continuity and momentum equations could then be reduced by eliminating all terms that consist of a change in density in time or space. Finally a one fluid model

was used within Flow3D. This utilized the aforementioned simplifying assumptions used for a one fluid model, to help reduce computation time.

3.2.2 Physics

There are a multitude of physics models that can be used within Flow3D, only two of which were selected to be appropriate for open channel flow through culverts. The first auxiliary model used was the gravity model. Gravity in the z-direction was set to 9.806 m/s^2, while gravity in the x-direction was adjusted to take into account the slope of the culvert model. This was done to allow the model to be in a horizontal orientation to prevent irregular fragments in the mesh that would occur along the length of the culvert barrel from the Fractional Area/Volume method (FAVOR) that Flow3D uses to capture the geometry.

The second physics model utilized was the viscosity and turbulence model due to the Reynolds number ranging between 94,000 and 326,000 for the physical model, indicating turbulent flow conditions. The viscous flow setting was used to better model the flow characteristics within the culvert. Since flow is known to have turbulent characteristics within CSP culverts, a turbulence model was used to represent these features. A series of tests were then developed using the different turbulence models available within Flow3D which are the Prandtl mixing length, one-equation turbulent energy model, two-equation k-ϵ model, renormalized group k-ϵ model, and a large eddy simulation model. Through these tests it was determined that the renormalized group k-

ϵ (RNG) turbulence model was the most efficient in this particular application, while still providing acceptable results. Also, the RNG turbulence model is generally the most robust transport turbulence model available within the Flow3D software (Flow-Science, 2009).

3.2.3 Fluids

Within Flow3D a comprehensive fluid database of different fluid properties is included. This database includes information regarding the density and viscosity among other key characteristics. The material properties that were used were water at 20^{o}C. This was deemed appropriate, considering the slight variation in density and viscosity with temperature, because the water within the laboratory at the University of Manitoba is generally close to 20^{o}C.

3.2.4 Meshing & Geometry

Flow3D has two meshing coordinate system options which are cylindrical or Cartesian coordinates. Cylindrical coordinates were initially considered because they would be ideal for capturing the culvert geometry accurately. However, within Flow3D, cylindrical coordinates are generally used for axisymmetric or annular domain problems, making them preferable for full pipe flow models. Since all of the modeled conditions were only partially full, a Cartesian coordinate system was found to be preferable.

A series of model geometries were developed at the beginning of the modeling phase to determine the most appropriate method of modeling flow conditions through CSP culverts. The first model was developed to try to limit the number of cells required to model the flow field within the domain. This model included half of the culvert cross section, with a length of 21 m. Symmetry was assumed along the centreline of the culvert by modeling flow in only half the cross-section. However, this tended to dampen the secondary circulations that would be expected within the culvert. This is because the assumption of symmetry within Flow3D does not allow for turbulent cross flow through the boundary condition.

The second model that was developed took these observations into account by including the full cross-section of the culvert. This model allowed for secondary circulations to develop within the culvert. However, the secondary circulations occurred in the opposite direction of what is expected within the culvert when compared to velocity profiles from Clark and Kehler (2011).

This then lead to the development of the final model geometry. The final model geometry included the headwater box geometry of the physical culvert model, as well as the full cross-section of the culvert for 21 m. By changing the geometry to include the headwater box, the secondary circulations developed in the appropriate direction. This is likely due to the incoming velocities and turbulence quantities within the culvert being

modeled more appropriately than assuming a constant velocity field at the inlet (Toews et al., 2011).

The geometry consisted of a headwater box which was 2.9 m in length (to the inlet of the culvert) and 2.8 m in width. A vertical head wall was assumed at the inlet to limit the number of cells required to capture the geometry of the inlet. This assumption was based on the findings of Hunt (2012), that the flow structure two diameters downstream from the inlet is very similar for different inlet configurations. Using these findings, and knowing the normal depth for a particular discharge in a culvert will not change, it can be taken that the velocity field for different inlet configurations will be very similar within the fully developed region. As previously mentioned, the culvert barrel portion of the model was a 0.8 m diameter, 21 m long, smooth horizontal pipe. The centre point of the culvert inlet was located at 2.90, 1.50, 0.50 (X, Y, Z) m and the centre point of the culvert at the outlet is located at 23.95, 1.50, and 0.50 m. The roughness of the culvert was determined by applying the log-law to the physical model results from Test 3 to determine the equivalent sand grain roughness of the corrugations. Additionally, for tests that include rock infill, a smooth surface was added at the appropriate location near the model bed, and was given an appropriate roughness value. This value was determined to be four times d_{50} of the gravel that was used within the physical model.

Mesh sensitivity tests were required to determine the appropriate mesh density for the Flow3D model. Two mesh blocks were used to capture the entire model domain. A coarse mesh block was used to capture the headwater box geometry simply to provide the CFD model with a better representation of the incoming velocities than an average velocity boundary condition. This mesh block was the same for all mesh configurations within the culvert. The mesh dimensions and number of cells for mesh block one can be found in Table 2. The second mesh block had different mesh densities, which were used to determine the required cell size to adequately model the flow field within a culvert, shown in Table 3.

Table 2: Mesh block 1 configuration

	Fixed Point	Number of Cells
X Direction	0.00	--
	2.00	20
	2.95	20
X Direction Total	--	40
Y Direction	0.00	--
	1.00	12
	2.00	20
	3.00	12
Y Direction Total	--	44
Z Direction	0.00	--
	0.75	15
Z Direction Total	--	15

Table 3: Mesh block 2 configurations

	Fixed Point	Mesh 1	Mesh 2	Mesh 3	Mesh 4
		Number of Cells	Number of Cells	Number of Cells	Number of Cells
X Direction	2.95	210	210	210	1050
	23.95				
Y Direction	1.05	23	30	45	45
	1.95				
Z Direction	0.05	18	25	35	35
	0.75				

A fifth mesh configuration was developed for the culvert barrel, which consisted of the same cell density for the bulk flow area as Mesh 2, while three nested meshes were utilized to better capture the culvert walls. However, the nested meshes were still unable to capture the corrugations of the culvert. The configuration for Mesh 5's nested mesh can be seen in Table 4. The developed mesh densities in the spanwise and vertical directions are depicted in Figure 4. The developed meshes were tested to ensure that further refinement would not lead to an improved result.

Table 4: Mesh 5 - nested mesh configurations

	Mesh 5 – Nested Mesh 1		Mesh 5 – Nested Mesh 2		Mesh 5 – Nested Mesh 3	
	Fixed Point	Number of Cells	Fixed Point	Number of Cells	Fixed Point	Number of Cells
X Direction	2.95	525	2.95	525	2.95	525
	23.95		23.95		23.95	
Y Direction	1.05	90	1.05	15	1.8	15
	1.95		1.2		1.95	
Z Direction	0.05	30	0.35	40	0.35	40
	0.35		0.75		0.75	

a)
Δx = 0.10 m

b)
Δx = 0.10 m

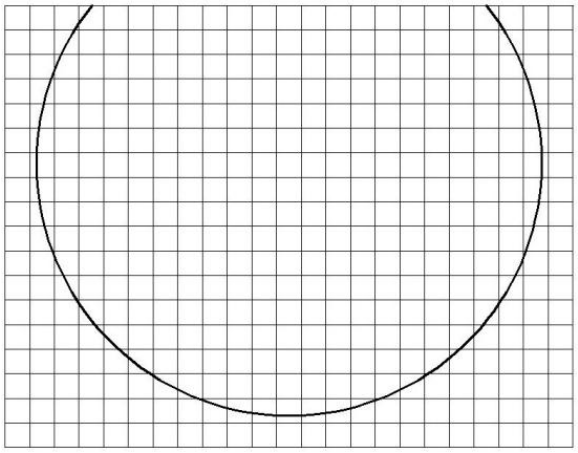

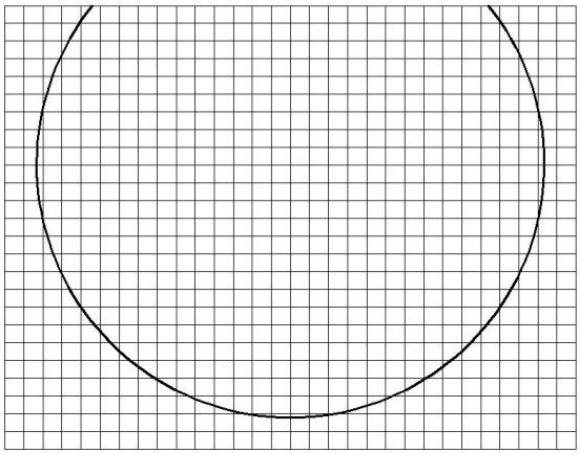

c)
Δx = 0.10 m

d)
Δx = 0.02 m

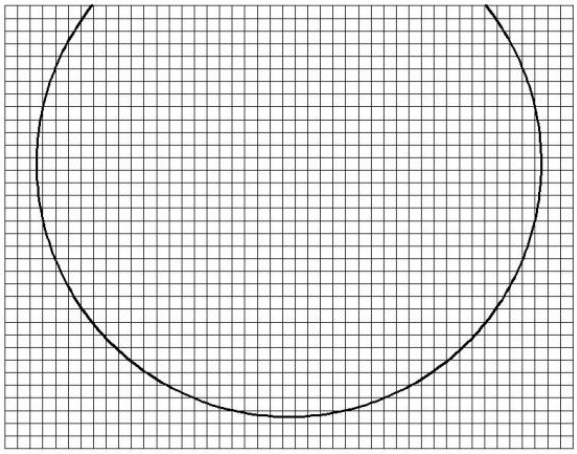

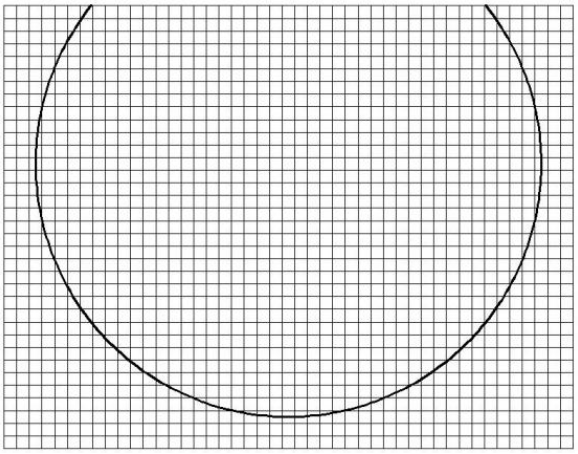

e)
Δx = 0.04 m

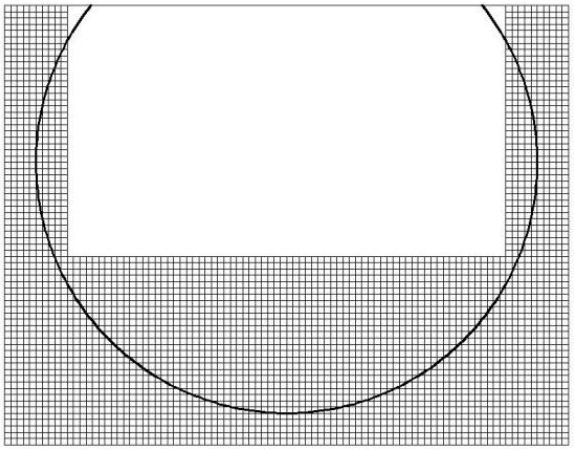

Figure 4: Mesh configurations as depicted from Table 3 & 4 - a) Mesh 1; b) Mesh 2; c) Mesh 3; d) Mesh 4; e) Nested meshes for Mesh 5

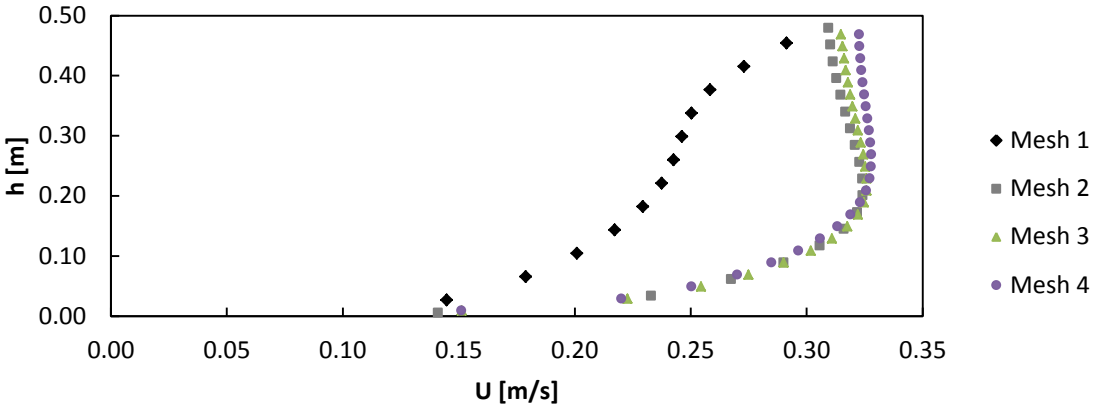

Figure 5: Test 1 mesh dependency check

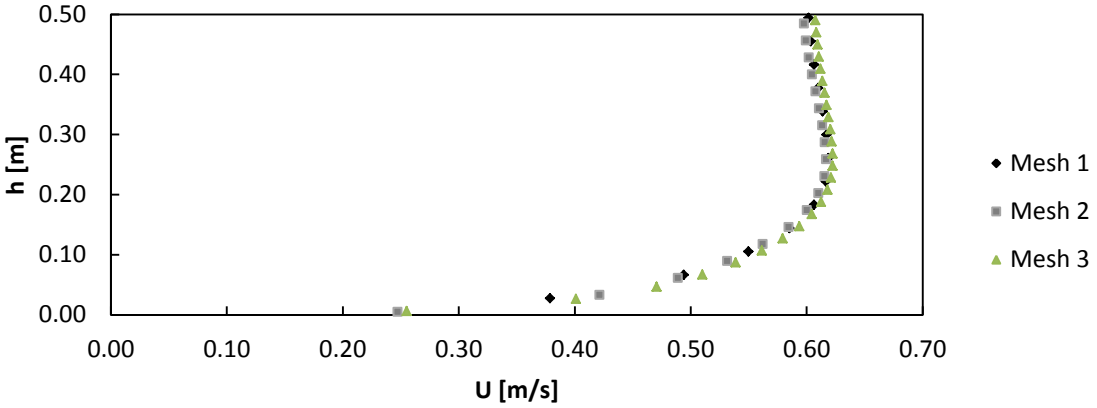

Figure 6: Test 3 mesh dependency check

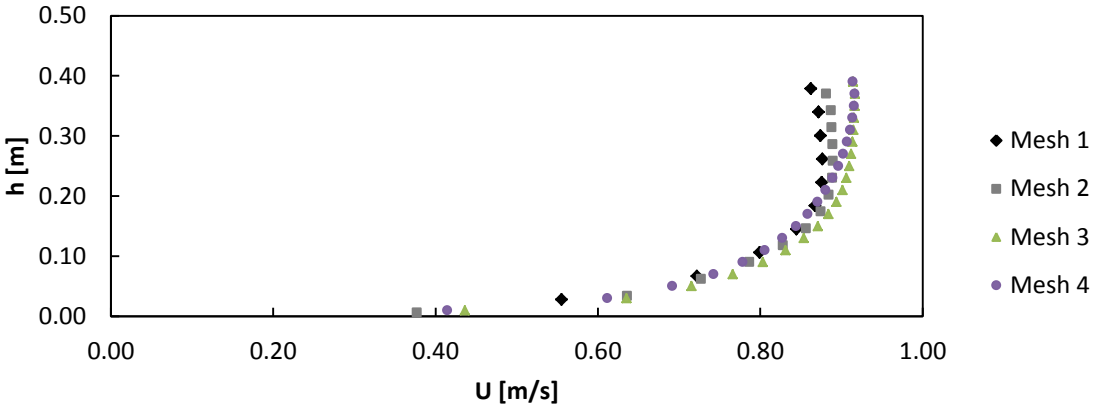

Figure 7: Test 5 mesh dependency check

Figures 5 to 7 show that there are small differences in the centreline profile within the developed region between the different developed meshes, excluding mesh 1 for test 1. However, there is a slight difference between mesh 2 and meshes 3 and 4 for test 5. Mesh 5 results were not obtained due to the significant increase in the number of active cells when compared against Mesh 4, exponentially increasing the CPU time seen in table 5, combined with consistent results being achieved between meshes 2 and 3, and meshes 3 and 4.

Table 5: Simulated time vs CPU time

Test	Mesh	CPU Time [days]	Simulated Time [s]	Ratio
1	1	1.2	700	154
	2	0.5	330	143
	3	1.1	401	240
	4	14.3	330	3742
3	1	0.6	617	88
	2	1.8	617	247
	3	6.2	617	865
	4	-	-	-
5	1	0.2	190	96
	2	0.3	190	155
	3	1.4	190	614
	4	30.3	412	6359

Due to these considerations, Mesh 3 was selected to be the most appropriate mesh density to accurately model the measured data within a timeframe that may be practical. Another important aspect was that this mesh was able to provide a good representation of the physical geometry of the model domain, which is demonstrated in Figure 8.

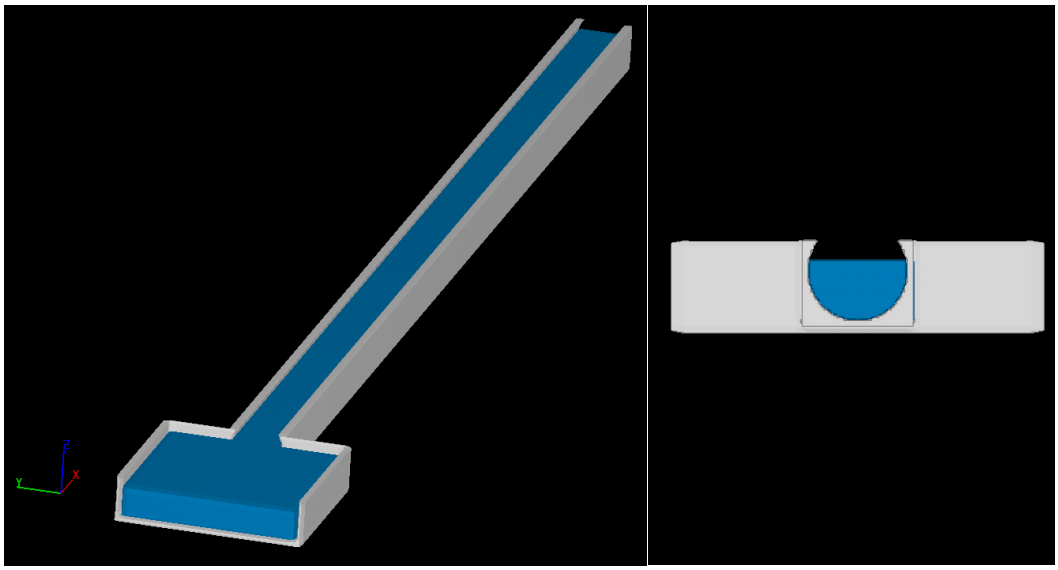

Figure 8: Final model domain

3.2.5 Boundaries

In Flow3D there are a multitude of boundary conditions available to the user depending on the desired application of the model. The boundary conditions used in all of the models are summarized in Table 6.

Table 6: Boundary conditions

Mesh Block	Boundary	Type
1	Xmin	Q
	Xmax	W
	Ymin	W
	Ymax	W
	Zmin	W
	Zmax	S
2	Xmin	W
	Xmax	P
	Ymin	W
	Ymax	W
	Zmin	W
	Zmax	S

Where Q is the volume flow rate boundary (Q and h), W is the wall boundary, S is the symmetry boundary, and P is the specified pressure boundary where the fluid depth (h) is specified. The pressure boundary was set to normal depth at the outlet and was assumed to be an appropriate representation because all test conditions are subcritical and controlled from the downstream portion of the physical model. However, for the volume flow rate boundary condition only the discharge was specified. This was done to prevent over specification of the CFD model and to allow a varying water surface profile to occur within the model. Finally, the reason for Xmax in mesh block 1 and Xmin in mesh block 2 being specified as wall boundaries are that a significant portion of the boundary is a wall boundary; however, Flow3D is able to recognize that flow does need to cross the boundary at the inlet of the culvert.

3.2.6 Initial Conditions

The initial conditions within the model consisted of setting the depth and velocity within the two mesh blocks. The depth was set to the expected normal depth within the culvert and the average velocity was assumed within the culvert. The initial velocity set within the headwater box was found by

$$U_{head} = \frac{Q}{2.8h} \quad [3.1]$$

where U_{head} is the streamwise velocity within the headwater box. The vertical velocity throughout the model was assumed to be in the downwards direction with a magnitude of 10% of the average velocity within the culvert. This was done to help initiate secondary circulations within the model.

3.2.7 Output

Data was saved for every 10 seconds of simulation time to minimize the result file size for each test, while still providing enough time steps to ensure that the model was working properly. Extra data that was used to ensure that the model was working included the hydraulic data set option which consisted of free surface elevation, Froude number, fluid depth, and the depth-averaged velocity.

3.2.8 Numeric

The numeric settings within the Flow3D models were based on recommendations from the user's manual with the exception of the minimum time step. The minimum time step was low at 0.000001 s to ensure that the time step would not force the model to exit before steady-state conditions had been met. The varying time-step was controlled by stability and convergence. The pressure solver used the GMRES implicit method, while the explicit solver was used to find the viscous stress. Finally, the momentum advection was modeled using the third order scheme to ensure that secondary circulations were not dissipated due to poor approximations from the first or second order schemes (Flow Science, 2012).

3.3 Data Processing

The data processing for this research consisted of processing the data from the physical model and the developed CFD models. The details for this process will be broken down into the physical modeling and CFD modeling procedure.

3.3.1 Physical Model Data Processing

The physical model data was organized into a folder which was labelled according to its slope, discharge, and infill depth. The velocity data was filtered to ensure that a correlation of greater than 50 was achieved for U, V, and W. This process included using the phase-space despiking method to eliminate the spikes from the measured data as set out by Goring and Nikora (2002). This method is based on the concept of a three-dimensional Poincaré map or phase-space plot where the variable and its derivatives are plotted against each other. The points are then enclosed by an ellipsoid defined by a set of criterion and the points outside of this ellipsoid are designated as spikes. When a spike was found it was then replaced by the overall mean of the signal. The method iterates until the number of good points does not change or the number of spikes goes to zero.

Once the data had been filtered for each data point location, the profile was then created using this filtered data. This was done using an in-house m-file to collect all data points and mirror them along the centreline of the two-dimensional profile. The averages for U, V, and W were calculated along with a multitude of turbulence

quantities. A new variable was then created for the normalized measured velocity (U_{meas}/U_{av}).

3.3.2 CFD Model Data Processing

The CFD models were labelled according to the same order as the physical model results as shown in Table 1. Each test required a different amount of simulation time to elapse. This difference resulted in a wide range of file sizes for each test, as well as a difference between the amounts of CPU time required to find a solution. Each test was separated into its corresponding folder depending on the CFD model properties. The CFD model properties consisted of the mesh density, surface roughness, and the boundary conditions.

Although Flow3D has a built-in results viewer, an external program was used to provide more flexibility with the analysis. Once steady-state was reached the flsgrf.* output files were then imported into Tecplot, each time-step could be observed within this file. Since the steady-state conditions were of interest, the data for the final time step was extracted. However, if the model reached quasi-steady-state the results were exported for the final 20 time-steps and averaged. This removed the subjectivity of selecting the "best" time-step throughout the simulated time period. Figure 9 shows that there was little change when averaging over 20 time-steps to obtain the two-dimensional velocity profile for Test 7.

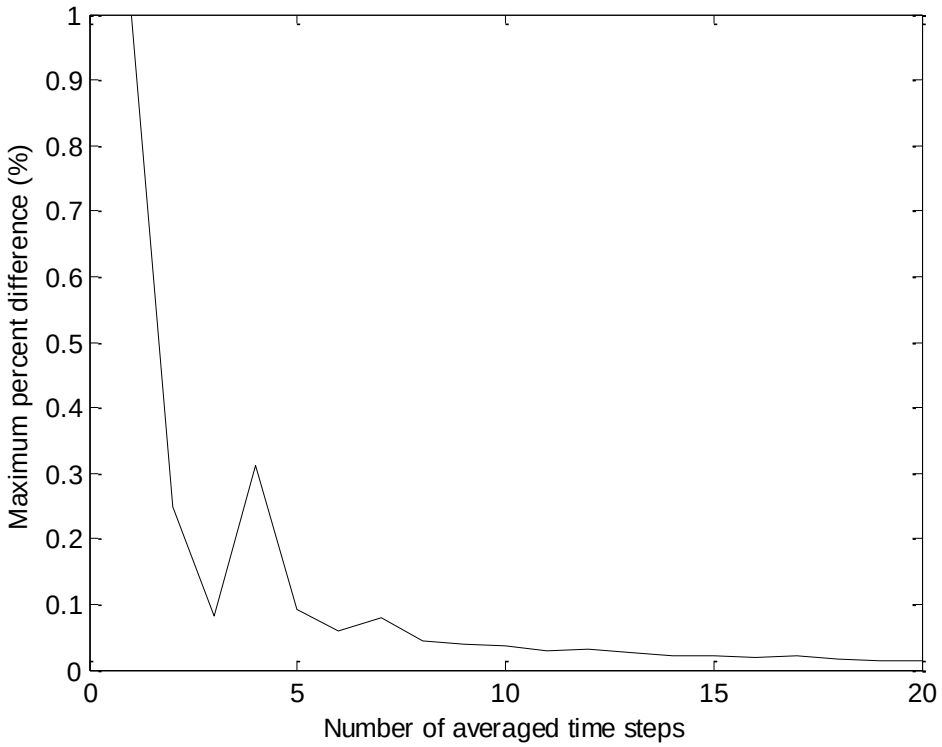

Figure 9: Maximum percent change between successive averaged result vs the number of averaged timed steps used to calculate the velocity profile for test 7

Cross-sectional data was extracted at 20.00 diameters downstream (18.90 m within the CFD model) from the inlet of the culvert within the model. The centreline was also extracted along the entire length of the culvert, which was then used to extract centreline profiles along the length of the culvert at 0.25, 1, 5, 10, 15, 20 and 25 diameters downstream of the culvert inlet.

Once the desired cross-sectional data was extracted, an additional variable was then calculated. This was done by finding the average streamwise velocity ($U_{av} = Q/A$)

within each distribution and dividing the predicted velocity by this calculated average at each point location. This new variable was then named U_{mod}/U_{av}.

3.3.3 Mesh Interpolation

The Flow3D mesh had node locations that did not exactly coincide with the measurement locations. In order to facilitate comparing the modeled and measured data at the same locations, the modeled data were linearly interpolated to the measured data point locations. This was done to reduce interpolation errors because the modeled data resolution was much finer, over the entire cross-section, than the measured data, as seen by Figure 10 below.

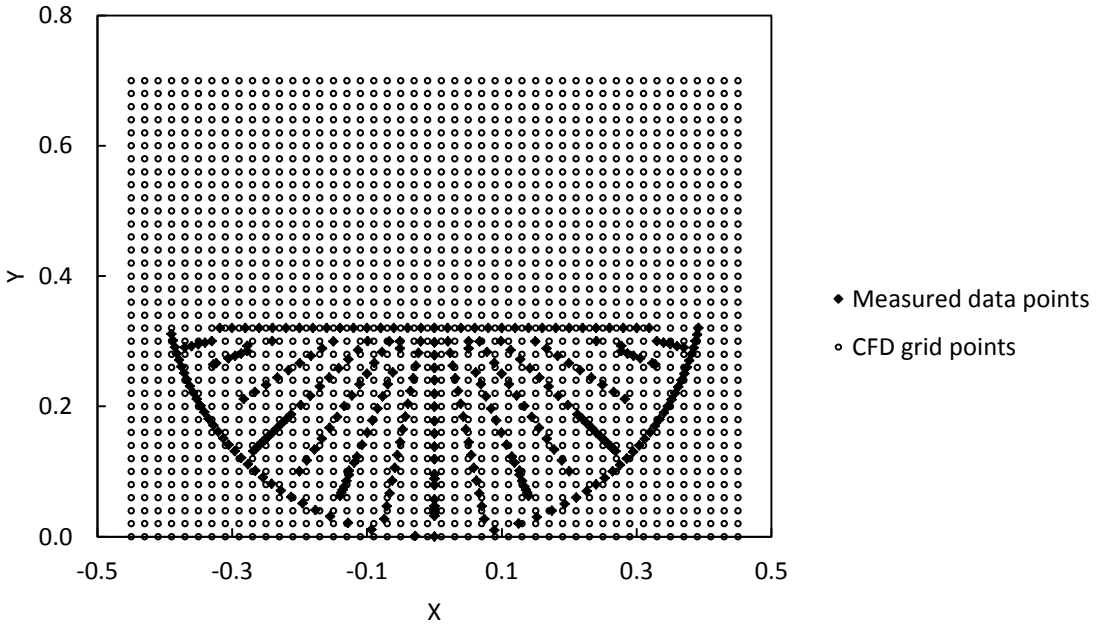

Figure 10: Test 1 measured data points and modeled data point locations

Chapter 4: Results and Analysis

The results and analysis portion of this research was completed using a combination of Excel, Matlab, and Tecplot software programs.

4.1 Introduction

Throughout this chapter only the results from several typical test conditions will be shown, while the remaining test conditions will be shown in Appendices A, B and C. A standard set of plots were used to allow an unbiased comparison between models. Each model's two-dimensional velocity distribution were plotted separately, and compared visually before detailed analysis was completed. Once these comparisons were made visually, inter-model comparisons were completed by using proportionality plots, and two-dimensional percent difference plots. Data was then extracted from the predictive model plots to show the percent area of the flow field that was within 5, 10, 15 and 20% of the measured normalized velocity (U_{meas}/U_{av}). Additionally, the cumulative percent area versus some threshold value (α) of U_{meas}/U_{av} was extracted to determine if there was a consistent relationship across all test conditions, where α ranged between 0.00 and 1.50, on an interval of 0.05 to provide a sufficiently detailed profile.

4.2 Physical Model Distributions

One of the objectives of using CFD to predict the flow field within CSP culverts, taking physical model measurements was required to verify the models ability to predict natural conditions. The physically measured two-dimensional velocity distributions for tests 1, 5, 6, 10, 13 and 16 are shown in Figure 11 to 16. The point locations on the two-dimensional distribution plots represent the locations where the physical measurements were taken, except for the points along the wetted perimeter. These points were forced to have velocity characteristics equal to zero to satisfy the no-slip boundary along the culvert wall, and were not included in any of the subsequent proportionality plots later in this chapter. They were necessary to include in order to facilitate generating accurate contour plots.

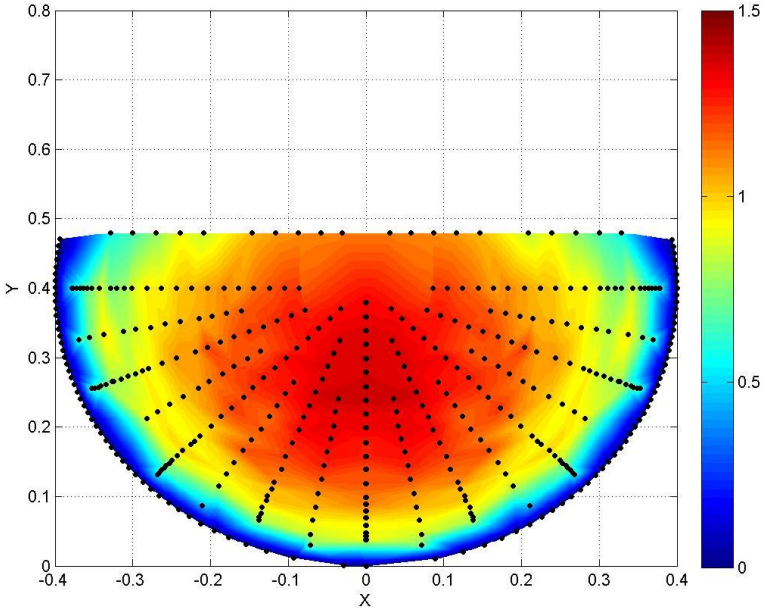

Figure 11: Test 1 – Measured normalized velocity (U_{meas}/U_{av})

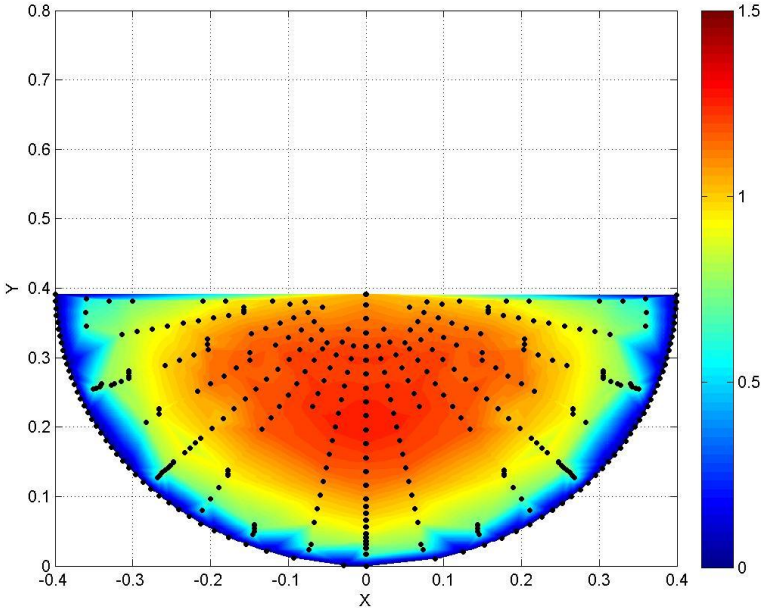

Figure 12: Test 5 – Measured normalized velocity (U_{meas}/U_{av})

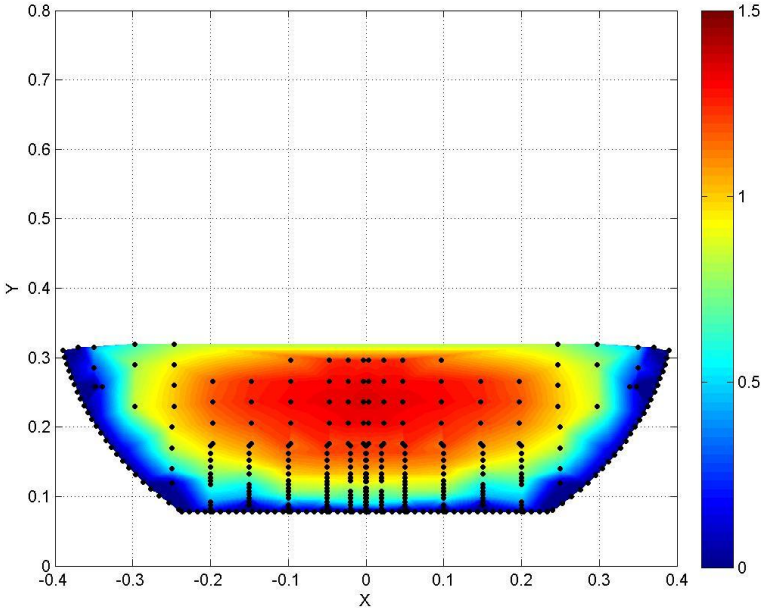

Figure 13: Test 6 – Measured normalized velocity (U_{meas}/U_{av})

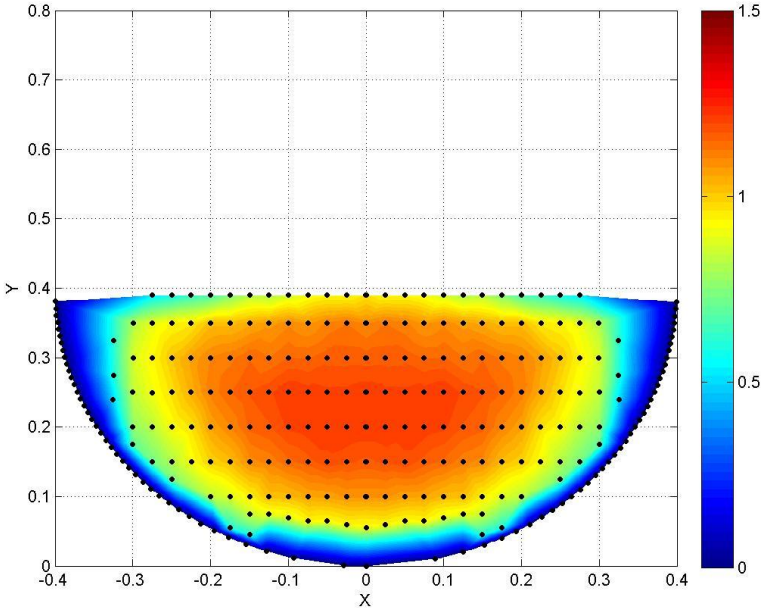

Figure 14: Test 10 – Measured normalized velocity (U_{meas}/U_{av})

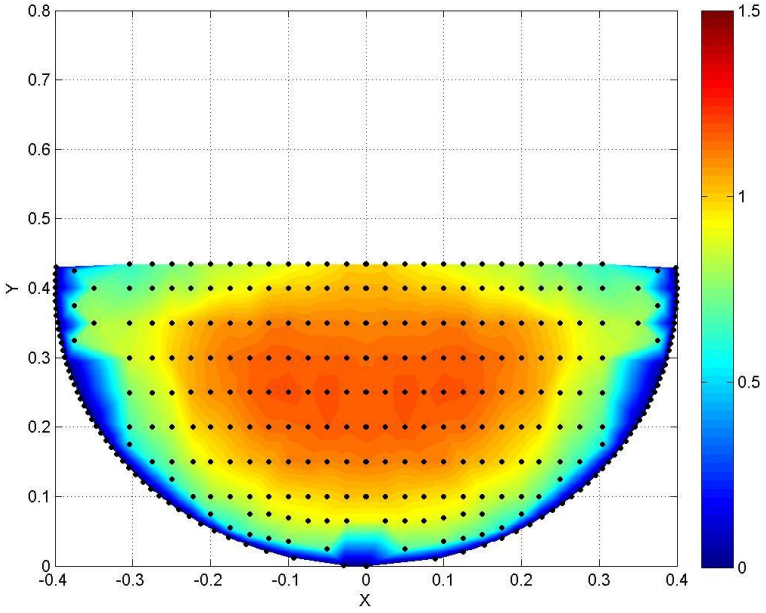

Figure 15: Test 13 – Measured normalized velocity (U_{meas}/U_{av})

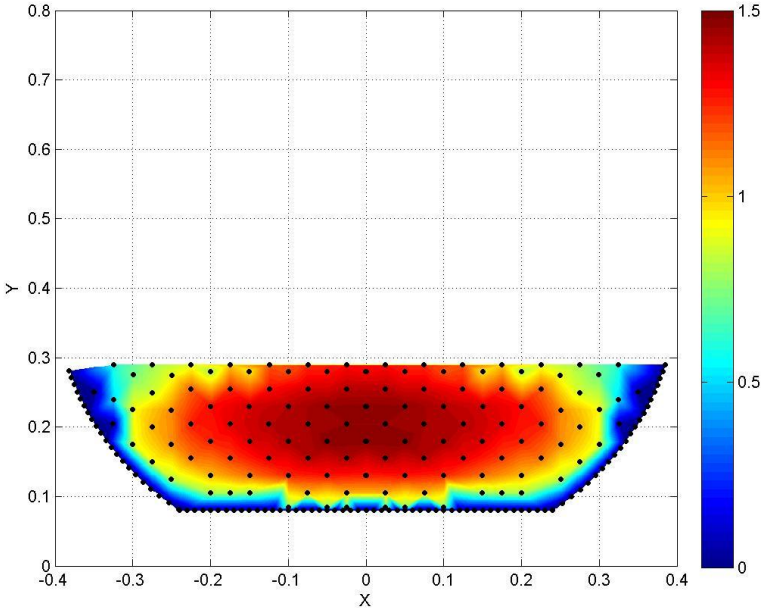

Figure 16: Test 16 – Measured normalized velocity (U_{meas}/U_{av})

A key observation to note is that the maximum velocity is suppressed from the water surface. This effect was due to the secondary circulations that were observed using the long-term averages of the secondary velocities taken by Kehler (2009). Another observation to take note of is the portion of the flow field that is less than the average velocity within these distributions. These aspects of the two-dimensional velocity profile were determined to be the most important to accurately model the velocity field within a culvert.

4.2.1 Current Prediction Method Comparison

Current fish passage regulations consider only one velocity, $U_{av} = Q/A$, when describing the hydraulic conditions within a culvert. This 'model' is in effect assuming that the two-dimensional streamwise velocity distribution is uniform, with the entire cross-section having a velocity of $U = U_{av}$. This 'model' was compared to the measured data to assess model performance. This was accomplished by calculating the percent difference between model and measurement on a grid. The measured velocity was linearly interpolated to this grid and the percent difference was calculated as

$$\%\ Difference = \frac{Uav - Umeas}{Umeas} * 100 \quad [4.1]$$

The percentage of the cross-sectional flow area where the model and measurements were within ±β percent difference (where β = 5, 10, 15, and 20) were determined for all test conditions, the results of which are shown below in Table 7 for tests without gravel infill and Table 8 for tests with gravel infill.

Table 7: Percentage of the cross-sectional flow area (%A) where the predicted velocity (Uav) is within ±β of the measured velocity for tests without gravel infill

Test	%A β = ±5%	%A β = ±10%	%A β = ±15%	%A β = ±20%
Test 1	12.6	27.5	42.8	59.2
Test 2	11.7	21.8	32.5	49.4
Test 3	15.2	32.2	49.7	70.9
Test 4	13.0	23.8	35.4	49.9
Test 5	16.0	30.3	48.3	68.7
Test 9	14.4	34.4	66.6	73.6
Test 10	15.5	32.5	53.3	69.0
Test 11	21.2	51.0	66.9	71.3
Test 12	11.7	23.3	37.2	56.2
Test 13	17.0	34.6	60.4	67.0
Test 14	17.9	37.5	58.9	65.5
Test 15	16.2	32.8	55.7	70.1
Average	15.2	31.8	50.6	64.2

Table 8: Percentage of the cross-sectional flow area (%A) where the predicted velocity (Uav) is within ±β of the measured velocity for tests with gravel infill

Test	%A β = ±5%	%A β = ±10%	%A β = ±15%	%A β = ±20%
Test 6	11.3	22.6	34.1	48.2
Test 7	11.9	23.3	35.7	51.3
Test 8	8.2	18.1	28.7	40.5
Test 16	9.0	18.5	27.0	37.5
Test 17	14.6	29.9	49.0	72.6
Average	11.0	22.5	34.9	50.0

Consider Test 1 as an example. A total of 12.6% of the cross-sectional flow area has a predicted velocity within ±5% of the measured velocity, whereas 59.2% of the cross-sectional flow area has a prediction that is within ±20% of the measured data.

It can be concluded that the current method of predicting the velocity field is not an accurate representation of the actual flow field within a culvert. It is important to be able to model the velocity gradient near the culvert wall, where the fish are likely to

swim as the velocities are significantly less than those in the centre of the channel and the average velocity. It is also important to note that the tests without gravel infill were slightly better represented on all four levels than the tests with gravel infill. This is likely due to the more complex secondary circulations that occur within culverts of this nature. The secondary circulations would be expected to be more complex due to the compound channel roughness and sharp corner regions of the channel geometry.

4.3 CFD Model Distributions

The predicted two-dimensional velocity distributions from the CFD model are shown in Figure 17 to 22 for the same test conditions (1, 5, 6, 10, 13, and 16).

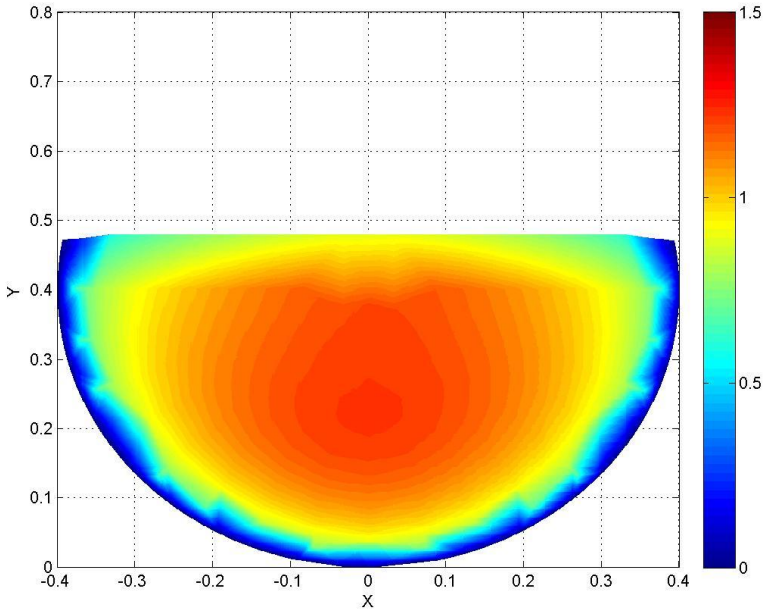

Figure 17: Test 1 – CFD predicted normalized velocity (U_{mod}/U_{av})

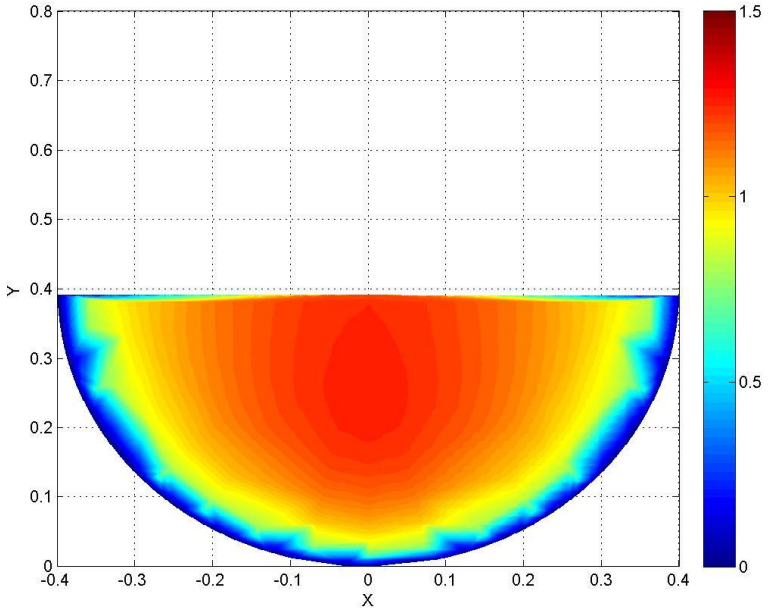

Figure 18: Test 5 – CFD predicted normalized velocity (U_{mod}/U_{av})

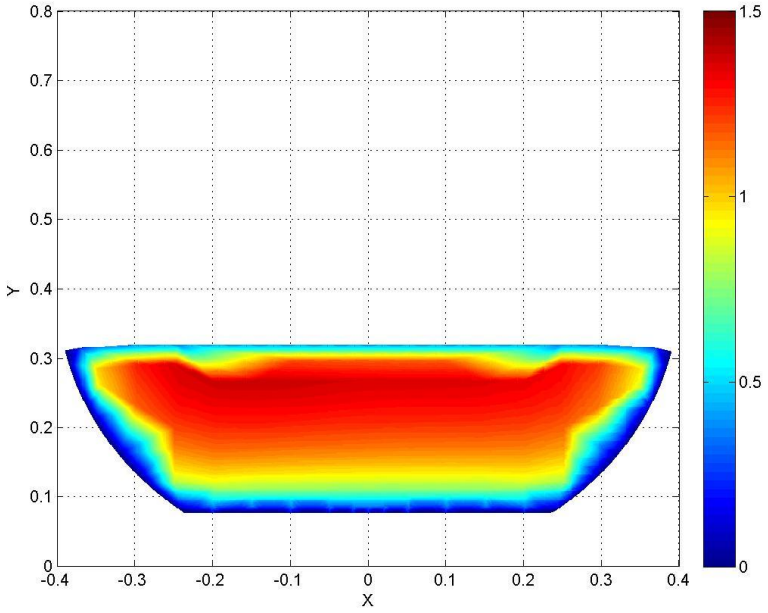

Figure 19: Test 6 – CFD predicted normalized velocity (U_{mod}/U_{av})

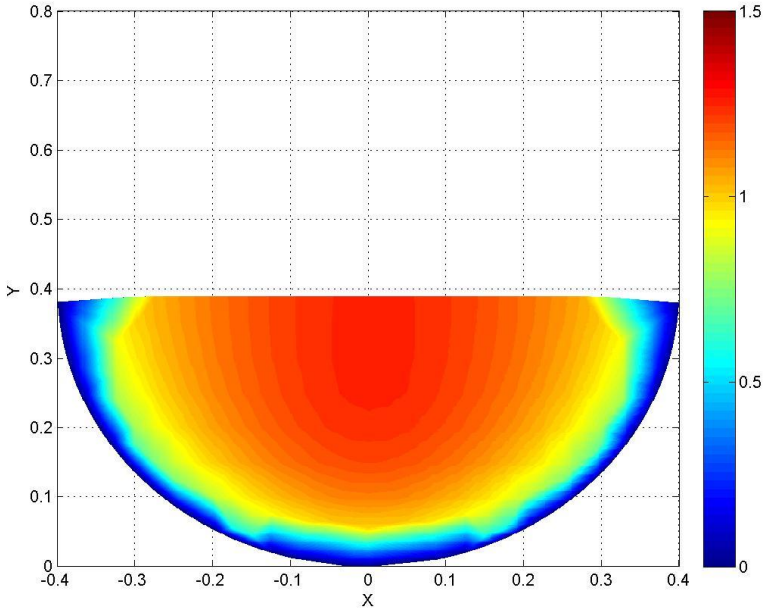

Figure 20: Test 10 – CFD predicted normalized velocity (U_{mod}/U_{av})

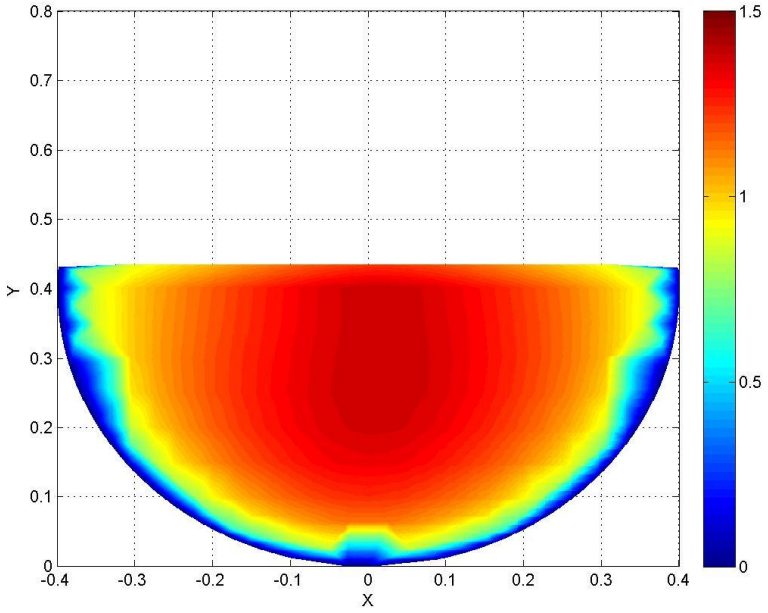

Figure 21: Test 13 – CFD predicted normalized velocity (U_{mod}/U_{av})

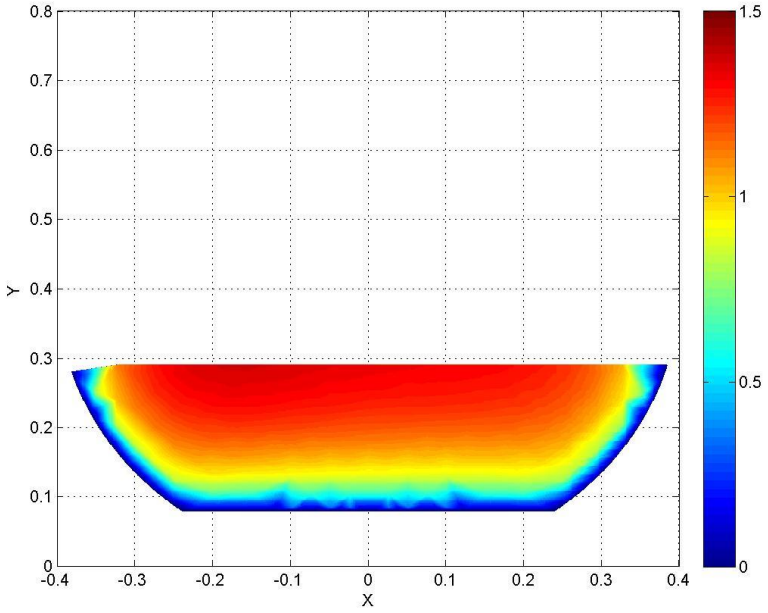

Figure 22: Test 16 - CFD predicted normalized velocity (U_{mod}/U_{av})

It can be seen that the Flow3D model has more accurately predicted the velocity distributions for tests without gravel infill than those with gravel infill. This is due to the maximum velocity being slightly suppressed from the water surface under these test conditions. However, for the models that included gravel infill the maximum velocity was forced closer to the water surface, further distorting the velocity profile. This is likely due to the k-ϵ turbulence model not being able to consistently model the velocity dip in shallow water depths. This was determined by visually inspecting the secondary circulations within the CFD model for each test condition. It was found that in tests with water depths below 0.398 m the model was not able to predict the secondary circulations in the appropriate direction.

Additionally, the centreline profiles were visually inspected to determine whether the CFD model has a developed region, similar to the physical model. The centreline profiles for tests 1-5 can be seen below. A continuous profile was extracted between the first cell above the culvert bed and the last cell below the water surface.

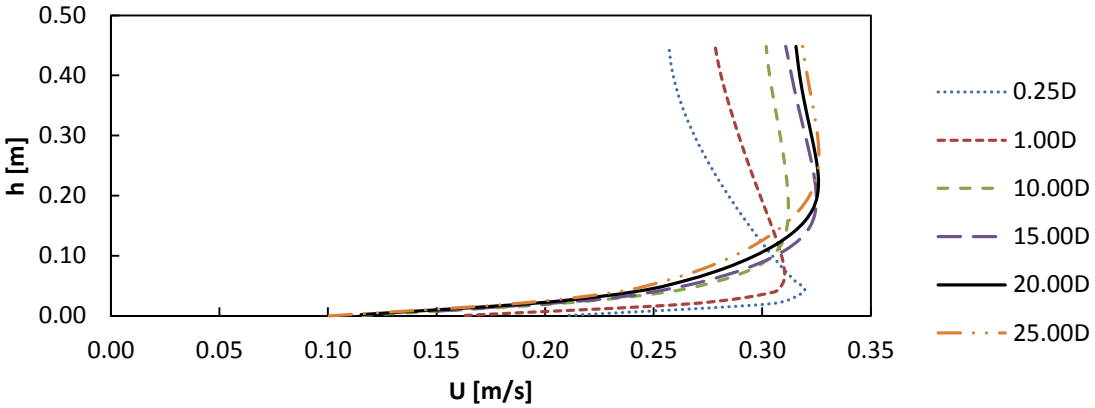

Figure 23: Test 1 CFD centreline development

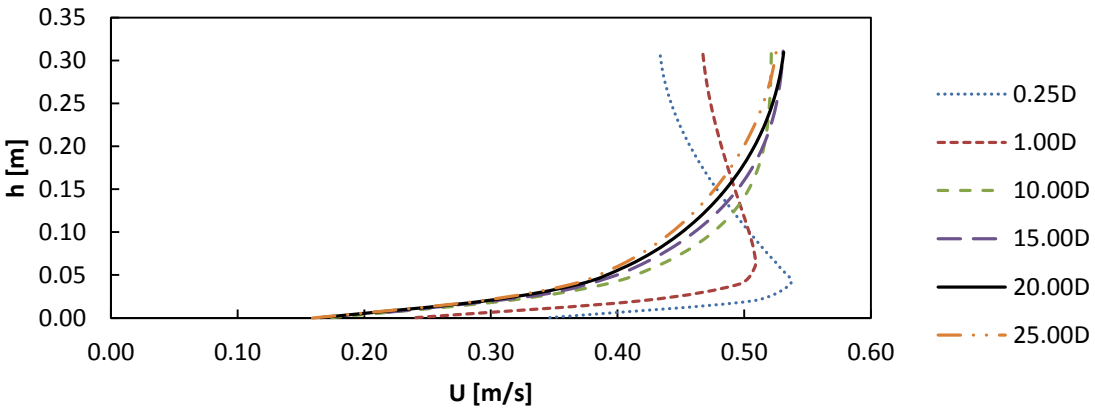

Figure 24: Test 2 CFD centreline development

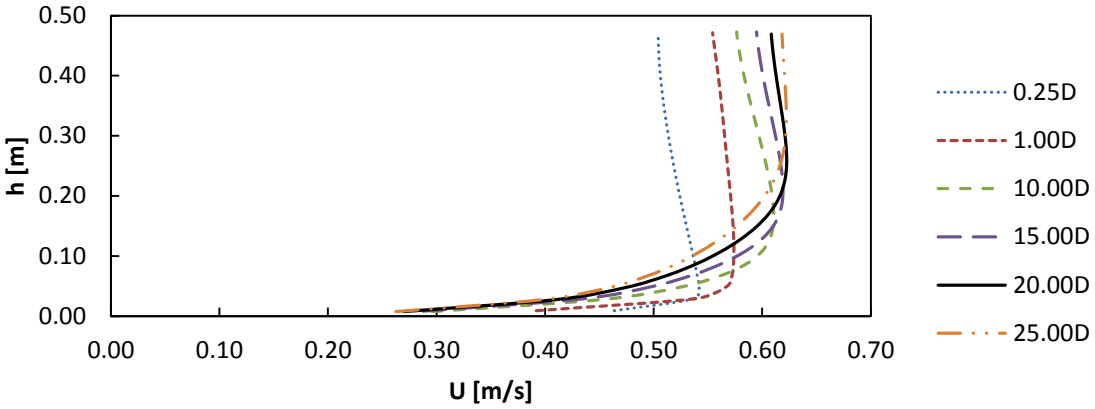

Figure 25: Test 3 CFD centreline development

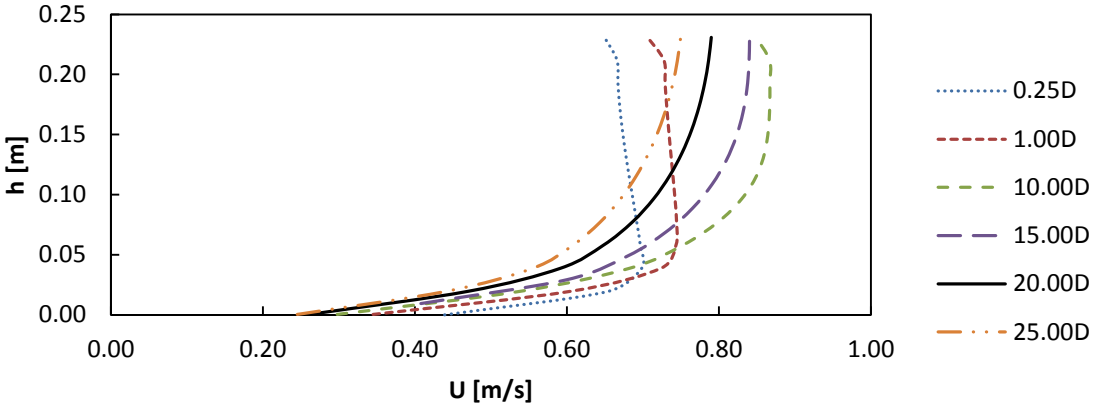

Figure 26: Test 4 CFD centreline development

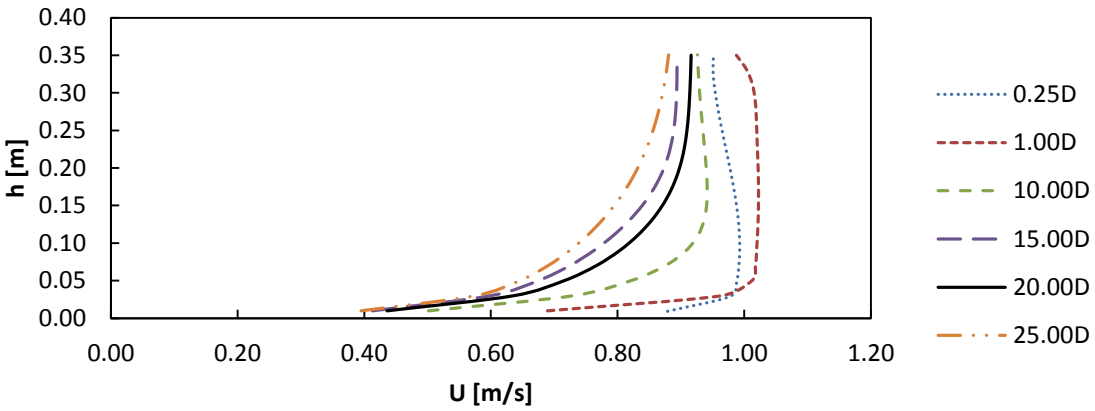

Figure 27: Test 5 CFD centreline development

It can be seen that in general there is a definite development region within the culvert model when comparing the centreline velocity profiles for 0.25, 1, 10 and 15D. This is similar to the observations made by Kehler (2009) on the physical model tests. The centreline velocity profiles become more consistent with respect to the downstream distance from the inlet when compared visually. In the region between 15-25D the centreline profiles take on a similar shape, and have a relatively consistent variation, with small differences between each subsequent profile.

4.3.1 CFD Model to Physical Model Comparison

The CFD model was compared to the physical model using several different figures and tools. The first of which was the proportionality plot where the predicted normalized velocities throughout the cross-section were plotted against the measured normalized velocities. A perfect relationship between these two values would result in a line of best fit to have a slope of one. Additionally, the R^2 value for a 1:1 slope and the line of best fit were calculated to determine the models performance. These figures are shown for tests 1, 5, 6, 10, 13 and 16.

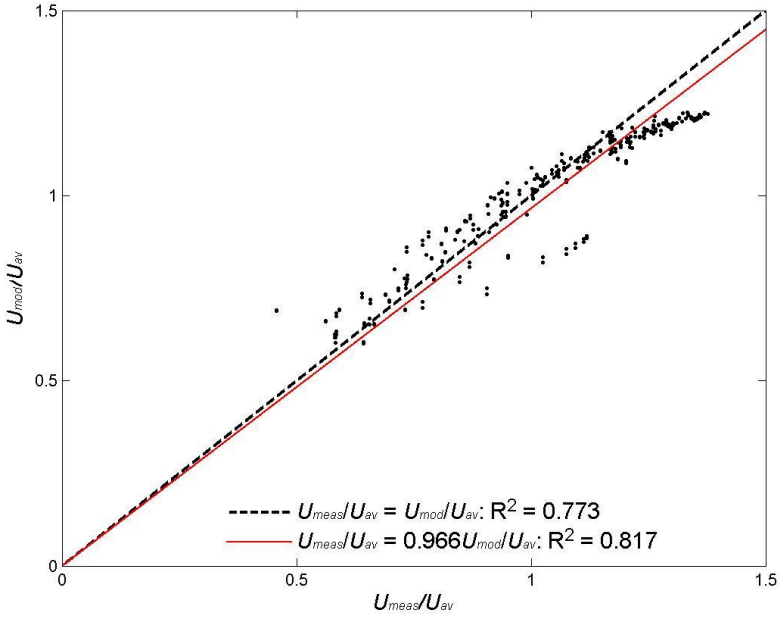

Figure 28: Normalized velocity predicted by the CFD model vs normalized measured velocity for Test 1

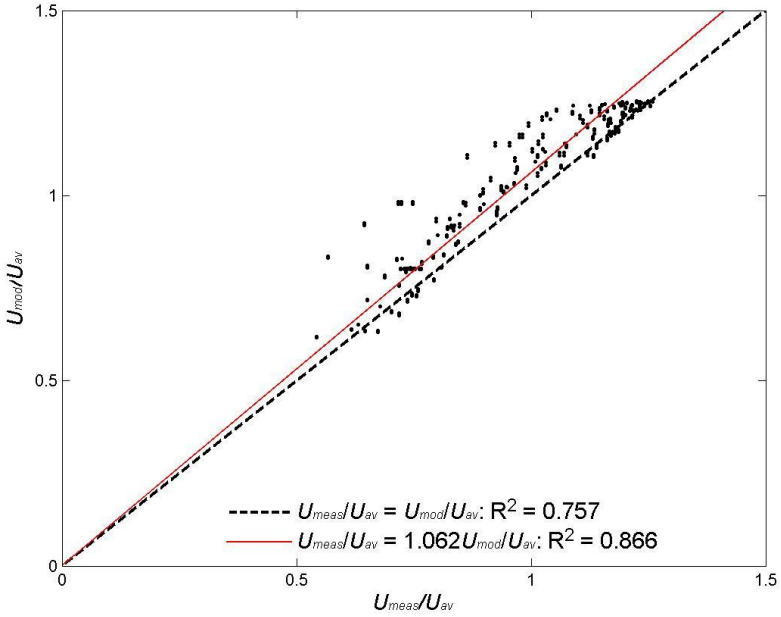

Figure 29: Normalized velocity predicted by the CFD model vs normalized measured velocity for Test 5

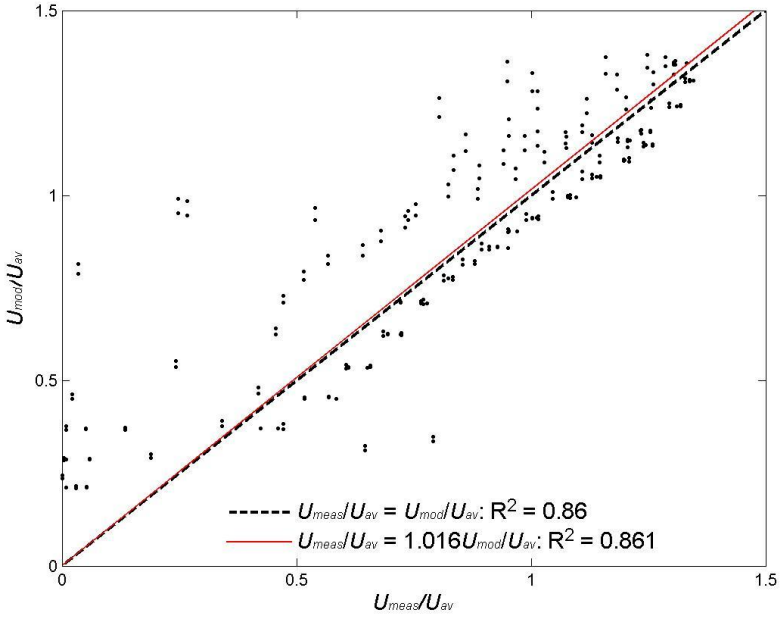

Figure 30: Normalized velocity predicted by the CFD model vs normalized measured velocity for Test 6

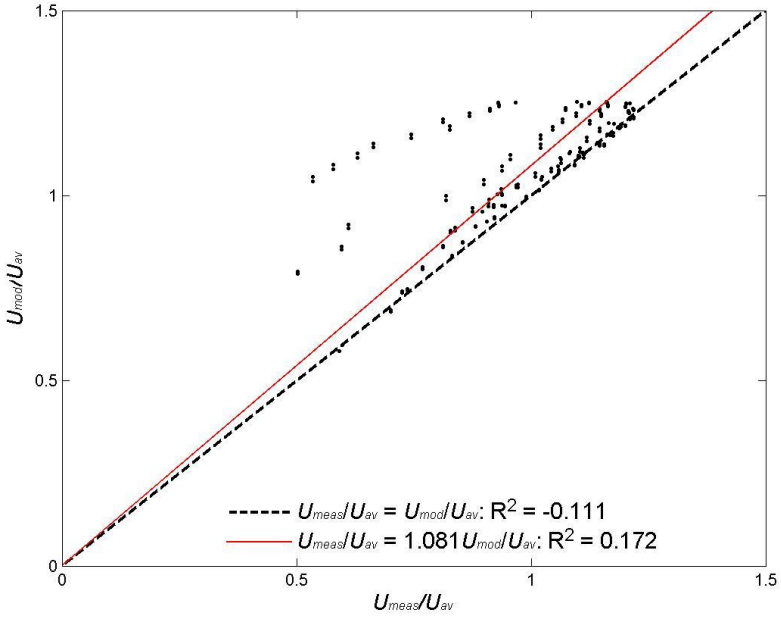

Figure 31: Normalized velocity predicted by the CFD model vs normalized measured velocity for Test 10

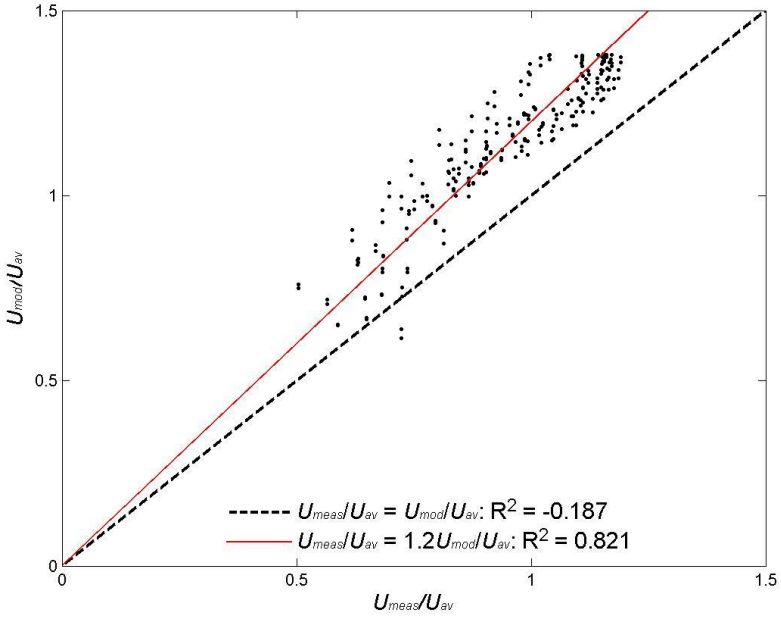

Figure 32: Normalized velocity predicted by the CFD model vs normalized measured velocity for Test 13

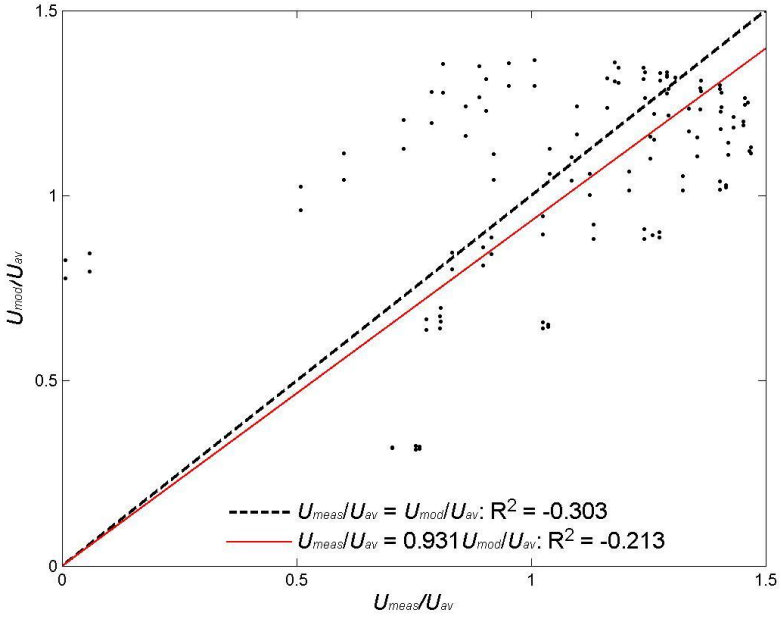

Figure 33: Normalized velocity predicted by the CFD model vs normalized measured velocity for Test 16

It can be seen that the general trend is close to a 1:1 slope ranging from 0.966 to 1.200 for tests without gravel infill, and 0.931 to 1.085 for tests with gravel infill. These results are summarized in Table 9 and Table 10, showing that the CFD model performs best for the test conditions to which it was calibrated in, tests 1-6, as expected. This can be seen from the R^2 value for the 1:1 and best fit lines. One of the objectives of this research was to determine whether a CFD model could be used in a predictive manner once calibrated to a physical model. Test conditions 7-17 were analyzed to determine how well the model was able to perform under predictive conditions. Looking at the 1:1 slope and R^2 values for tests 9-15, it would appear that the CFD model did not work well. However, the R^2 values significantly improve for the best fit line, showing that in general the scatter within the proportionality plots is relatively low. This is particularly true for tests 12-15, while tests 9-11 do not improve as much.

Table 9: CFD proportionality plot summary for tests without gravel infill

Test	1:1 R^2	Best Fit Slope	Best Fit R^2
Test 1	0.773	0.966	0.817
Test 2	0.699	0.989	0.705
Test 3	0.777	1.036	0.833
Test 4	0.854	1.022	0.862
Test 5	0.757	1.062	0.866
Test 9	-0.325	1.061	-0.070
Test 10	-0.111	1.081	0.172
Test 11	0.209	1.080	0.393
Test 12	0.651	1.031	0.684
Test 13	-0.187	1.200	0.821
Test 14	0.207	1.144	0.782
Test 15	0.456	1.083	0.513

However, for the rock infill tests none of the models, outside of the calibrated test condition, performed well. All other test conditions showed large amounts of scatter about the line of best fit. This is demonstrated by the negative to low R^2 values obtained from these models.

Table 10: CFD proportionality plot summary for tests with gravel infill

Test	1:1 R^2	Best Fit Slope	Best Fit R^2
Test 6	0.860	1.016	0.861
Test 7	-1.215	1.085	-1.164
Test 8	-1.069	1.050	-1.040
Test 16	-0.303	0.931	-0.213
Test 17	0.190	0.914	0.260

These results were expected based on visual inspection of the CFD two-dimensional velocity profiles. As an additional means of objectively assessing the CFD results, a two-dimensional plot of the percent difference between the predicted and measured streamwise velocities was produced for each test. The percent differences were calculated in a manner similar to that used when comparing U_{av} to U_{meas} (section 4.2.1), with U_{av} being replaced by U_{mod}. This provided a method to determine where the largest errors occurred within the CFD model, while also determining the percentage of the flow area that was modeled well. These results can be seen in Figure 34 to 39 for the same representative test conditions and are summarized in Table 11 and Table 12.

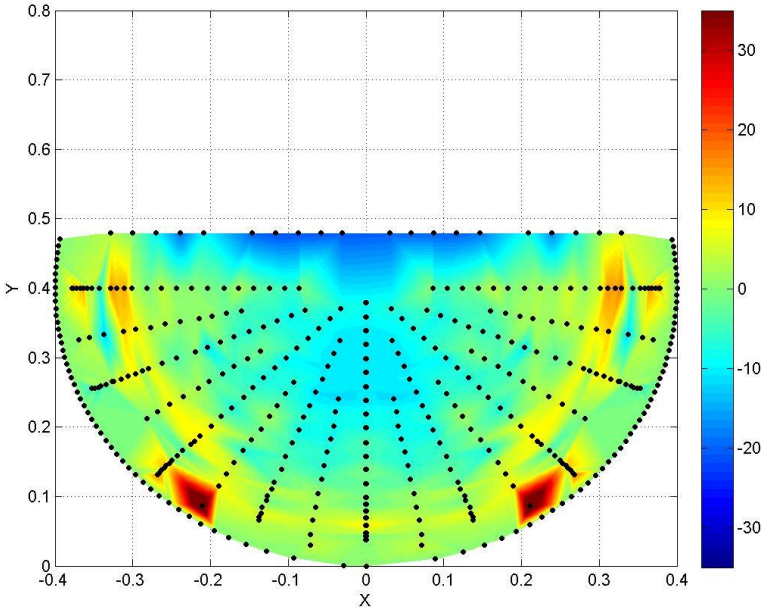

Figure 34: CFD percent difference two-dimensional distribution for Test 1 (%)

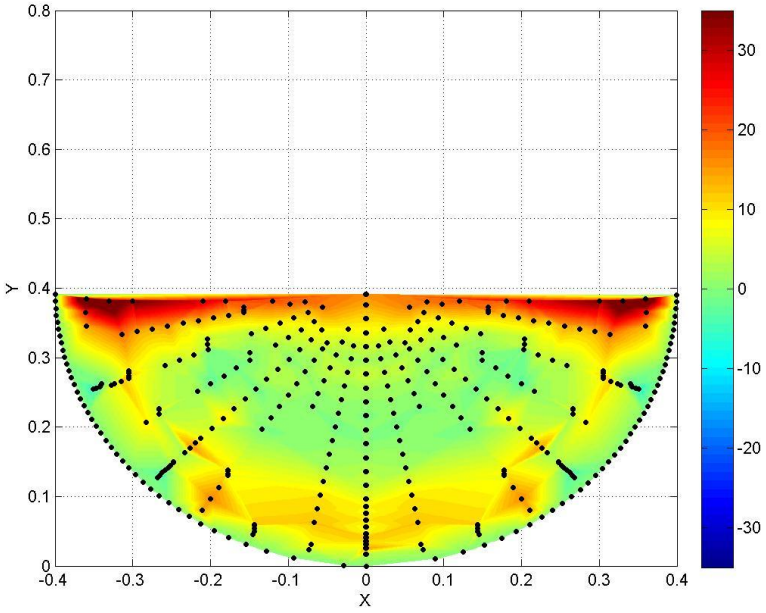

Figure 35: CFD percent difference two-dimensional distribution for Test 5 (%)

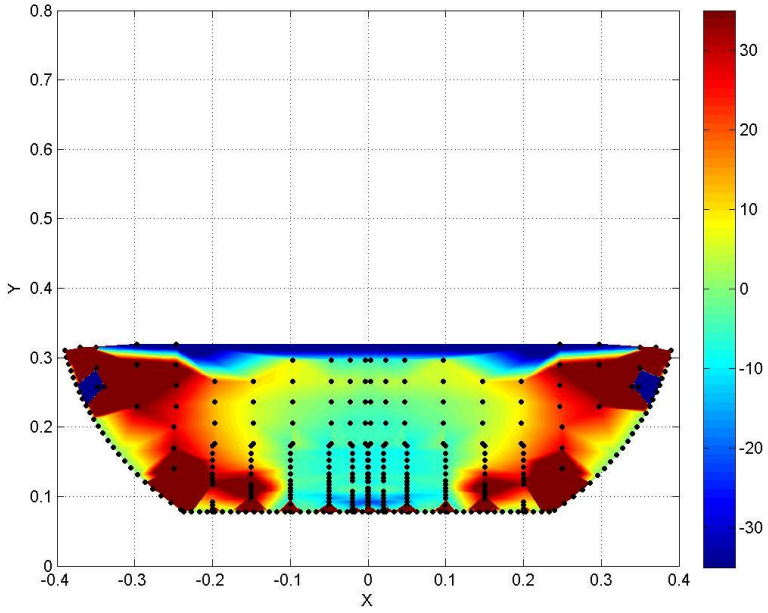

Figure 36: CFD percent difference two-dimensional distribution for Test 6 (%)

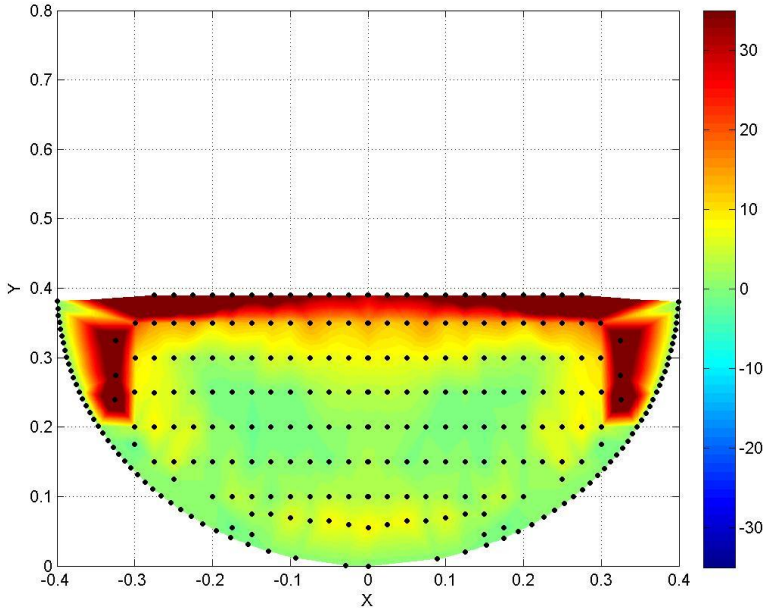

Figure 37: CFD percent difference two-dimensional distribution for Test 10 (%)

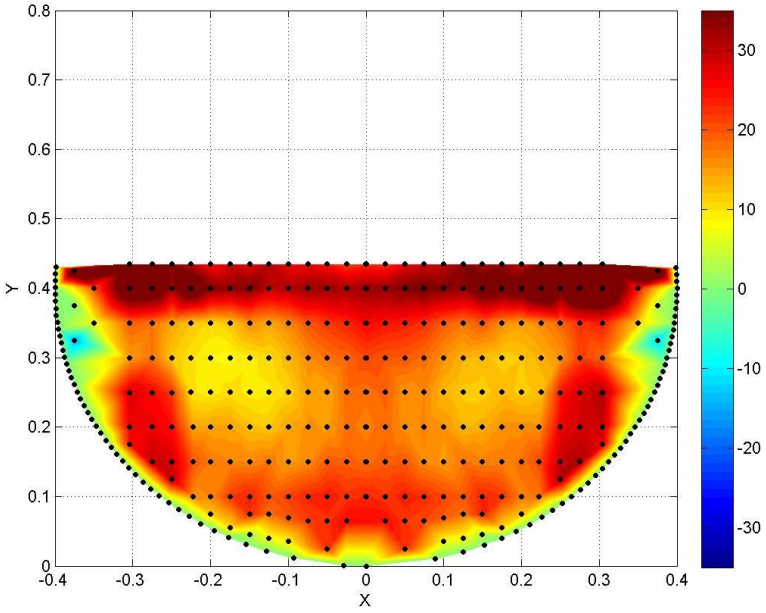

Figure 38: CFD percent difference two-dimensional distribution for Test 13 (%)

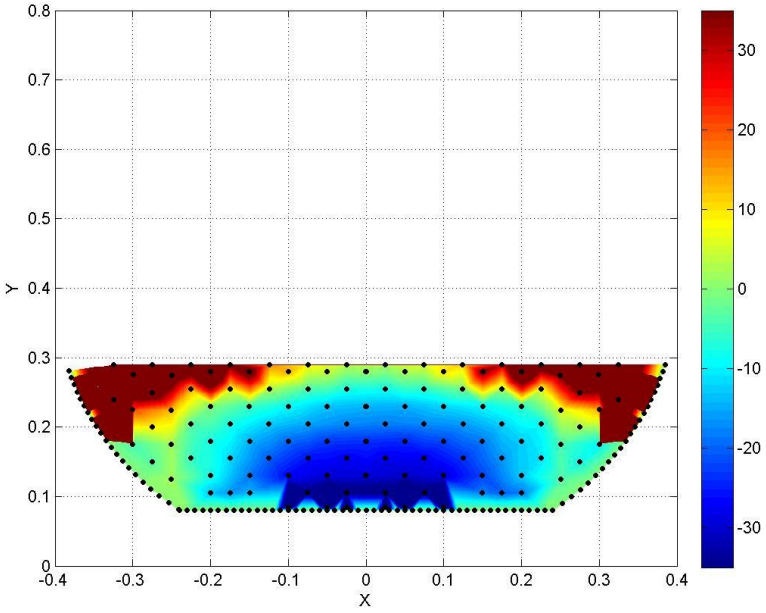

Figure 39: CFD percent difference two-dimensional distribution for Test 16 (%)

The plots demonstrate that the largest errors occur along the water surface and in sharp corners, either between the water-wall or wall-gravel regions. These areas have the most complex secondary circulations within the flow field. This is particularly true for tests with gravel infill where four circulation zones would be expected, thereby adding to the complexity of their secondary circulations over tests without gravel infill. These plots illustrate that the models do in fact, perform better than they had appeared to earlier when strictly using the R^2 values. Data from these plots were extracted to determine the percentage of the cross-sectional flow area (%A) where the predicted velocity (U_{mod}) is within ±β of the measured velocity. The model still generally performs the best for test conditions 1-5, as expected from calibration. When comparing the CFD modeled velocities for tests with and without gravel infill, there is still a definite improvement over using the average velocity to predict the flow field (see Tables 7 and 8). This is due to the streamwise velocity gradient from the culvert wall giving a better representation than using the average velocity to predict the entire flow field. There is a significant increase in all percent area groups, where approximately 25% of the flow area is modeled more accurately than using the bulk average velocity for tests without gravel infill.

Table 11: Percentage of the cross-sectional flow area (%A) where the predicted velocity (*Umod*) is within ±β of the measured velocity for tests without gravel infill

Test	%A β = ±5%	%A β = ±10%	%A β = ±15%	%A β = ±20%
Test 1	55.1	85.3	95.2	98.5
Test 2	53.4	84.3	96.3	98.4
Test 3	55.8	87.8	94.2	97.1
Test 4	54.1	75.4	83.7	86.6
Test 5	48.9	76.9	90.5	95.2
Test 9	57.6	82.4	89.3	92.2
Test 10	54.7	72.0	78.0	80.2
Test 11	26.4	50.9	67.4	75.8
Test 12	59.1	73.7	83.0	88.7
Test 13	5.6	12.5	31.4	60.2
Test 14	6.2	34.3	61.9	78.4
Test 15	9.1	25.8	52.1	66.5
Average	40.5	63.4	76.9	84.8

There is little difference between test conditions when comparing the percentage of the cross-sectional flow area where the predicted velocity is within ±β of the measured velocity, even considering that the proportionality plot suggested test 6 was significantly better than the four remaining tests for tests with gravel infill. This suggests that the bulk area of the flow is modeled accurately for all test conditions, while the corners and surface within these models are likely not well modeled for test conditions 7, 8, 16, and 17. There is still an improvement over using the bulk average velocity; however, it is not as significant as for the test conditions without gravel infill. This improvement ranges from 13 to 21.2% of the flow area for tests with gravel infill, which is still a significant portion of the cross-sectional flow area.

Table 12: Percentage of the cross-sectional flow area (%A) where the predicted velocity (*Umod*) is within ±β of the measured velocity for tests with gravel infill

Test	%A β = ±5%	%A β = ±10%	%A β = ±15%	%A β = ±20%
Test 6	25.4	46.0	54.5	61.7
Test 7	27.9	44.3	52.3	57.8
Test 8	24.1	43.2	54.1	59.9
Test 16	19.8	35.6	49.8	61.7
Test 17	22.8	43.8	69.5	76.4
Average	24.0	42.5	56.1	63.5

4.4 Empirical Model Distributions

Through visual inspection along with detailed analysis of the velocity profiles for the physical and CFD models it was concluded that it would be beneficial to also compare the empirical equation from Clark and Kehler (2011) for predicting the two-dimensional velocity distribution within the fully developed region. These distributions were developed in a similar manner to those used by Kehler (2009) using an in-house MatLab script. It is important to note that only tests without gravel infill can be compared due to the limitations of the empirical equation. Figure 40 to 43 show the cross-sectional plots of the streamwise velocities predicted by the empirical equation (U_{ck}) for tests 1, 5, 10, and 13, respectively.

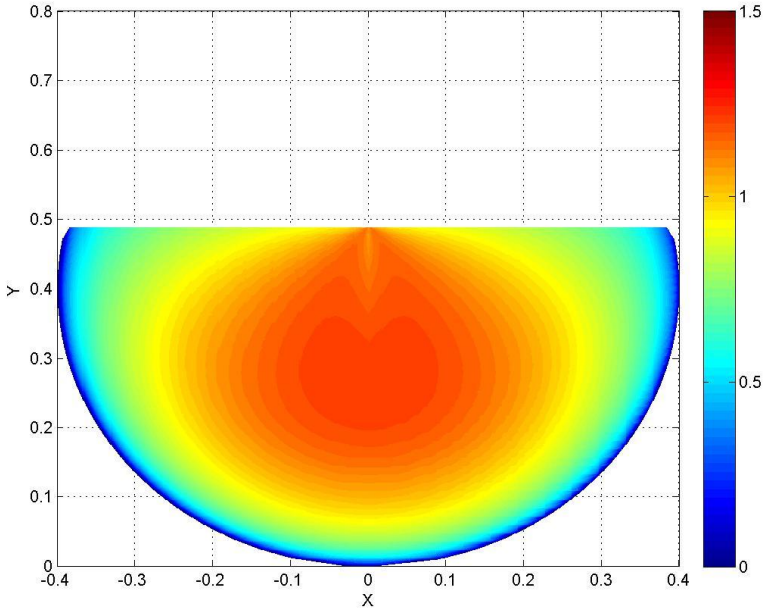

Figure 40: Test 1 - Empirical normalized velocity (U_{ck}/U_{av})

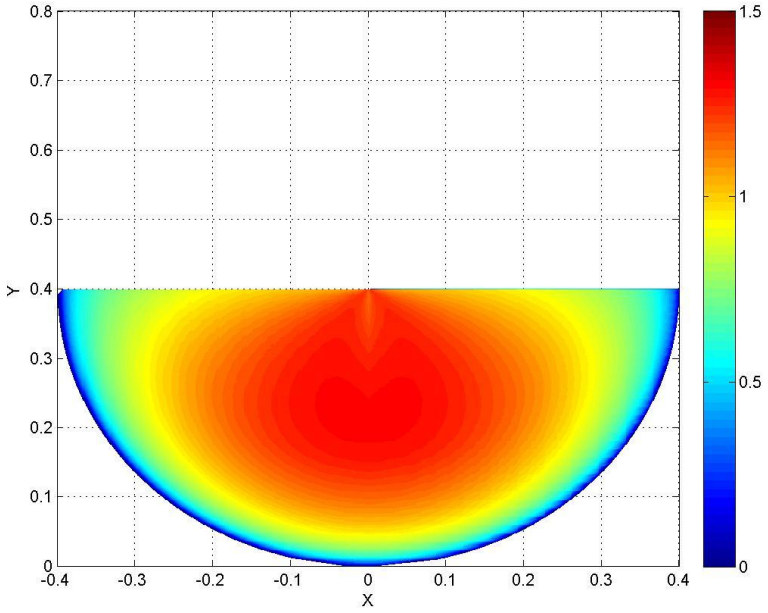

Figure 41: Test 5 - Empirical normalized velocity (U_{ck}/U_{av})

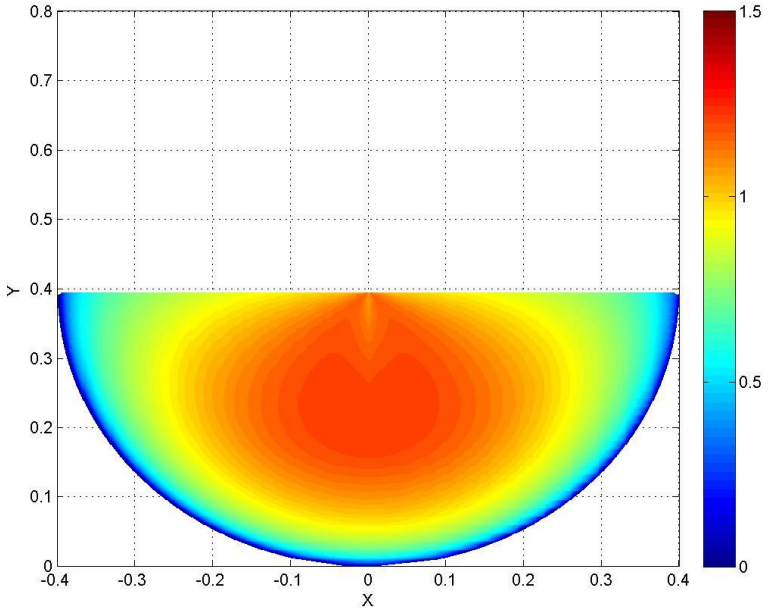

Figure 42: Test 10 - Empirical normalized velocity (U_{ck}/U_{av})

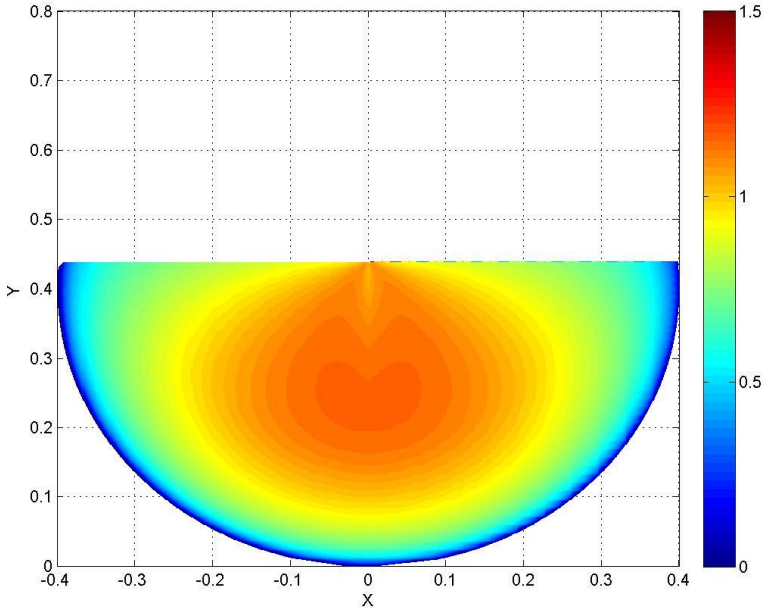

Figure 43: Test 13 - Empirical normalized velocity (U_{ck}/U_{av})

Since this empirical model was developed using the conditions for tests 1-5 it would be expected that they would produce strong correlations. These equations were able to provide a reasonable prediction of the two-dimensional velocity distribution within the fully developed region. The empirical equations velocity distributions do a good job predicting that the maximum velocity is depressed below the water surface, as well as a significant percent of the overall flow area is less than the average velocity for each test condition.

4.4.1 Empirical Equations to Physical Model Comparison

The empirical equation results were analysed in the same manner used for the CFD model, where U_{ck} represents the streamwise velocity predicted by the empirical equations from Clark and Kehler (2011). By first presenting the proportionality plots, the summary from these plots, then progressing into the percent difference plots and similarly the summary table for these figures as well.

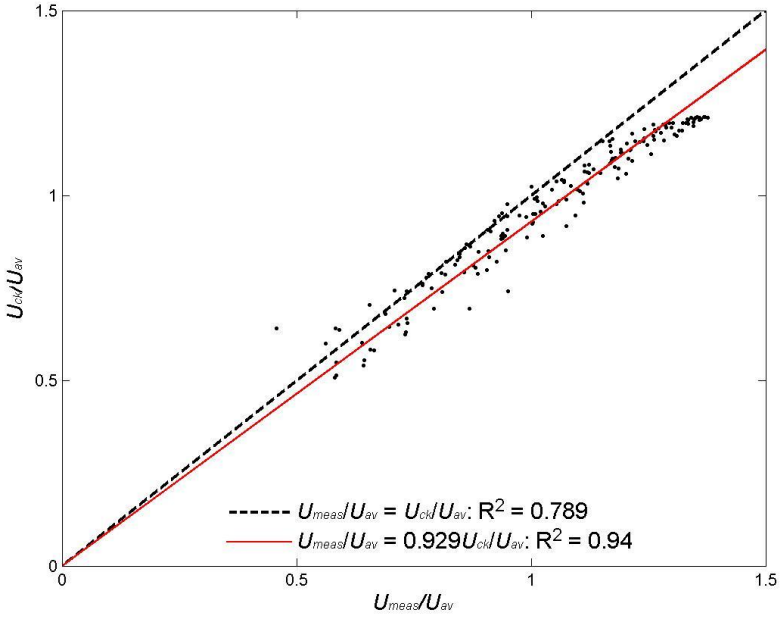

Figure 44: Empirical equation normalized predicted velocity vs normalized measured velocity for Test 1

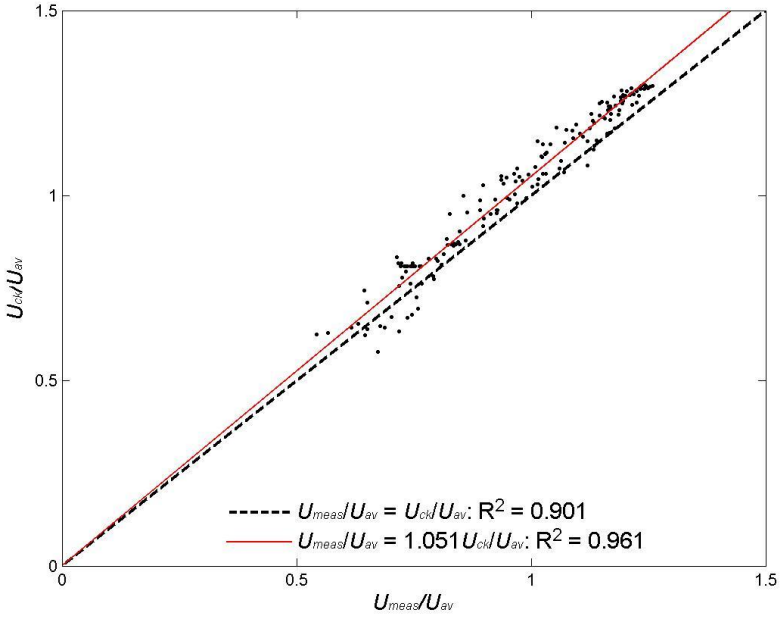

Figure 45: Empirical equation normalized predicted velocity vs normalized measured velocity for Test 5

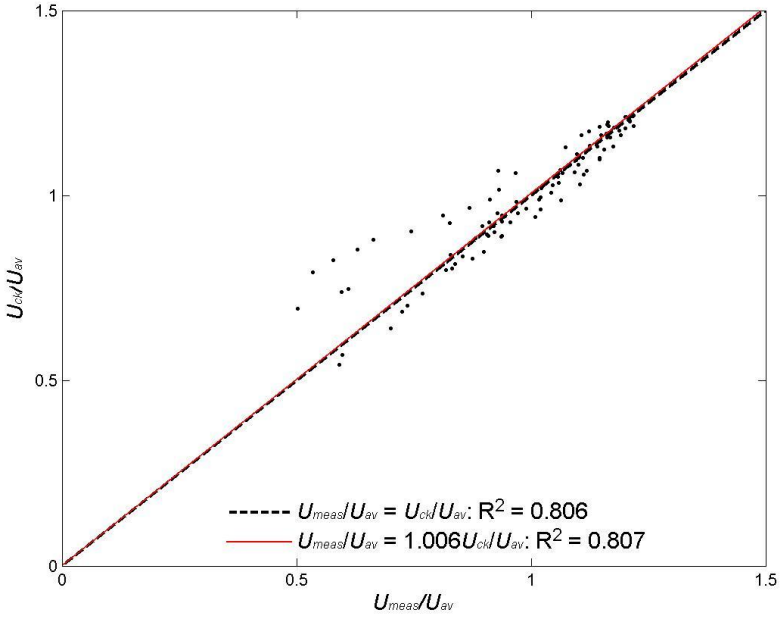

Figure 46: Empirical equation normalized predicted velocity vs normalized measured velocity for Test 10

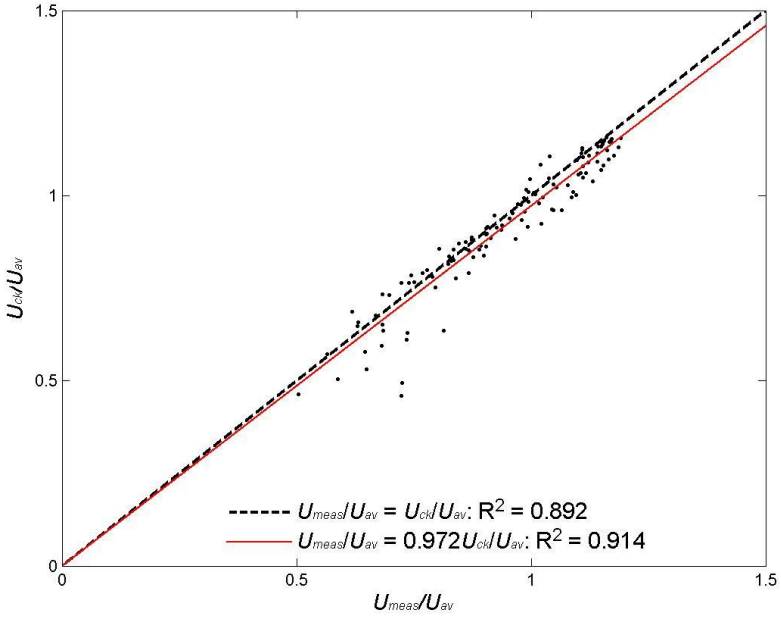

Figure 47: Empirical equation normalized predicted velocity vs normalized measured velocity for Test 13

The proportionality plots demonstrate that the empirical equation performs well over the entire range of the test conditions. The best fit line slope ranged from 0.883 to 1.105 with R^2 values ranging from 0.550 to 0.971 (seen in Table 13), showing that the model does a relatively good job of predicting the velocity field within the fully developed region.

Table 13: Empirical equation proportionality plot summary for tests without gravel infill

Test	1:1 R^2	Best Fit Slope	Best Fit R^2
Test 1	0.789	0.929	0.940
Test 2	0.967	1.012	0.971
Test 3	0.904	1.050	0.971
Test 4	0.938	1.013	0.943
Test 5	0.901	1.051	0.961
Test 9	0.374	0.917	0.682
Test 10	0.806	1.006	0.807
Test 11	0.866	1.003	0.866
Test 12	0.122	0.883	0.775
Test 13	0.892	0.972	0.914
Test 14	0.140	1.105	0.550
Test 15	0.855	1.004	0.856

The empirical equations were also compared using the percent difference plots where U_{ck} was used instead of U_{av}. It was expected that a larger percent of the area would be within the bounds set due to the fact that the R^2 values were comparatively higher than the CFD models results, combined with slopes closer to 1:1.

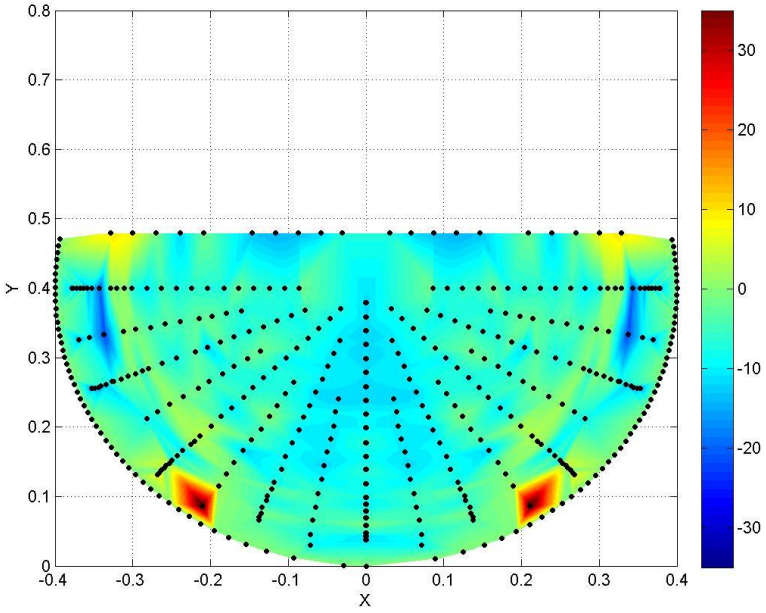

Figure 48: Empirical equation percent difference two-dimensional distribution for Test 1 (%)

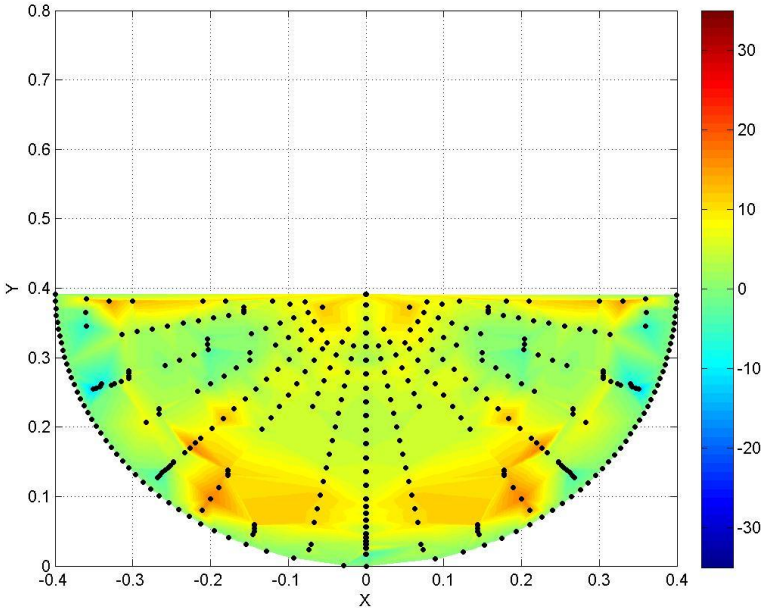

Figure 49: Empirical equation percent difference two-dimensional distribution for Test 5 (%)

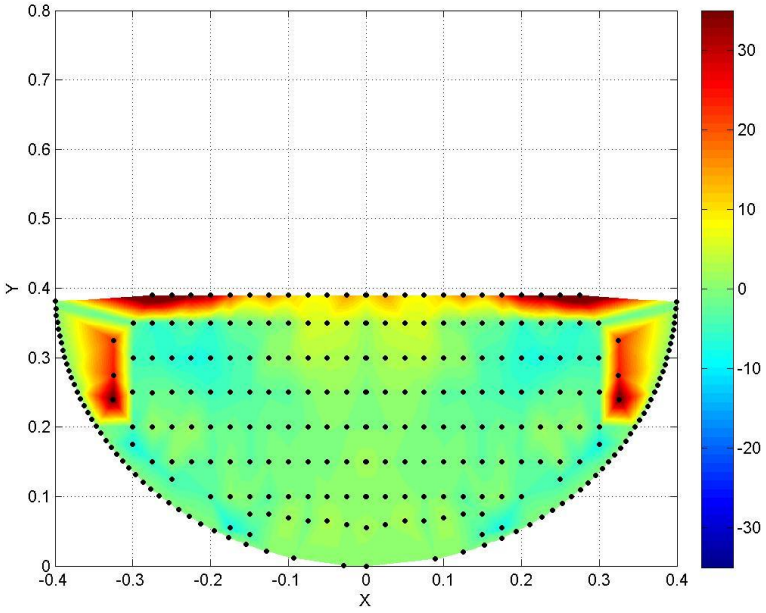

Figure 50: Empirical Equation percent difference two-dimensional distribution for Test 10 (%)

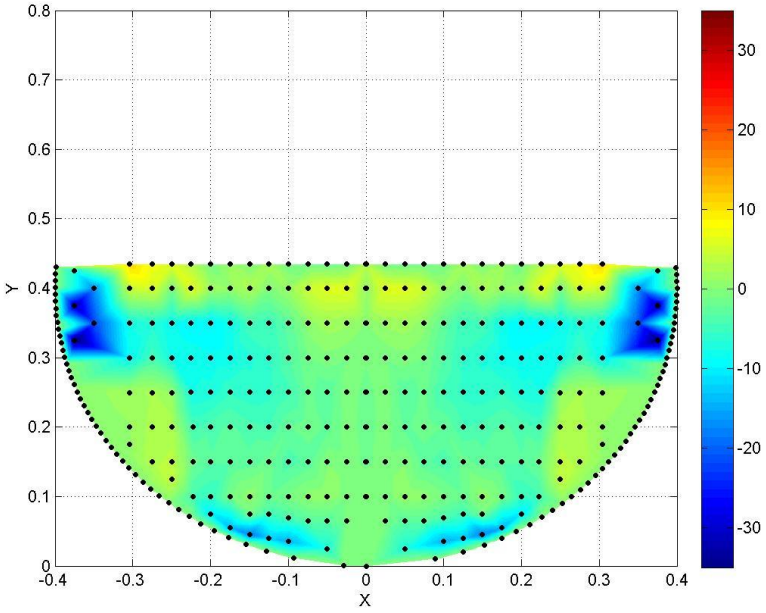

Figure 51: Empirical Equation percent difference two-dimensional distribution for Test 13 (%)

Table 14: Percentage of the cross-sectional flow area (%A) where the predicted velocity (*Uck*) is within ±β of the measured velocity for tests without gravel infill

Test	%A β = ±5%	%A β = ±10%	%A β = ±15%	%A β = ±20%
Test 1	37.6	86.2	98.2	99.2
Test 2	95.7	99.6	100.0	100.0
Test 3	53.4	96.2	99.8	100.0
Test 4	69.0	80.7	82.5	83.3
Test 5	49.1	87.5	99.5	100.0
Test 9	29.5	65.0	83.0	91.9
Test 10	73.6	84.9	87.1	88.3
Test 11	52.1	81.1	90.6	91.4
Test 12	19.6	36.2	82.9	96.5
Test 13	70.5	93.2	96.6	98.1
Test 14	35.7	57.7	72.5	82.2
Test 15	65.8	82.8	88.0	89.7
Average	54.3	79.3	90.1	93.4

Generally, the model performed well. This was shown by the increase in the higher percent areas for each β value, suggesting that the empirical equation did not only perform better when looking at the R^2 value, but also that a larger percentage of the flow area was modeled more accurately. These results show that for the test conditions used here, on average, 79.3% of the flow cross-sectional area was predicted within an accuracy of ±10%, and 93.4% of the cross-sectional area was predicted with an accuracy of ±20%.

4.5 Simplified Cumulative Percent Area Method

As previously mentioned, current fish passage regulations are based on describing the complex flow conditions within a culvert using a single average velocity. The results thus far demonstrate that a CFD model can provide a better estimate of streamwise water

velocities in a culvert, yet this comes with a considerable investment of finances and time. The empirical equations of Clark and Kehler (2011) were found to be a reasonable representation of the streamwise water velocities in a CSP culvert. Although this method can be programmed without the use of expensive software, there is still an investment of time that is required.

It was decided to use the empirical equation to try to develop an even more basic means of assessing the flow conditions in a CSP culvert within the fully developed region. Specifically, a simple method to predict the percentage of the cross-sectional flow area with a velocity less than U_{av} may be beneficial to culvert designers and regulators. This type of tool would allow designers to quickly say, for example, that 55% of the flow area has a velocity less than U_{av}.

Additionally, since physical measurement values of U/U_{av} did not range below 0.5 and the flow along the boundary would be expected to follow the law of the wall, where velocity does not vary linearly, it was decided that the empirical equations provided a more appropriate comparison method. The empirical equation also provided more flexibility in terms of being able to develop a much finer mesh to extract data from, avoiding interpolation errors. Streamwise velocity data was extracted for all test conditions without gravel infill, on an interval size of 0.05 U/U_{av}. The cumulative area was then averaged over all test conditions at these intervals to develop a relationship. These average values are shown below in Figure 52. The fitted lines are given by

equation 4.2. The utility of this plot can be demonstrated using the following example. A culvert designer can quickly find the $U/U_{av} = 1$ ordinate, move vertically to the fitted line, and then horizontally to the vertical axis to see that this corresponds to approximately 55% of the area. Similarly, 25% of the flow area will have a velocity less than or equal to $U/U_{av} = 0.8$.

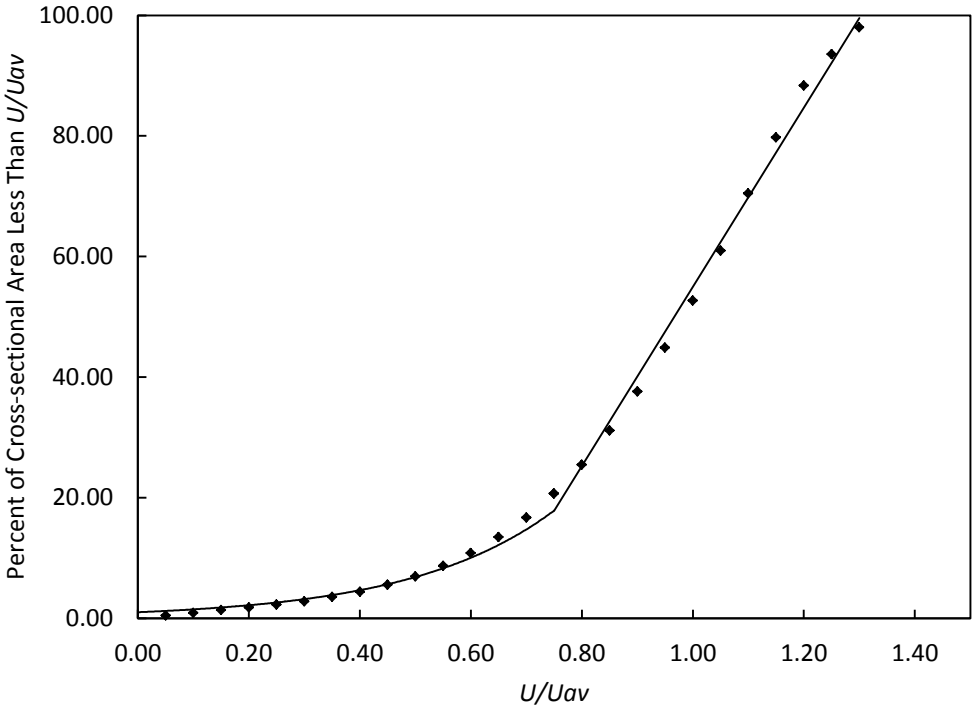

Figure 52: Development of cumulative percent cross-sectional area less than U/Uav vs U/Uav relationship within the fully developed region

$$Cumulative\ \%A = \begin{matrix} 148.58\left(\frac{U}{Uav}\right) - 93.62 & for\ \frac{U}{Uav} > 0.75 \\ e^{3.84U/Uav} & for\ \frac{U}{Uav} \leq 0.75 \end{matrix} \qquad [4.2]$$

Equation 4.2 provided excellent results for the averaged data. An R^2 value of 0.997 and root mean squared error (RMSE) of 3.844 were achieved when compared to the measured velocity profiles. This relationship was then applied to each individual test

condition for the measured velocity profiles. The developed relationship performed extremely well over all individual test conditions and is shown in Table 15.

Equations 2.10, 2.11 and 2.12 were also used to determine if the House et al. (2005) developed equation, for predicting the cumulative percent area less than some threshold velocity within a streambed simulation culvert, also applied to CSP culverts. House et al. (2005) developed relationship also performed well; however, an averaged data set could not be compared since the β_1 function in equation 2.8 makes this method test specific. Equation 4.2 was found to perform better by comparing the average R^2 and RMSE values for tests 1-15, with the RMSE being approximately half that of the House et al. (2005) equations. Additionally, it is important to note that when the House et al. (2005) relationship was applied to the measured data, the model only predicted that approximately 85% of the flow area was less than U/Uav = 1.50, showing a large discrepancy at the upper limit.

Table 15: Developed relationships performance

	Developed Relationship		**House et al. (2005)**	
Test	**R^2**	**RMSE**	**R^2**	**RMSE**
Averaged Data	0.997	3.844	-	-
Test 1	0.993	5.518	0.977	12.123
Test 2	0.976	9.824	0.972	8.482
Test 3	0.996	3.488	0.953	13.687
Test 4	0.989	6.902	0.990	7.192
Test 5	0.997	3.759	0.994	8.212
Test 9	0.991	5.398	0.977	12.514
Test 10	0.994	5.723	0.989	10.038
Test 11	0.991	6.497	0.987	11.129
Test 12	0.991	6.160	0.989	7.720
Test 13	0.996	4.676	0.994	9.651
Test 14	0.993	6.411	0.992	10.850
Test 15	0.994	5.157	0.984	11.337
Average	0.992	5.793	0.983	10.245

Since equation 4.2 was able to perform well under a broad range of tests (experimental data ranged from h/D = 0.271-0.543), the relationship was then applied to a series of h/D values that ranged between 0.20 and 0.80 on an increment of 0.05 for a single slope. The relationship was only applied for one slope because upon closer inspection of the empirical equations the predicted normalized velocity is not a function of slope. Considering the empirical equations (equations 2.13 and 2.14) and substituting in the relationships for U^+, t^+, T^+, and U_{*dp} as defined in Chapter 2 and using the relationship $\ln(A) - \ln(B) = \ln(\frac{A}{B})$, the empirical equations then become:

$$U = \sqrt{gRS}\left[1.1 - 1.39\left(\frac{d_p}{p}\right)^2\right]\left[\ln\left(\frac{t\left(1.1-1.39\left(\frac{d_p}{p}\right)^2\right)}{k_s}\right) + A_o\right] \quad for\ t < 0.36T \qquad [4.3]$$

$$U = \sqrt{gRS}\left[1.1 - 1.39\left(\frac{d_p}{p}\right)^2\right]\left[\ln\left(\frac{t\left(1.1-1.39\left(\frac{d_p}{p}\right)^2\right)}{k_s}\right) + A_o\right] -$$

$$\sqrt{gRS}\left(1 - \frac{2d_p}{P}\right)\left[\frac{t-0.36T}{0.64T}\right] \quad for\ t \geq 0.36T \qquad [4.4]$$

The predicted velocity is then a function of $\sqrt{S}$. Noting that Manning's equation is used to predict the average velocity it can be seen that U_{av} is also a function of $\sqrt{S}$. Therefore, by normalizing the predicted velocity by the average velocity, the normalized predicted velocity profile will not be a function of the slope.

It has been demonstrated that the model performs well over all test conditions, with a minimum R^2 value of 0.991, and maximum RMSE of 6.970 as seen in Table 16. Additionally, it can be seen that the developed relationship performs best over the mid-range of the theoretical tests due to the majority of the physical model tests and empirical equations being calibrated within this range.

Table 16: Theoretical tests for cumulative percent area with a velocity less than U/U_{av} comparison between equations 2.13 & 2.14 and equation 4.2

h/d	R^2	RMSE
0.20	0.994	5.368
0.25	0.995	4.731
0.30	0.996	3.980
0.35	0.997	3.611
0.40	0.997	3.289
0.45	0.998	2.486
0.50	0.998	2.225
0.55	0.998	2.382
0.60	0.998	2.742
0.65	0.997	3.363
0.70	0.996	4.348
0.75	0.994	5.543
0.80	0.991	6.970
Avg	0.999	2.049

Chapter 5: Conclusions and Future Work

5.1 Summary

Current legislation requires that an efficient fishway shall be provided where it is necessary for the public's best interest (R.S.C., 1985, c. F-14). The current guidelines for culvert fishways require that the average velocity be below 1 m/s for culverts shorter than 25 m or 0.8 m/s for culverts longer than 25 m, and potentially lower if the prolonged swimming speed of the local fish species is below these thresholds. These guidelines are set to ensure that fish are able to navigate the full length of the culvert. In essence this means that a single average velocity calculated from a design discharge is used to describe the complex flow conditions within a partially filled culvert.

However, research has indicated that these regulations may be overly conservative. This is because the average velocity does not provide an accurate representation of the velocity field within the fully developed region. A significant portion of the velocity field within the fully developed region has been observed to be below the average velocity. Fish will likely use these areas, as opposed to swimming against water that is flowing faster than the average velocity. Physical models have also shown that the maximum velocity within the fully developed region is suppressed from the water surface. This feature has been attributed to secondary circulations that have been observed from measurements. Additionally, research has been completed on the inlet region where it

was found that the flow structure two diameters downstream from the inlet is similar for all inlet configurations.

Although physical modeling is important to determine new flow characteristics, it can be beneficial to model flow using CFD, since it can potentially cut costs while in the design phase of any project. There has been a multitude of CFD models that have been applied and verified for different applications. However, there has been little research that has combined CFD modeling and culvert hydraulics, which lead to the current research plan to be carried out.

The current research consisted of completing physical tests at low slopes that ranged between 0.028% and 0.468%, typical to Manitoba's low surface gradients, with a 21 m long, 0.8 m diameter CSP culvert. The tests were completed with and without gravel infill to determine the velocity distributions that are expected within a CSP culvert. A CFD model was then calibrated to six tests and verified against an additional eleven test conditions. The test conditions without gravel infill were then tested against the empirical equations developed by Clark and Kehler (2011). These results were then used to determine if there is a relationship between the cumulative percent area less than some threshold velocity.

5.2 Conclusions

Several key attributes were further confirmed for open channel flow through culverts by acquiring physically measured profiles within the fully developed region for tests with and without gravel infill. One such attribute demonstrated that the maximum velocity is suppressed from the surface due to secondary circulations, and is forced toward the water surface as the water depth is decreased. Also, a significant portion of the flow field was observed to be below the average velocity for all test conditions. These characteristics were determined to be the most important to model when using CFD.

The current method, U_{av}, of predicting the flow conditions within a culvert is to calculate the average velocity. This method is overly simplistic when modeling the velocity distribution within the fully developed region. Physical model results have shown that a velocity gradient exists near the rough culvert walls, and that complex velocity distributions occur within a partially-filled CSP culvert. When comparing the predicted average velocity to the physical model results, on average, only 32% of the cross-sectional flow area was predicted with an accuracy of ±10%, and only 64% of the area was predicted with an accuracy of ±20%. This demonstrates that using the average velocity provides a poor prediction of the streamwise velocity distribution in a CSP culvert.

On average, the current prediction method only predicts 23% of the flow cross-sectional area with an accuracy of ±10%, and only 50% of the flow area was predicted with an

accuracy of ±20% for test conditions with gravel infill. These percent differences indicate that using the average velocity to predict the flow field performs slightly better for test conditions without gravel infill than tests with gravel. This is likely due to the added complexities of the secondary circulations attributed to compound channel roughness and sharp corners that are seen in tests with gravel infill.

The developed CFD model performed relatively well predicting the velocity profile within the fully developed region for tests that were deeper than 0.398 m. The model was able to predict the secondary circulations in the expected direction for these test conditions, which in result facilitated the maximum velocity to be slightly suppressed from the water surface. Additionally, the CFD model provided a better representation of the velocity gradient that occurred near the CSP culvert wall than the average velocity does when compared against the physically measured velocity distributions. However, the model failed to accurately predict flows in shallow tests and tests with gravel infill. This was likely due to the complexities of secondary circulation cells that are observed within similar geometry to these test conditions.

Centreline profiles were also extracted along the length of the CFD culvert model. From these profiles it was found that the model was able to predict a developing region, where there was significant change in the centreline velocity profile, between 0 and 15 diameters downstream of the culvert inlet. This compared well with the physically measured developing region, which was found to range between 5.95 and 12.11

diameters downstream of the culvert inlet (Kehler, 2009). The centreline velocity profile then becomes more stable after 15 diameters downstream and maintains a similar shape and velocity up to 25 diameters downstream.

When the CFD model was compared against the measured data, all test conditions had a slope close to 1:1 when plotted against each other. However, the model performed best for tests conditions 1-6. On average, 63% of the cross-sectional flow area was predicted with an accuracy of ±10%, and 85% of the flow area was predicted with an accuracy of ±20% for test conditions without gravel infill. The model performed poorest for test conditions with gravel infill that the model was not calibrated to (7, 8, 16, and 17) when comparing the R^2 value. However, the percent difference values showed, on average, 24% of the cross-sectional flow area was predicted with an accuracy of ±10% and 64% of the flow area was predicted with an accuracy of ±20% which was consistent over all tests with gravel infill. The percent difference plots also indicated that the model performed significantly better for tests without gravel infill. Even though the model did not always perform exceptionally well, the percent difference plots show a significant improvement on the current method of predicting the velocity field, while also providing a means of approximating flow conditions in the developing region.

The empirical equations developed by Clark and Kehler (2011) performed well for the test conditions without gravel infill. The empirical equations provided an accurate representation of the flow field within the fully developed region with the maximum

velocity suppressed from the water surface, and a large percent of the flow field below the average velocity. Comparing the empirical equation to the measured data, on average, 79% of the flow area is predicted with an accuracy of ±10%, and 93% of the flow area is predicted with an accuracy of ±20%. These results along with the proportionality plots indicate that there was a significant improvement using these equations over the CFD model.

The empirical equations were then used to develop a relationship for the cumulative percent area below some threshold velocity (Y_v). Equation 4.2 was able to predict the cumulative percent area below some threshold velocity for all of the physically measured tests with an R^2 = 0.997 and an RMSE of 3.844 for the average test condition, and an average R^2 = 0.992 and RMSE of 5.793 when applied to individual tests. House et al. (2005) developed relationship, for streambed simulation culverts, also performed well with an average R^2 = 0.983 and RMSE = 10.245. However, House et al.'s (2005) relationship only predicts approximately 85% of the flow area to be below $U/Uav =$ 1.5, whereas the measured data indicates that 100% of the area was below this point. Therefore, the developed relationship provides a more accurate representation of Y_v for h/D between 0.271 and 0.543 in CSP culverts. The developed relationship also performed well when tested against theoretical tests between h/D = 0.2 and 0.8, with a minimum R^2 = 0.991, and maximum RMSE = 6.970.

Overall, the results indicate that the empirical equation is a much more reliable means of predicting the velocity field within the fully developed region than the CFD model. However, both models do perform better than the current method of using Uav to predict the flow field within CSP culverts and the CFD model provides the added benefit of predicting the flow field within the developing region as well. Additionally, equation 4.2 for the cumulative percent area below some threshold velocity provides a simple and accurate tool that can be used to describe the velocity distribution within CSP culverts in the fully developed region.

5.3 Future Works

Within the project there are several potential areas of research that should be followed in the future to increase the understanding and accuracy of modeling culvert hydraulics. The following list provides an outline of potential topics that should be explored.

1) Additional testing in culverts with gravel infill to determine the effects of secondary circulations under these conditions, and to potentially develop an empirical relationship similar to that of Clark and Kehler (2011) for culverts with gravel infill.
2) Application of a higher order turbulence model than what was available with the commercially available software used within this research. Possible higher order turbulence models include the Reynolds stress model applied by Reece (1977) or the modified k-ϵ turbulence model applied by Naot and Rodi (1982).

3) Physical modeling of gradually varied flow conditions should be explored to determine their effect on the velocity profile. In addition, determine the backwater effects and their benefits to fish passage.

4) Collaboration between hydraulic researchers and fish biology researchers. Although both are important individually, communication should continue to be improved to ensure that the most important portions of the culvert are being explored.

5) Combine the latest findings in hydraulics and biological understanding of fish passage through culverts to develop a field program to select sites for observation of an operating culvert. The program could collect hydraulic data (such as water velocities, gradually varied flow profiles, and operating conditions) and the fish passage success rates (number of fish passed, fish passage attempts, etc.) for all species present.

Works Cited

Abbs, T. J., Kells, J. A., & Katopodis, C. (2007). A Model Study of the Hydraulics Related to Fish Passage Through Backwatered Culverts. *18th Canadian Hydrotechnical Conference - Canadian Society of Civil Engineers*, (pp. 1-13). Winnipeg, Manitoba,.

Behlke, C. E., Kane, D. L., McLean, R. F., & Travis, M. D. (1991). *Fundamentals of Culvert Design for Passage of Weak-Swimming Fish.* Fairbanks, AK, USA: Alaska DOT & PF.

Chanel, P. G., & Doering, J. C. (2008). Assessment of Spillway Modeling Using Computational Fluid Dynamics. *Canadian Journal of Civil Engineering*, 1481-1485.

Chow, V. T. (1959). *Open Channel Hydraulics.* McGraw-Hill College.

Clark, S. P., & Kehler, N. (2011). Turbulent Flow Characteristics in Circular Corrugated Culverts at Mild Slopes. *Journal of Hydraulic Research, 49:5*, 676-684.

Corrugated Steel Pipe Institue. (2007). *Handbook of Steel Drainage & Highway Construction 2nd Canadian Edition.* American Iron and Steel Institute.

Cotel, A. J., Webb, P. W., & Tritico, H. (2006). *Do Brown Trout Choose Locations with Reduced Turbulence?* American Fisheries Society.

Demuren, A. O., & Rodi, W. (1986). Calculation of Flow and Pollutant Dispersion in Meandering Channels. *Journal of Fluid Mechanics, 172*, 63-92.

Department of Fisheries and Oceans. (1996). *Manitoba Stream Crossing Guidelines for the Protection of Fish and Fish Habitat.*

Ead, S. A., Rajaratnam, N., Katopodis, C., & Ade, F. (2000). Turbulent Open-Channel Flow in Circular Corrugated Culverts. *Journal of Hydraulic Engineering*, 750-757.

Flow Science. (2012). Retrieved from www.flow3d.com.

Flow-Science. (2009). *Flow-3D User Manual* (Vol. Version 9.4).

Goring, D. G., & Nikora, V. I. (2002). Despiking Acoustic Doppler Velocimeer. *Journal of Hydraulic Engineering, 128*(1), 117-126.

Hinze, J. O. (1975). *Turbulence.* McGraw Hill.

House, M. R., Pyles, M. R., & White, D. (2005, February). Velocity Distributions in Streambed Simulation Culverts Used for Fish Passage. *Journal of the American Water Resources Association*, 209-217.

Hunt, M. (2012). *Velocity Distributions Near the Inlet of Corrugated Steel Pipe Culverts.* Winnipeg, MB: University of Manitoba.

Kane, D. L., Behlke, C. E., Gieck, R. E., & McLean, R. F. (2000). *Juvenile Fish Passage Through Culverts in Alaska: A Field Study.* Fairbanks, AK: Alaska Department of Transportation & Public Facilities.

Katopodis, C. (1992). *Introduction to Fishway Design.* Department of Fisheries and Oceans Canada.

Kehler, N. J. (2009). *Hydraulic Characteristics of Fully Developed Flow in Circular Culverts.* MSc Thesis, University of Manitoba, Department of Civil Engineering, Winnipeg.

Khan, L. A., Wicklein, E. A., & Teixeira, E. C. (2006). Validation of a Three-Dimensional Computational Fluid Dynamics Model of a Contact Tank. *Journal of Hydraulic Engineering, 132*, 741-746.

Knight, D. W., & Sterling, M. (2000). Boundary Shear in Circular Pipes Running Partially Full. *Journal of Hydraulic Engineering*, 263-275.

Kopeinig, T. (2004). *Numerical Study of Flow Through a Culvert - Investigation on Various Modifications Using a 3D Turbulent Navier-Stokes Code.* Diploma Thesis, Leopold-Franzens-University, Institute of Hydraulic Engineering, Innsbruck, Austria.

Kwak, D., Reynolds, W. C., & Ferziger, J. H. (1975). *Three-dimensional Time-dependent Computation of Turbulent Flow.* NASA NGR-05-020-622 Report No. TF-5.

Leschziner, M. A., & Rodi, W. (1979, October). Calculation of Strongly Curved Open Channel Flow. *Journal of the Hydraulics Division*, 1297-1314.

Magura, C. (2007). Velocity Structure in an Embedded Corrugated Steel Pipe Model. *18th Canadian Hydrotechnical Conference* (pp. 1-10). Winnipeg: Canadian Society of Civil Engineers.

Mangin, S. F. (2010). *Development of an Equation Independent of Manning's Coefficient n for Depth Prediction in Partially-Filled Circular Culverts.* MSc Thesis, Youngstown State University, Department of Civil and Environmental Engineering.

McEnroe, B. M., & Malone, T. (2008). *Hydraulic Resistance of Small-Diameter Helically Corrugated Metal Pipe.* Univserity of Kansas, Department of Civil, Environmental and Architectural Engineering. Kansas Department of Transportation.

McGraw-Hill Companies, Inc. (2002). *McGraw-Hill Concise Encyclopedia of Physics.* New York: McGraw-Hill Companies, Inc.

Motayed, A. K., & Krishnamurthy, M. (1980). Composite Roughness of Natural Channels. *J. Hyd. Div.*, 1111-16.

Naot, D., & Rodi, W. (1982, August). Calculation of Secondary Currents in Channel Flow. *Journal of the Hydraulics Division*, 948-968.

Neill, C. R. (2001). *Guide to Bridge Hydraulics.* Transportations Association of Canada.

Nezu, I., & Nakagawa, H. (1993). *Turbulence in Open-Channel Flows.* A. A. Balkema.

Nikuradse, J. (1932). Similarity for turbulent flow in smooth pipes. *VDI-Forschungsheft*(No. 356).

Reece, G. J. (1977). *A Generalized Reynolds-stress Model of Turbulence.* MSc Thesis, University of London, Faculty of Engineering.

Rouse, H. (1946). *Elementary Fluid Mechanics.* New York: Wiley.

SonTek. (2001). SonTek ADVField Technical Documentation. San Diego, CA, USA.

Straub, L. G., & Morris, H. M. (1950). *Hydraulic Tests on Corrugated Metal Culvert Pipes.* University of Minnesota.

Sturm, T. W. (2010). *Open Channel Hydraulics, 2nd Edition.* McGraw Hill.

Toews, J. S., Clark, S. P., & Kehler, N. J. (2011). Towards a Better Understanding of Hydraulics in Culverts. *2011 CSCE Annual General Meeting & Conference - 20th Canadian Hydrotechnical Conference*, (pp. HY-19-p1-10). Ottawa.

Williams, G. P. (1970). Manning Formula - A Misnomer? *J. Hyd. Div., ASCE 96, no. HY1*, pp. 193-199.

Yen, B. C. (2001). On Establishing Uniform Channel Flow With Tail Gate. *Water & Maritime Engineering*, 281-283.

Yeung, H. (2001). Modelling of Service Reservoirs. *Journal of Hydroinformatics*, 165-172.

Appendix A – Physical Model Results

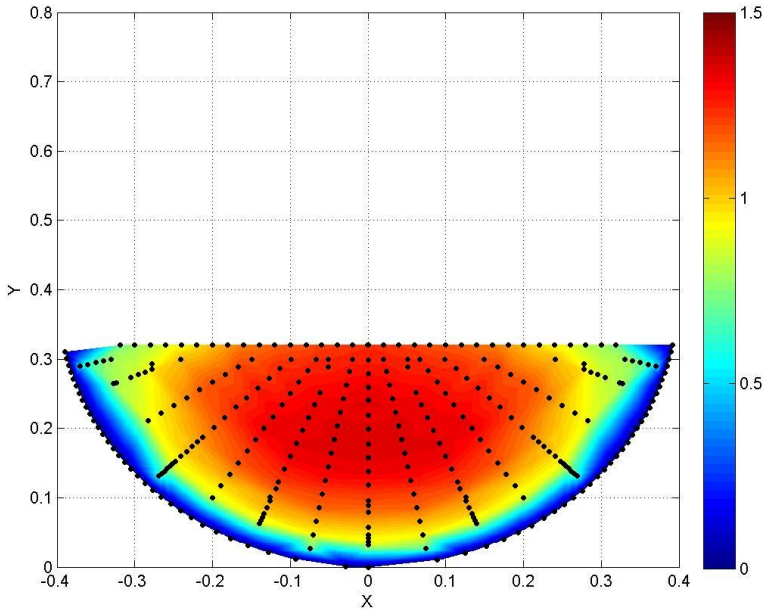

Figure 53: Test 2 - Normalized measured velocity (U_{meas}/U_{av})

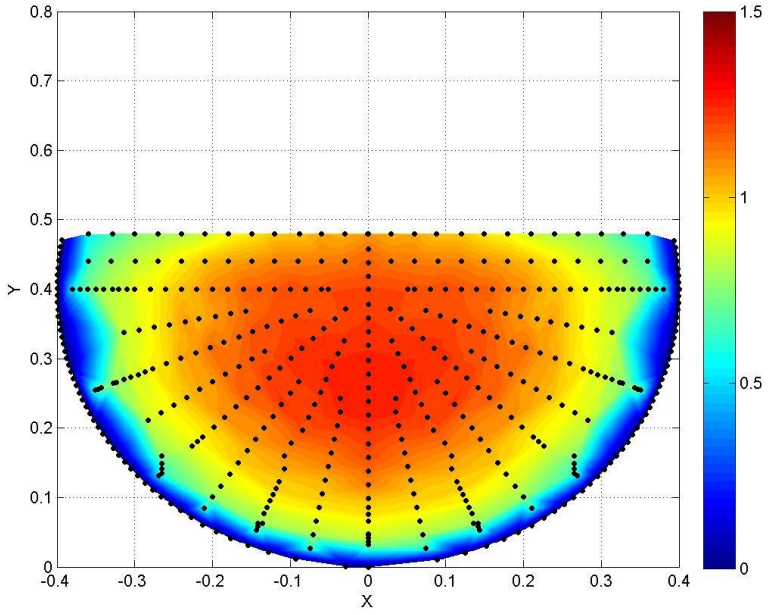

Figure 54: Test 3 - Normalized measured velocity (U_{meas}/U_{av})

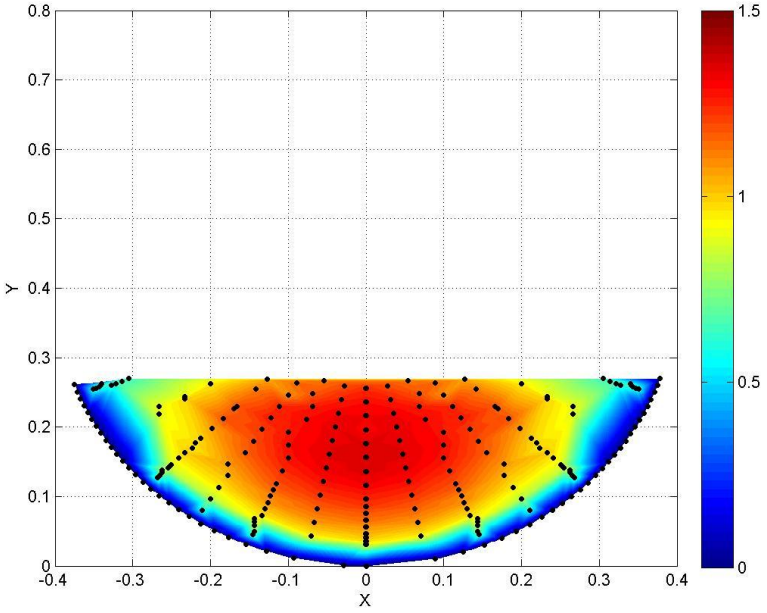

Figure 55: Test 4 - Normalized measured velocity (U_{meas}/U_{av})

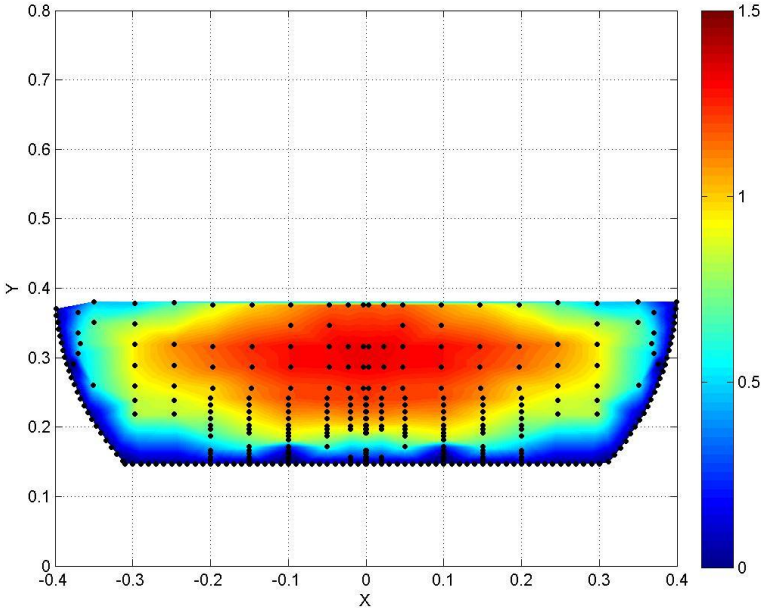

Figure 56: Test 7 - Normalized measured velocity (U_{meas}/U_{av})

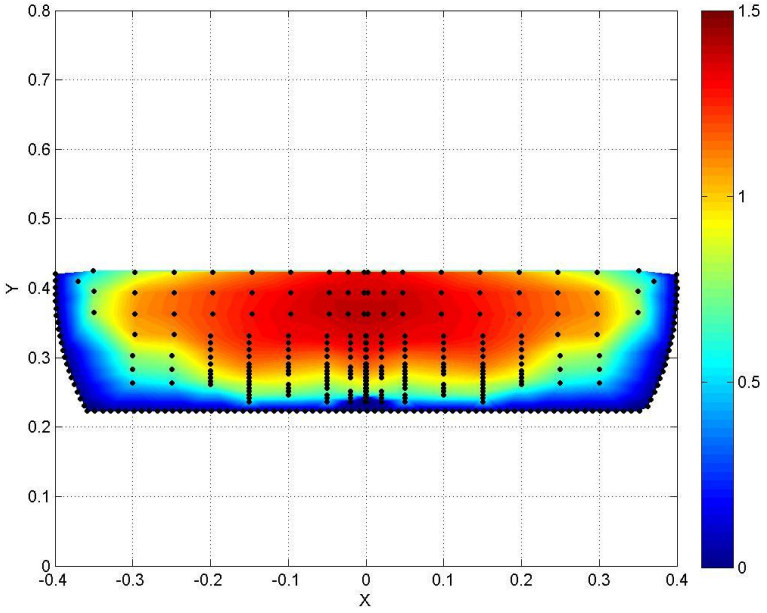

Figure 57: Test 8 - Normalized measured velocity (U_{meas}/U_{av})

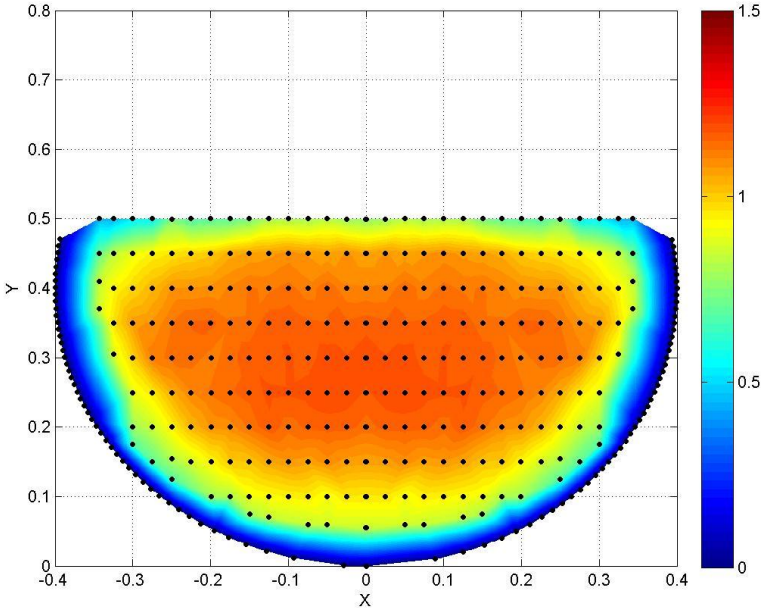

Figure 58: Test 9 - Normalized measured velocity (U_{meas}/U_{av})

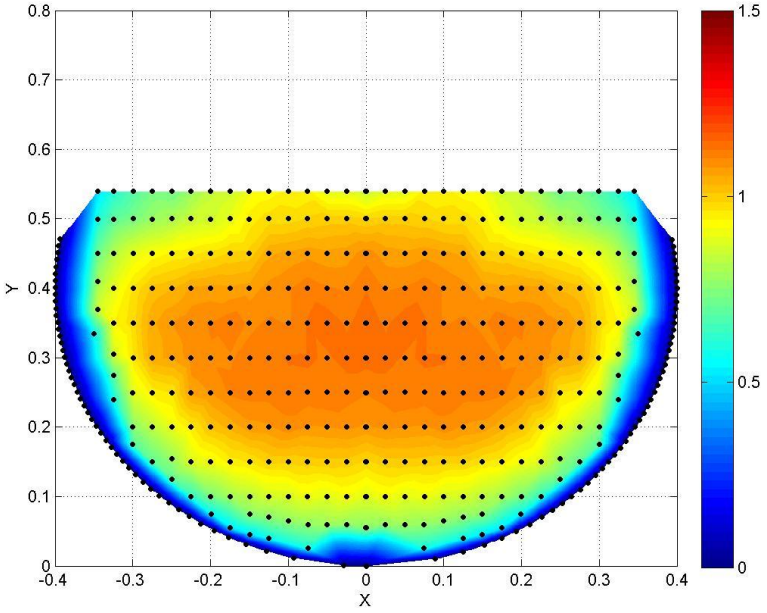

Figure 59: Test 11 - Normalized measured velocity (U_{meas}/U_{av})

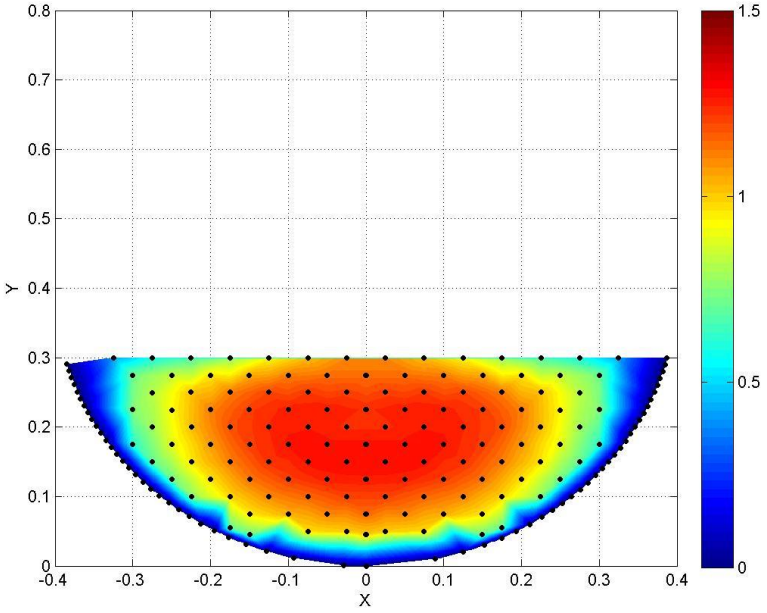

Figure 60: Test 12 - Normalized measured velocity (U_{meas}/U_{av})

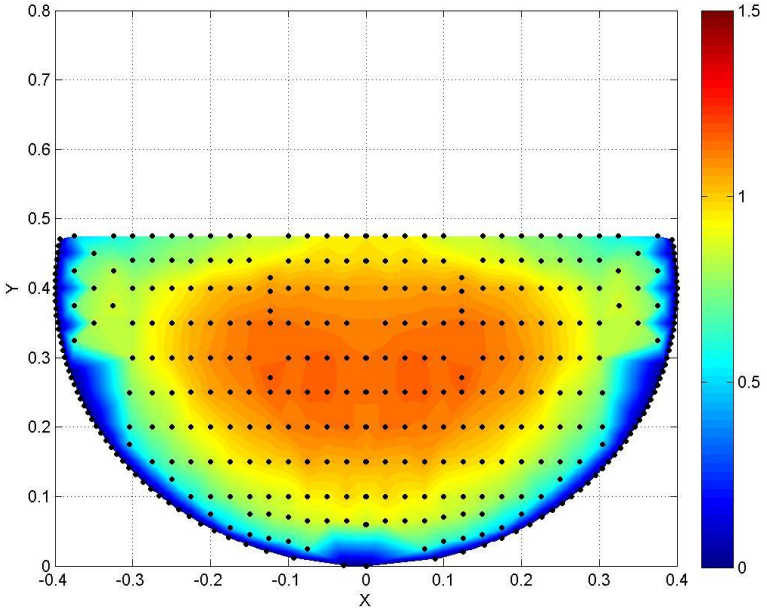

Figure 61: Test 14 - Normalized measured velocity (U_{meas}/U_{av})

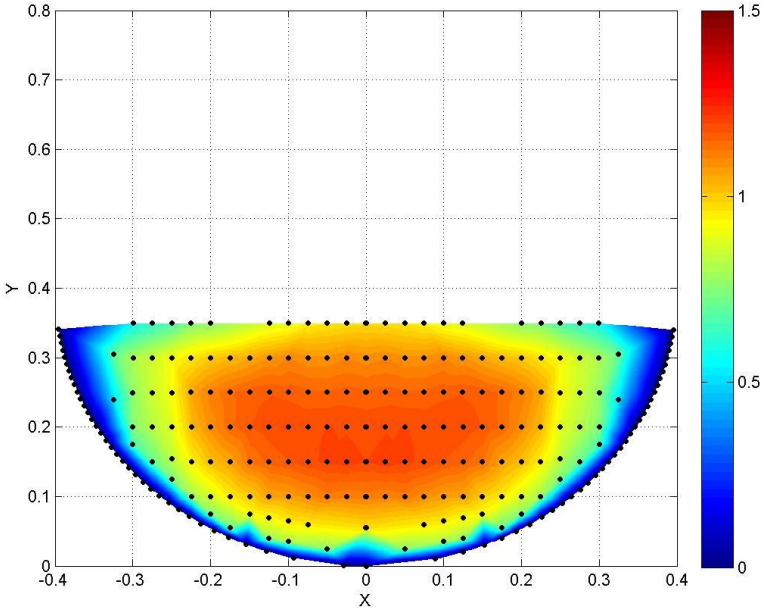

Figure 62: Test 15 - Normalized measured velocity (U_{meas}/U_{av})

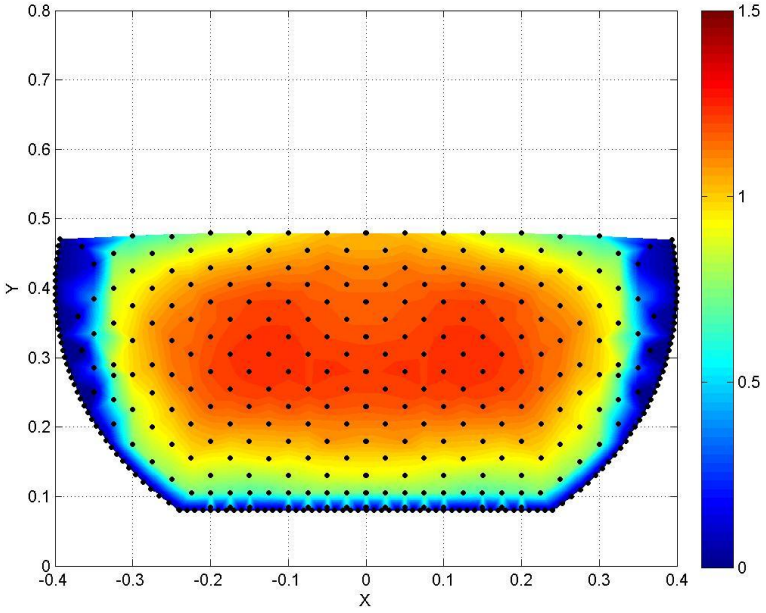

Figure 63: Test 17 - Normalized measured velocity (U_{meas}/U_{av})

Appendix B – CFD Model Results

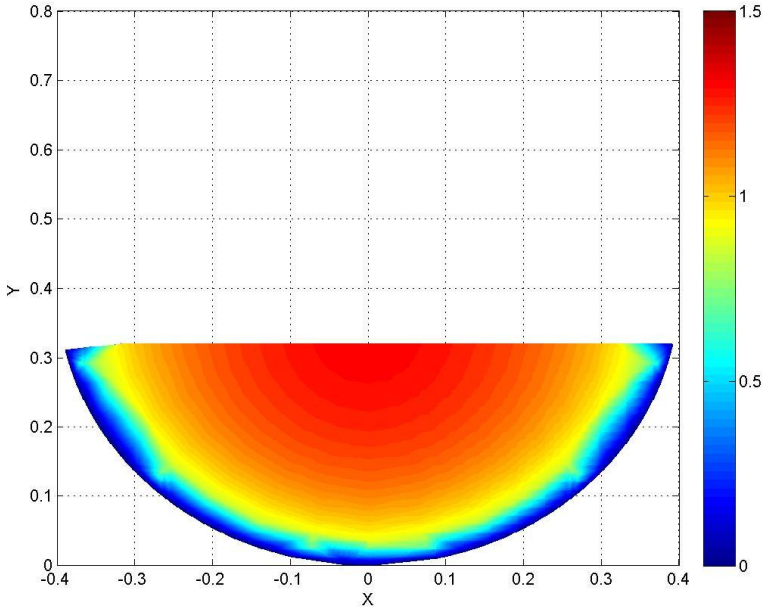

Figure 64: Test 2 - Normalized CFD predicted velocity (U_{mod}/U_{av})

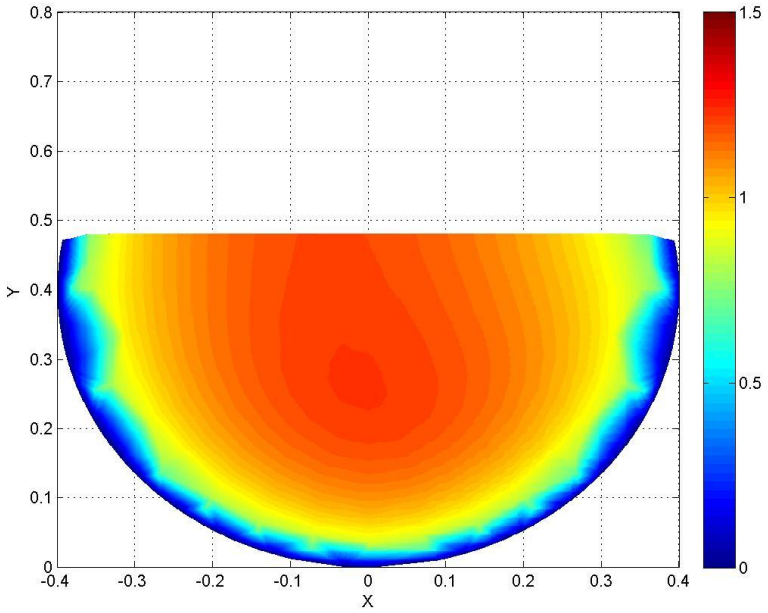

Figure 65: Test 3 - Normalized CFD predicted velocity (U_{mod}/U_{av})

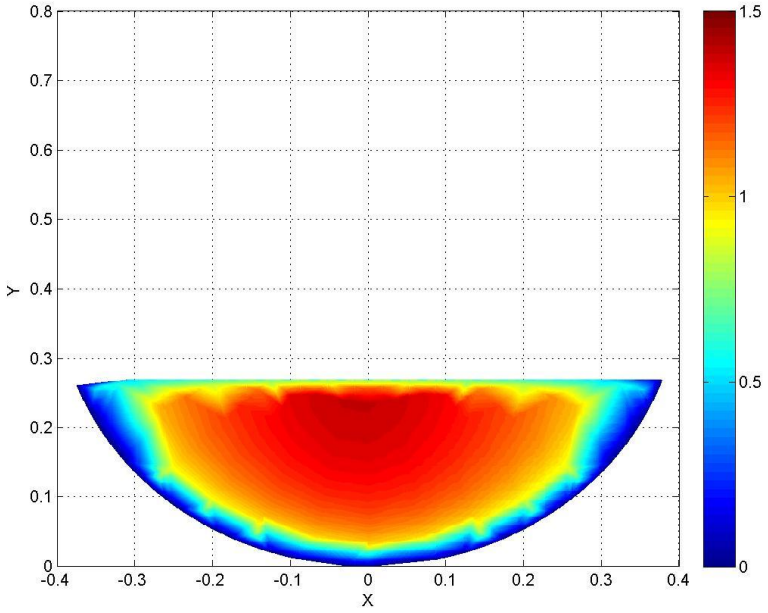

Figure 66: Test 4 - Normalized CFD predicted velocity (U_{mod}/U_{av})

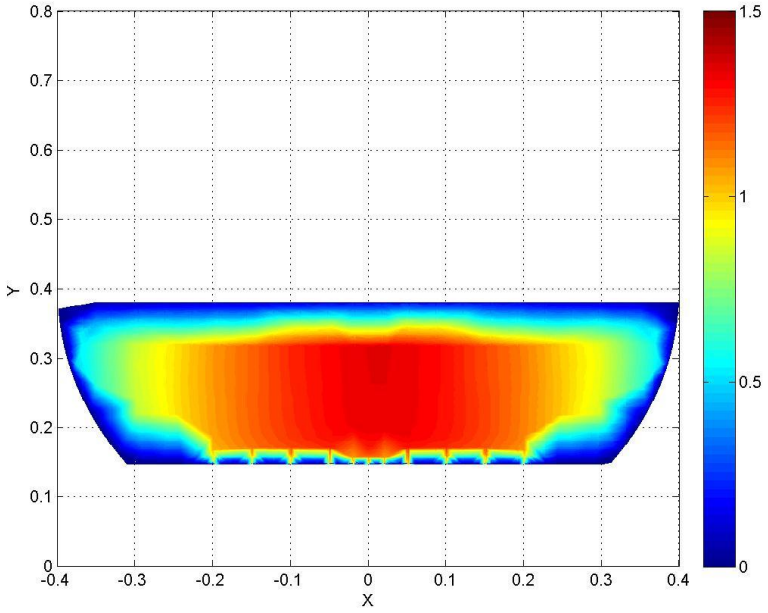

Figure 67: Test 7 - Normalized CFD predicted velocity (U_{mod}/U_{av})

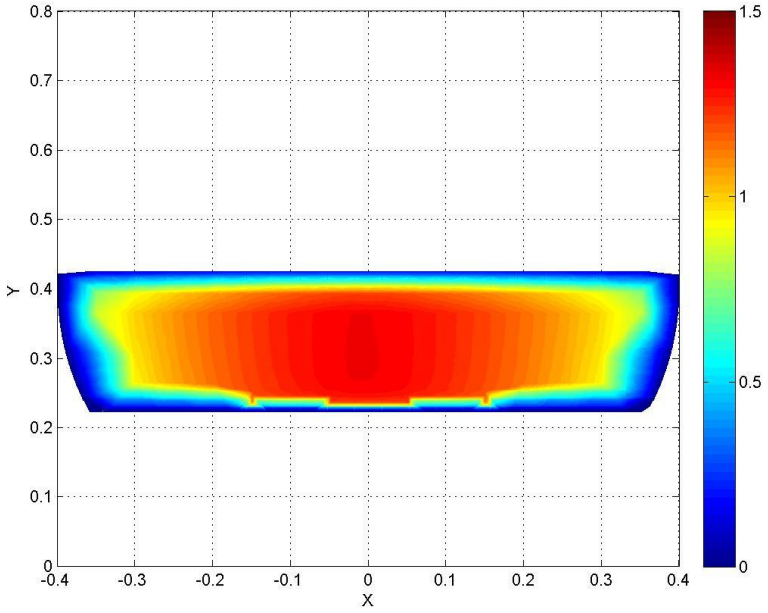

Figure 68: Test 8 - Normalized CFD predicted velocity (U_{mod}/U_{av})

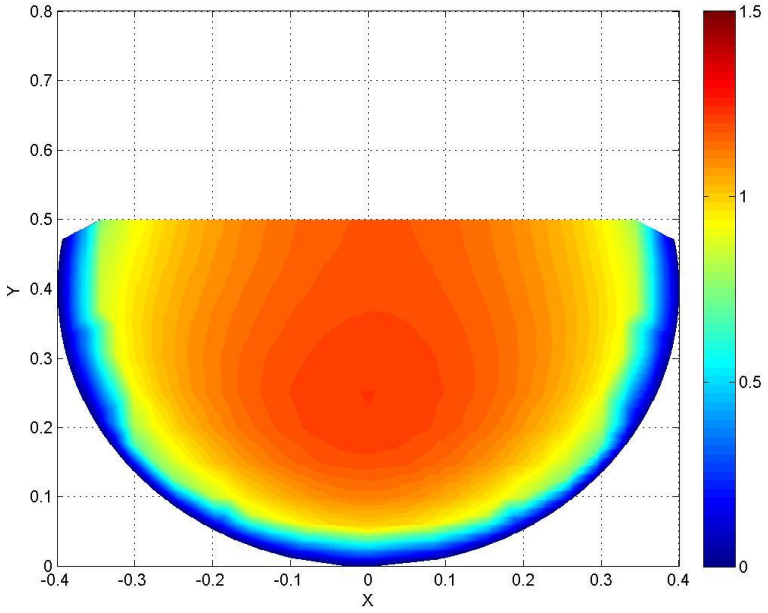

Figure 69: Test 9 - Normalized CFD predicted velocity (U_{mod}/U_{av})

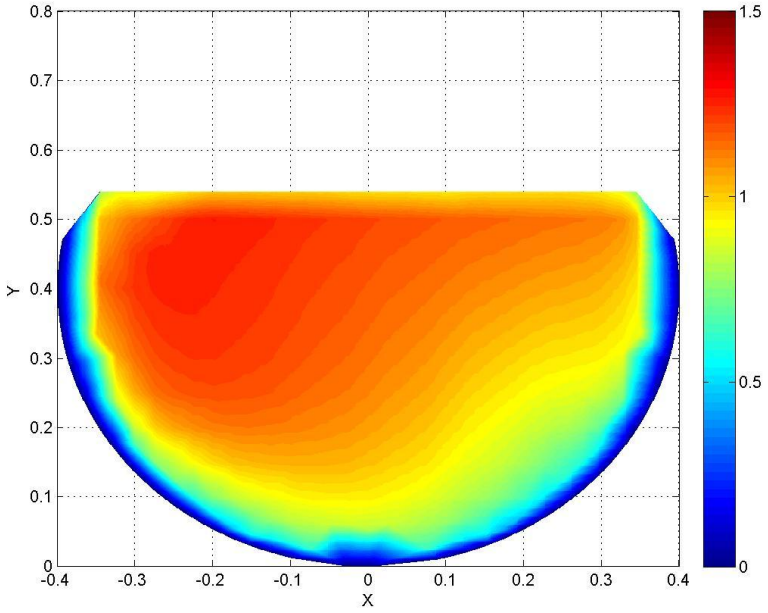

Figure 70: Test 11 - Normalized CFD predicted velocity (U_{mod}/U_{av})

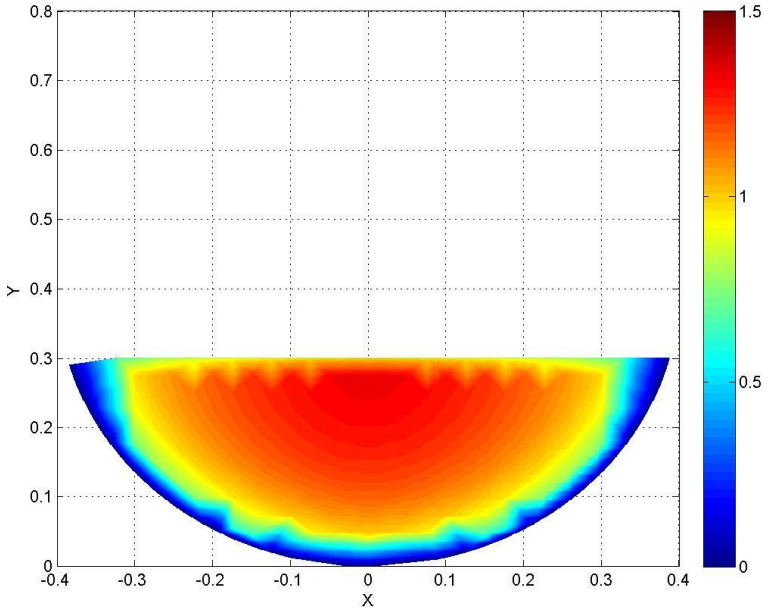

Figure 71: Test 12 - Normalized CFD predicted velocity (U_{mod}/U_{av})

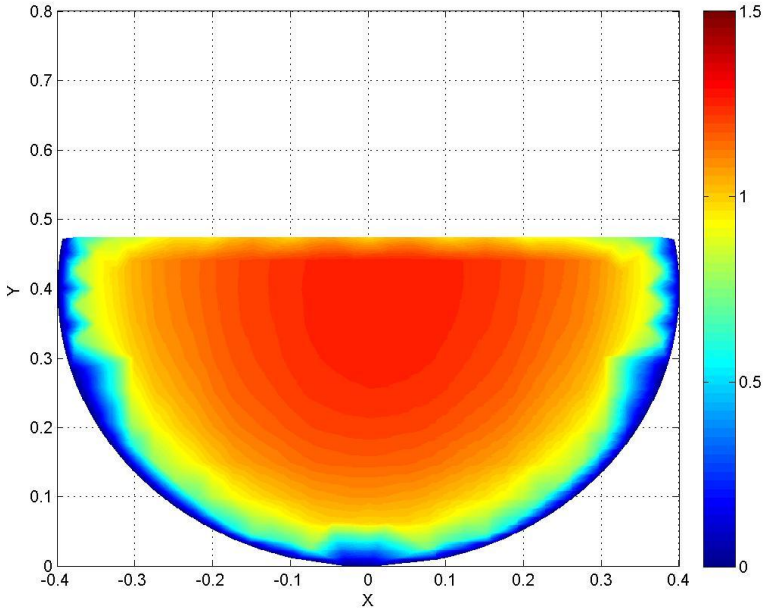

Figure 72: Test 14 - Normalized CFD predicted velocity (U_{mod}/U_{av})

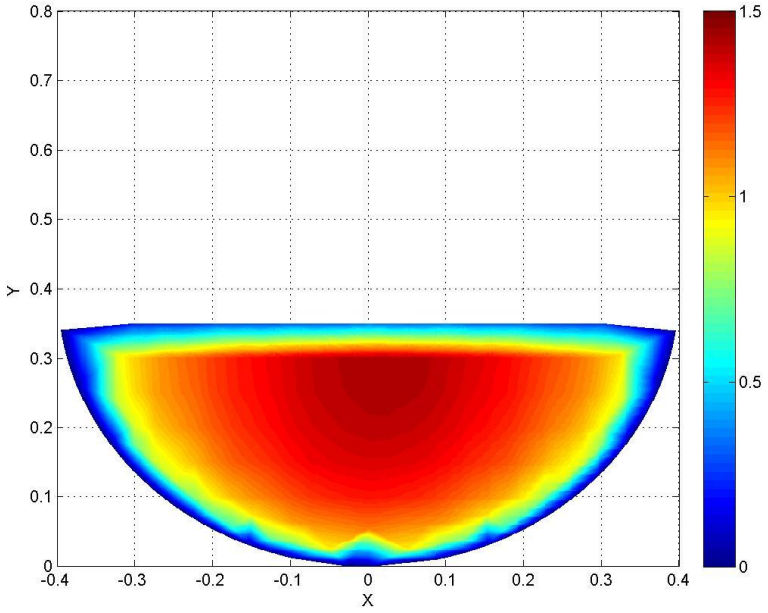

Figure 73: Test 15 - Normalized CFD predicted velocity (U_{mod}/U_{av})

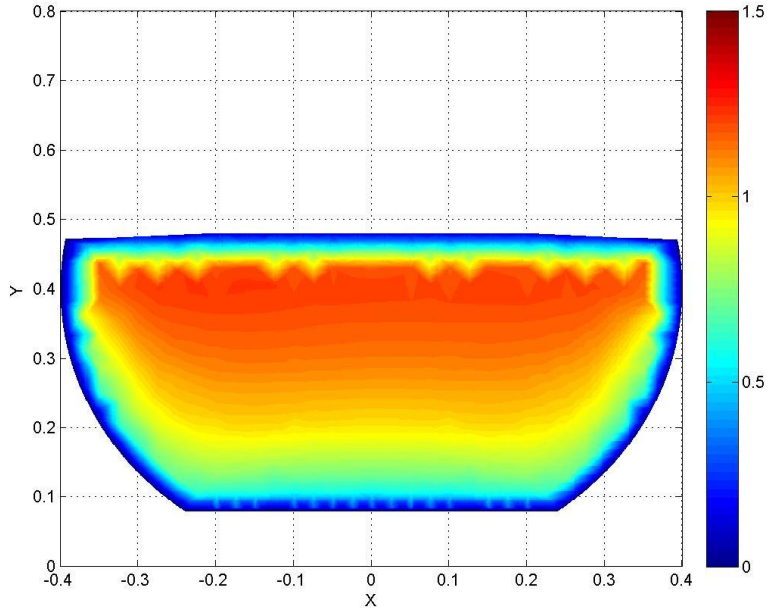

Figure 74: Test 17 - Normalized CFD predicted velocity (U_{mod}/U_{av})

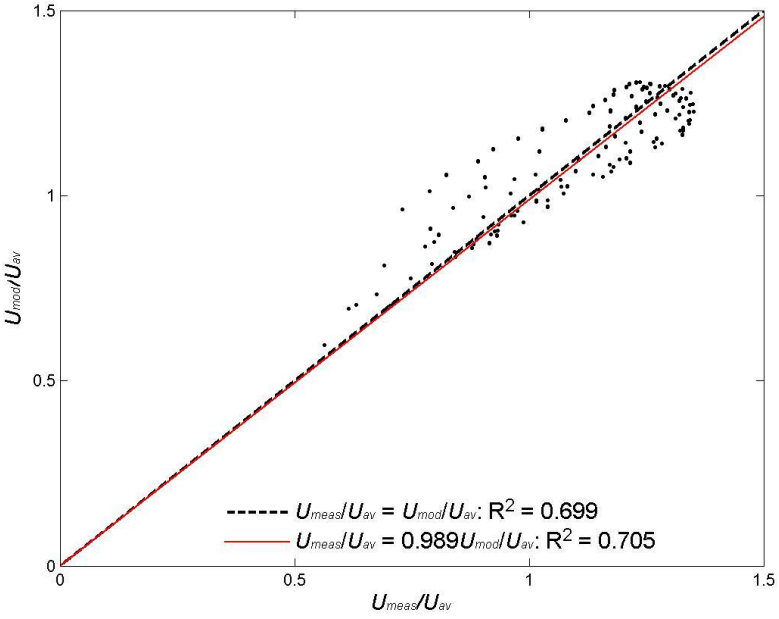

Figure 75: Normalized velocity predicted by the CFD model vs normalized measured velocity for Test 2

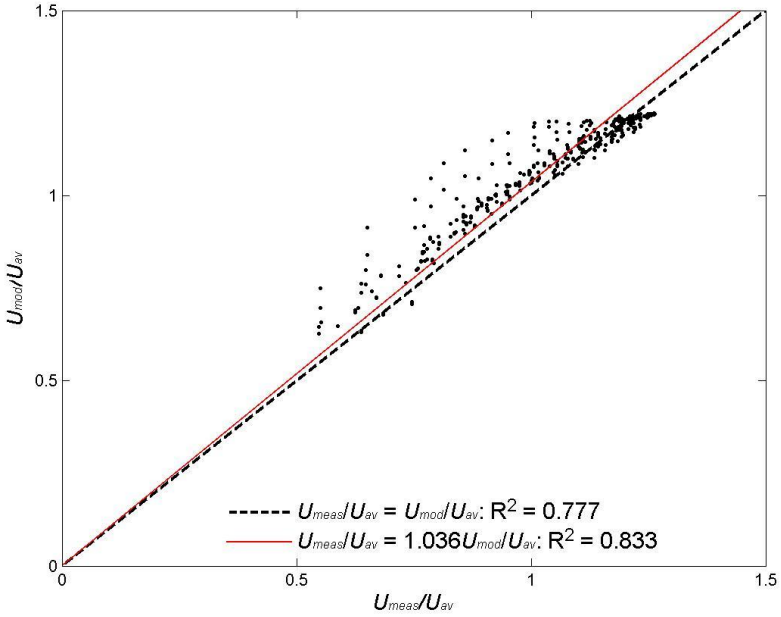

Figure 76: Normalized velocity predicted by the CFD model vs normalized measured velocity for Test 3

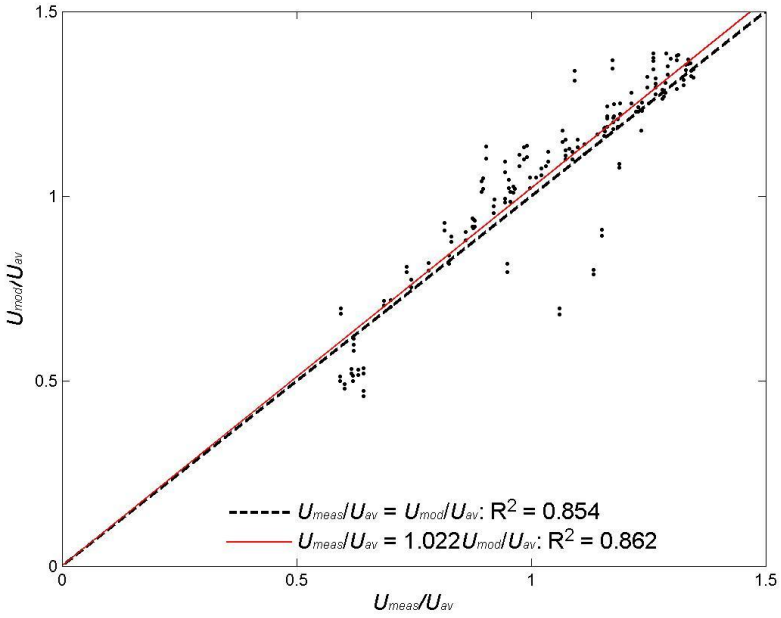

Figure 77: Normalized velocity predicted by the CFD model vs normalized measured velocity for Test 4

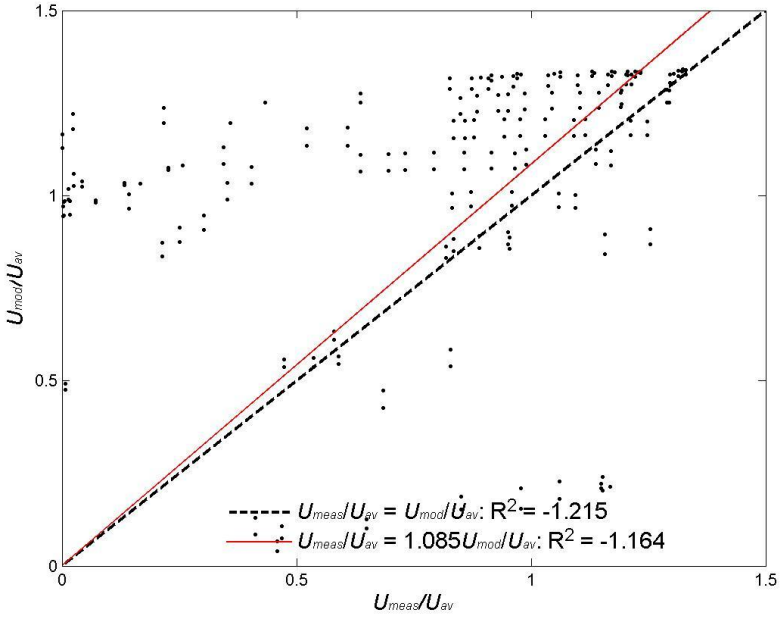

Figure 78: Normalized velocity predicted by the CFD model vs normalized measured velocity for Test 7

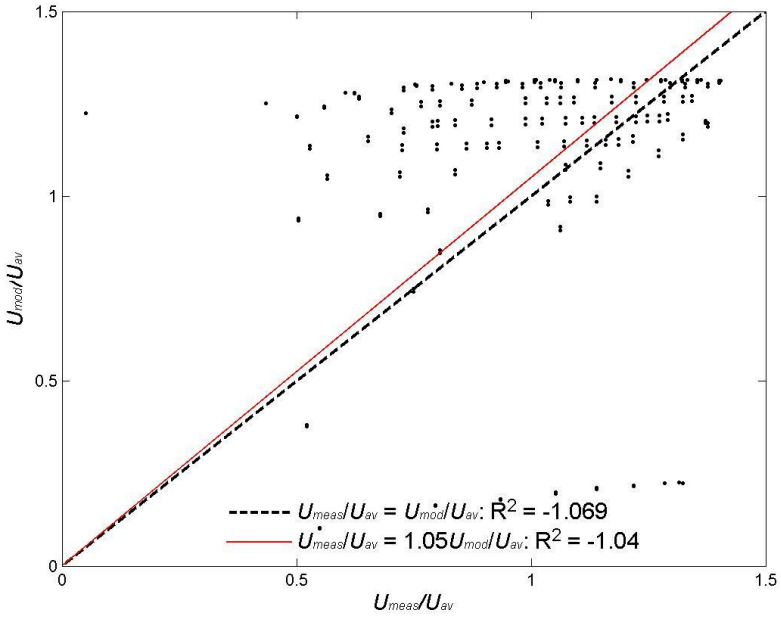

Figure 79: Normalized velocity predicted by the CFD model vs normalized measured velocity for Test 8

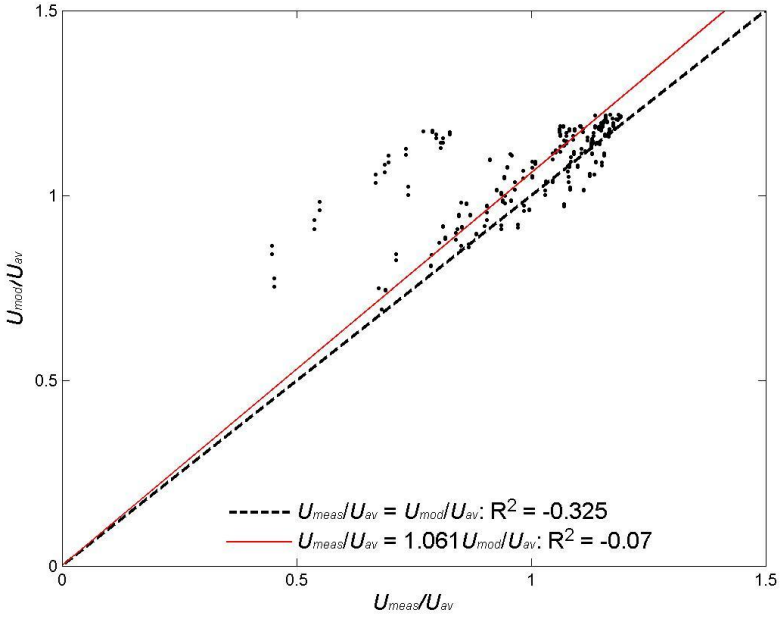

Figure 80: Normalized velocity predicted by the CFD model vs normalized measured velocity for Test 9

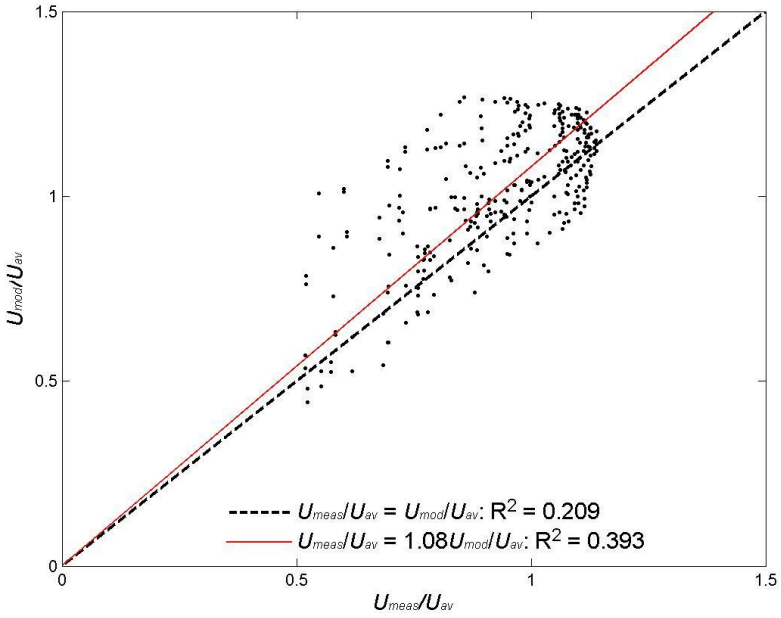

Figure 81: Normalized velocity predicted by the CFD model vs normalized measured velocity for Test 11

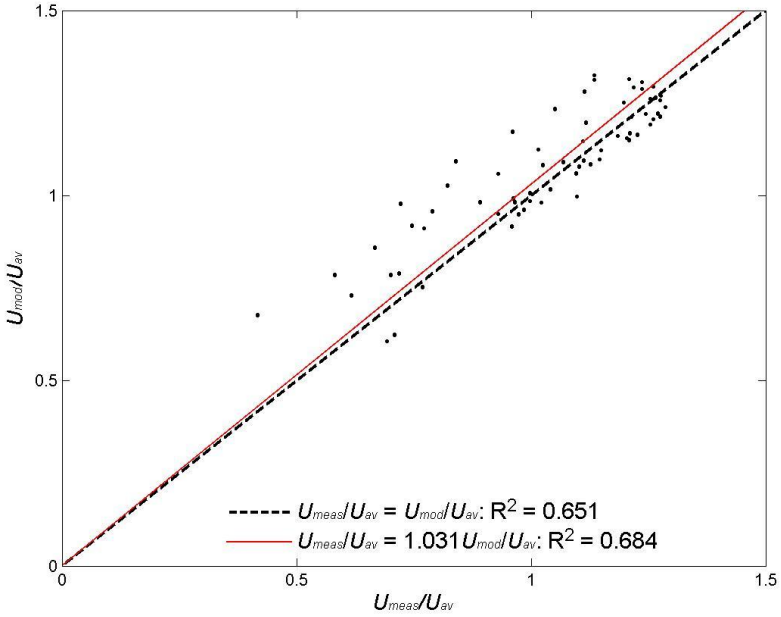

Figure 82: Normalized velocity predicted by the CFD model vs normalized measured velocity for Test 12

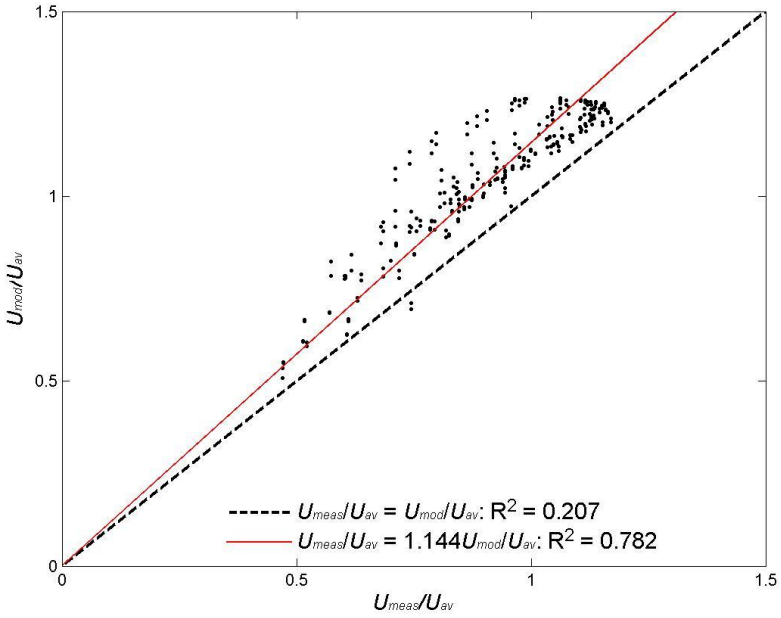

Figure 83: Normalized velocity predicted by the CFD model vs normalized measured velocity for Test 14

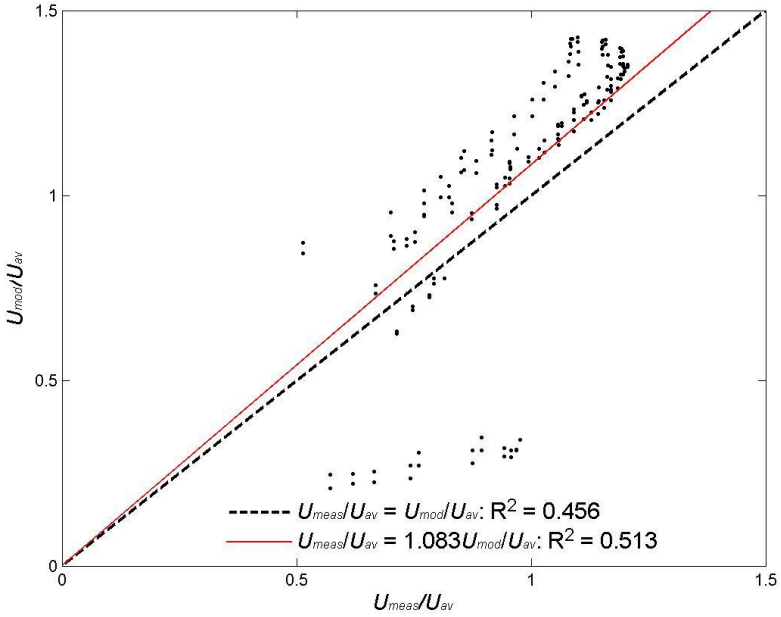

Figure 84: Normalized velocity predicted by the CFD model vs normalized measured velocity for Test 15

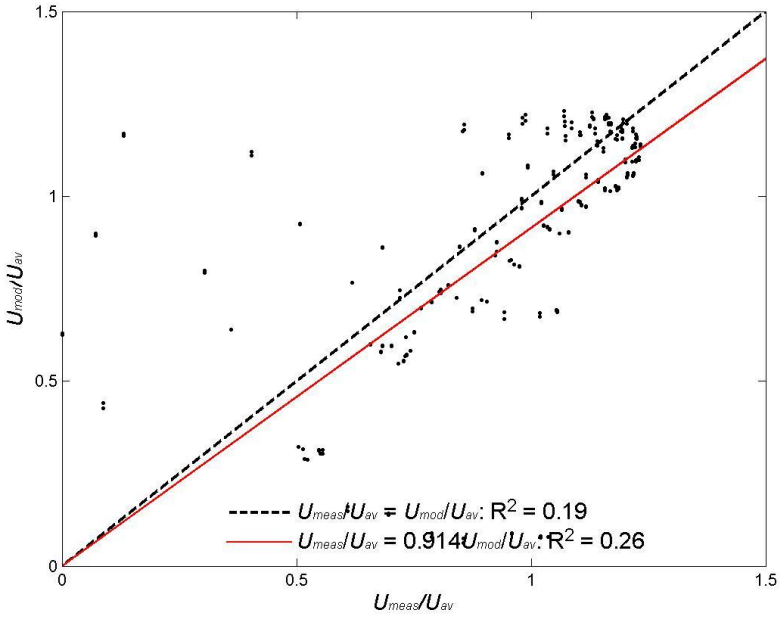

Figure 85: Normalized velocity predicted by the CFD model vs normalized measured velocity for Test 17

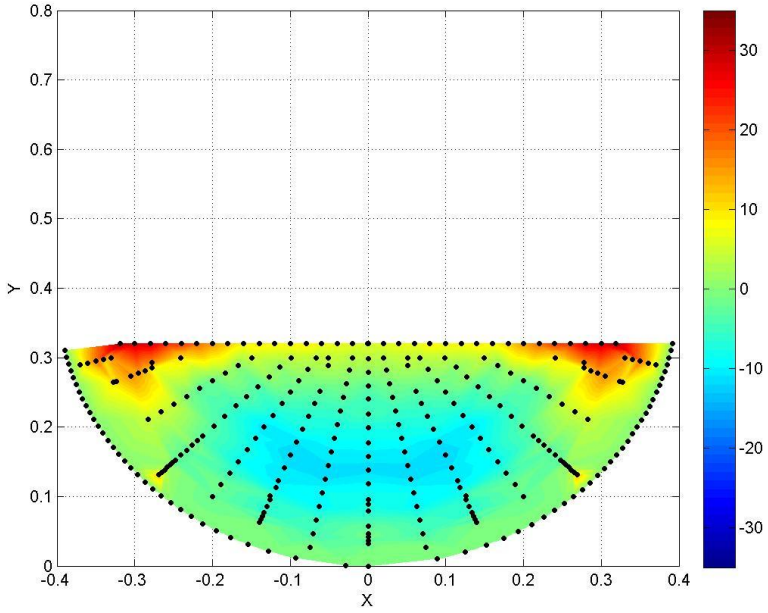

Figure 86: CFD percent difference two-dimensional distribution for Test 2 (%)

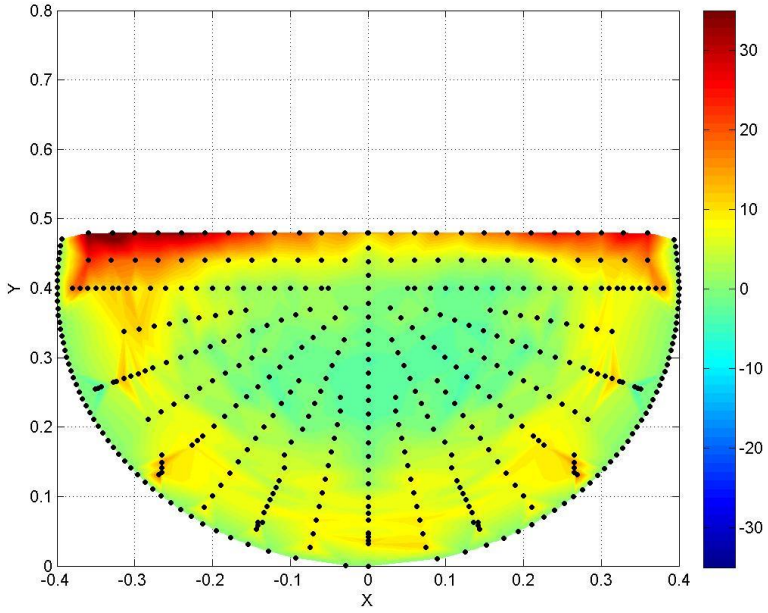

Figure 87: CFD percent difference two-dimensional distribution for Test 3 (%)

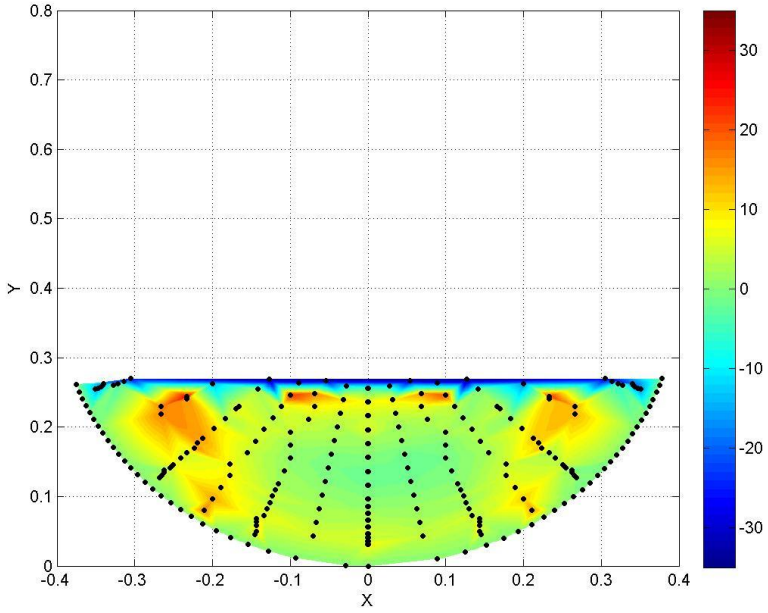

Figure 88: CFD percent difference two-dimensional distribution for Test 4 (%)

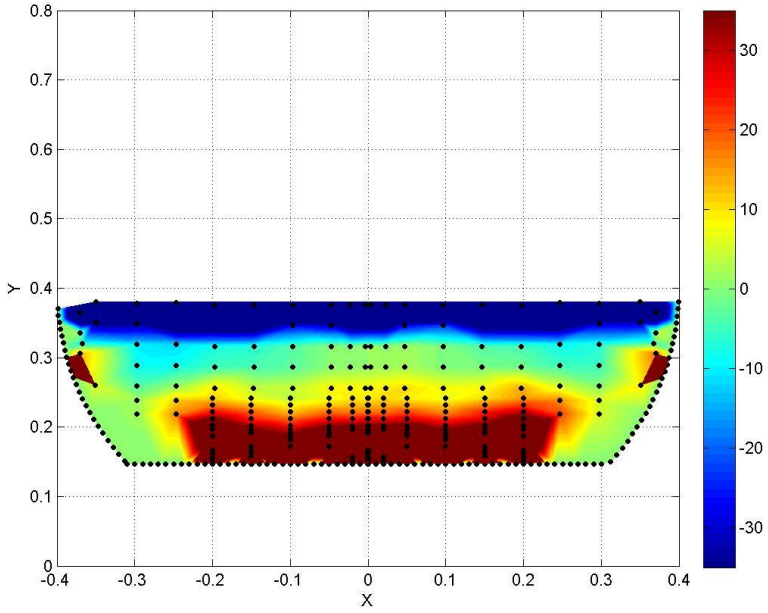

Figure 89: CFD percent difference two-dimensional distribution for Test 7 (%)

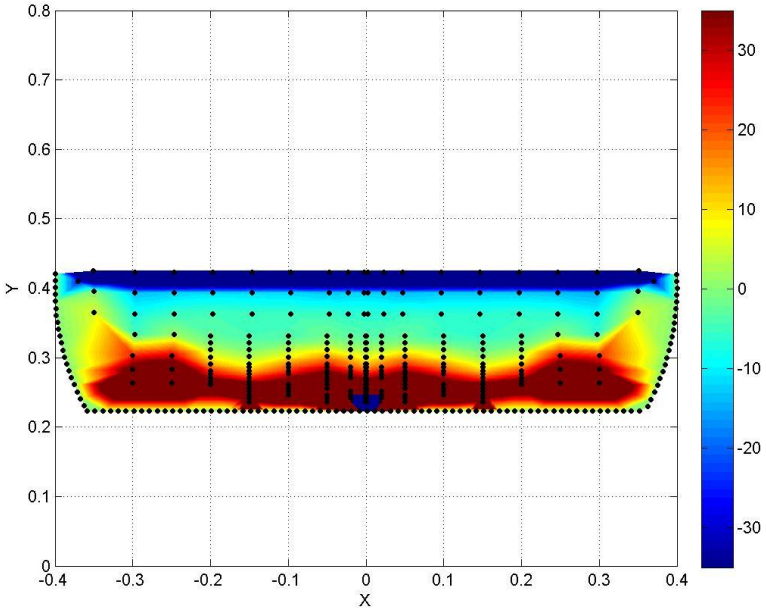

Figure 90: CFD percent difference two-dimensional distribution for Test 8 (%)

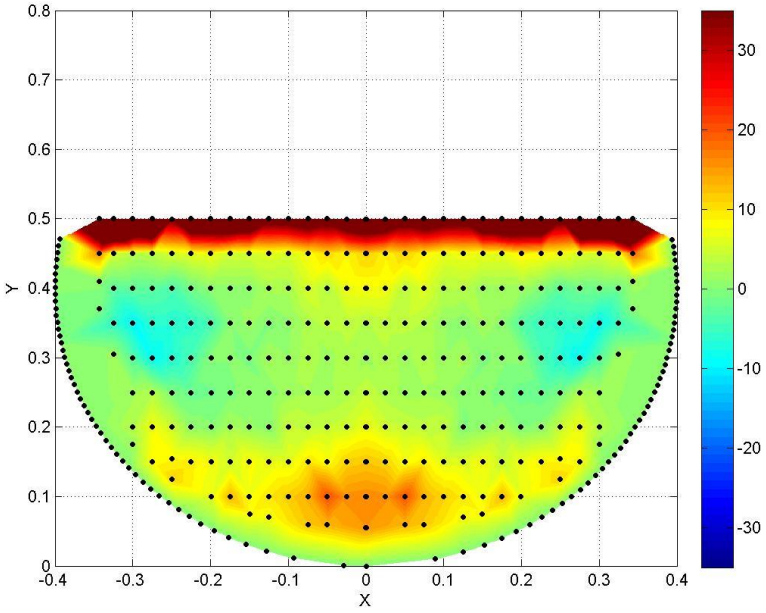

Figure 91: CFD percent difference two-dimensional distribution for Test 9 (%)

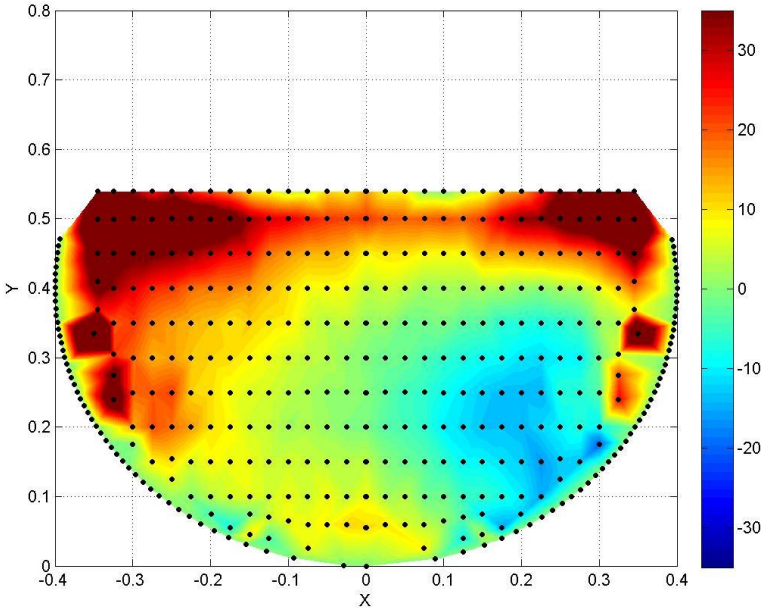

Figure 92: CFD percent difference two-dimensional distribution for Test 11 (%)

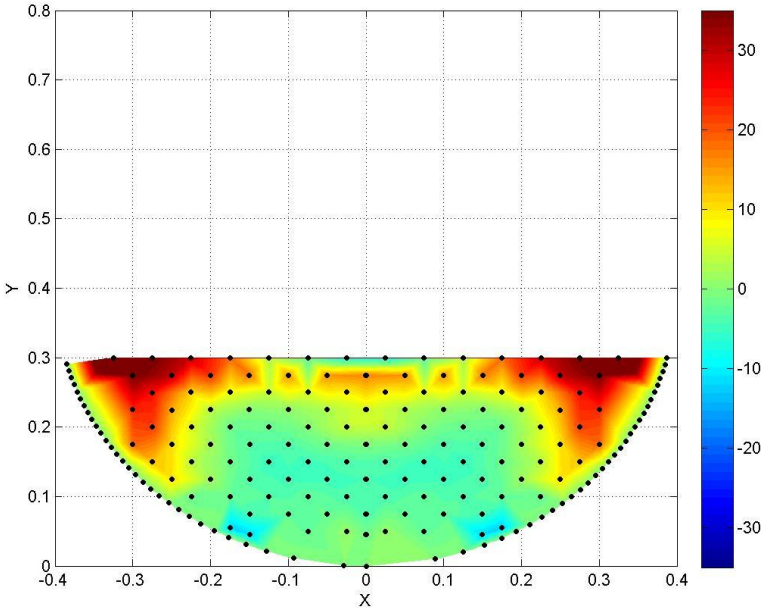

Figure 93: CFD percent difference two-dimensional distribution for Test 12 (%)

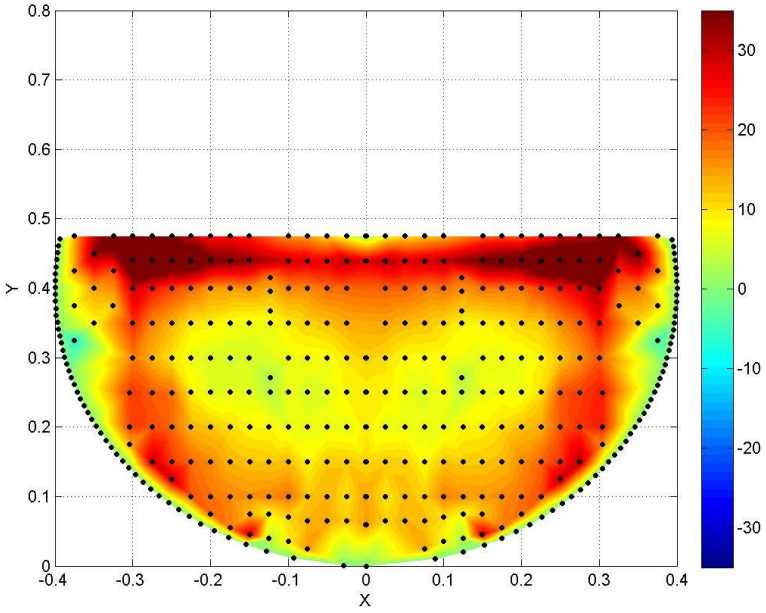

Figure 94: CFD percent difference two-dimensional distribution for Test 14 (%)

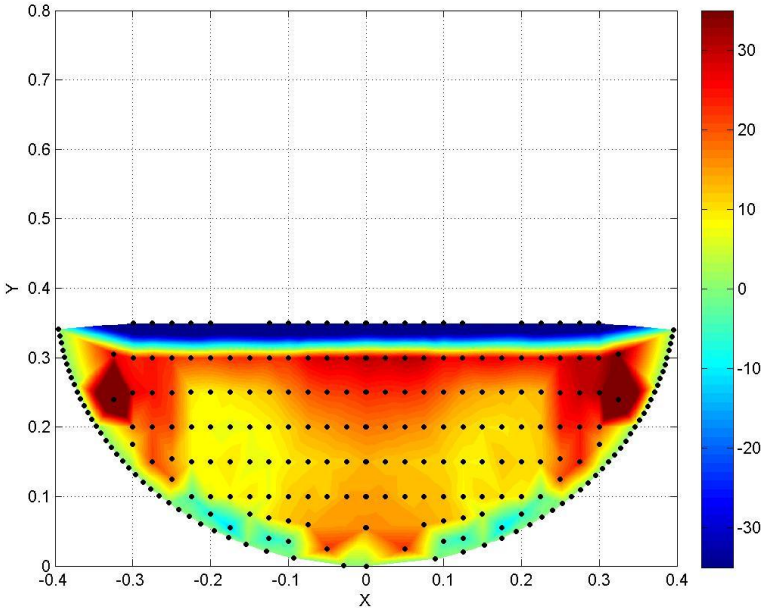

Figure 95: CFD percent difference two-dimensional distribution for Test 15 (%)

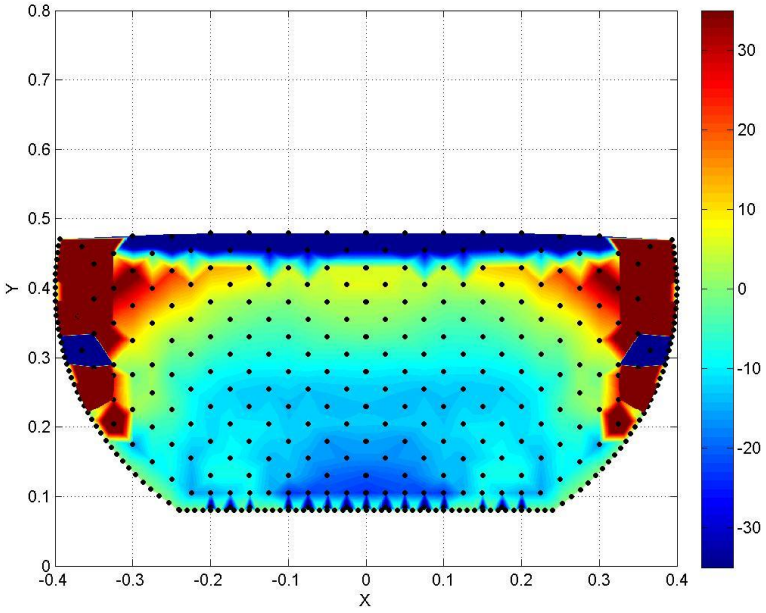

Figure 96: CFD percent difference two-dimensional distribution for Test 17 (%)

Appendix C – Empirical Equation Results

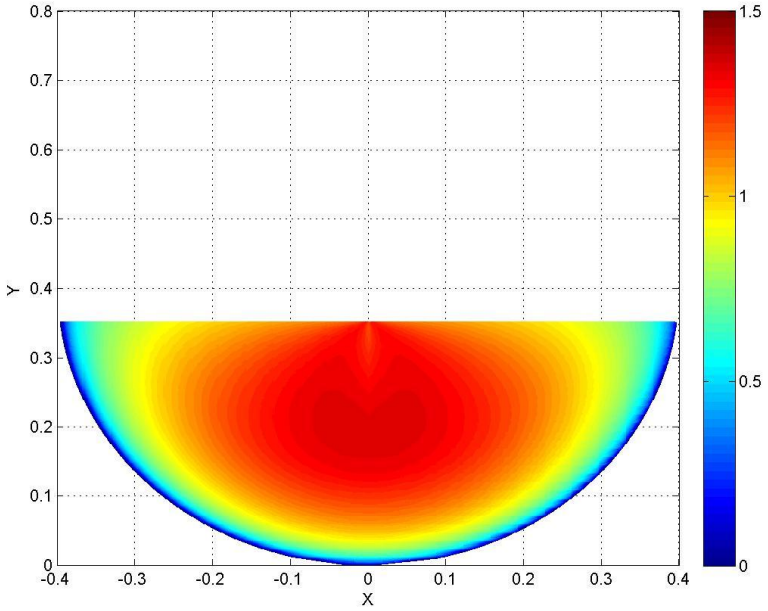

Figure 97: Test 2 - Normalized Empirical Equation predicted velocity (U_{ck}/U_{av})

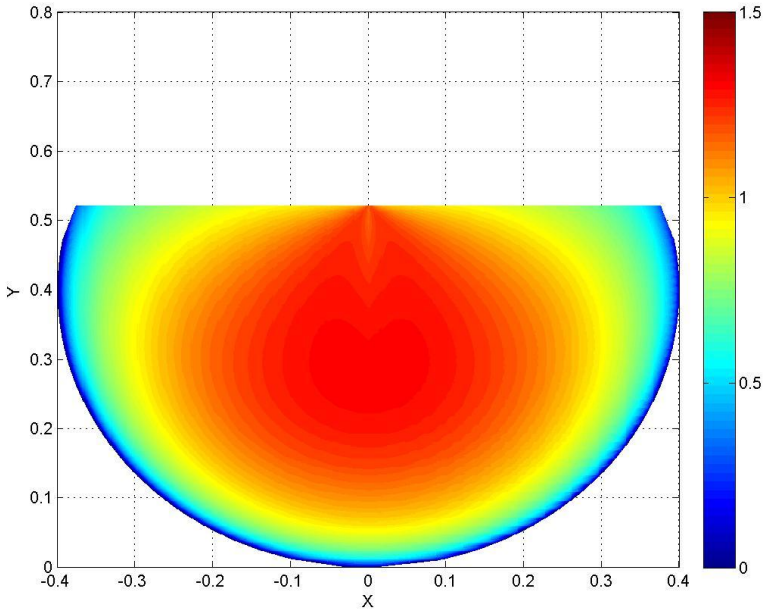

Figure 98: Test 3 - Normalized Empirical Equation predicted velocity (U_{ck}/U_{av})

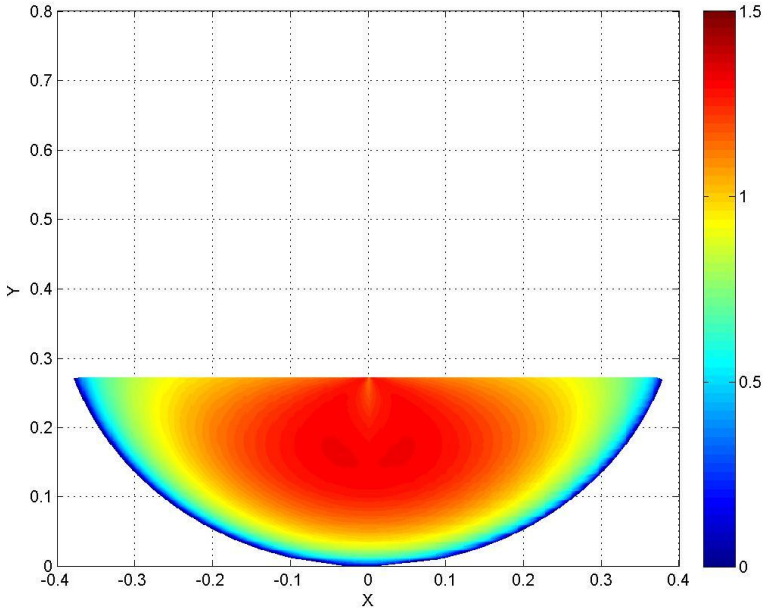

Figure 99: Test 4 - Normalized Empirical Equation predicted velocity (U_{ck}/U_{av})

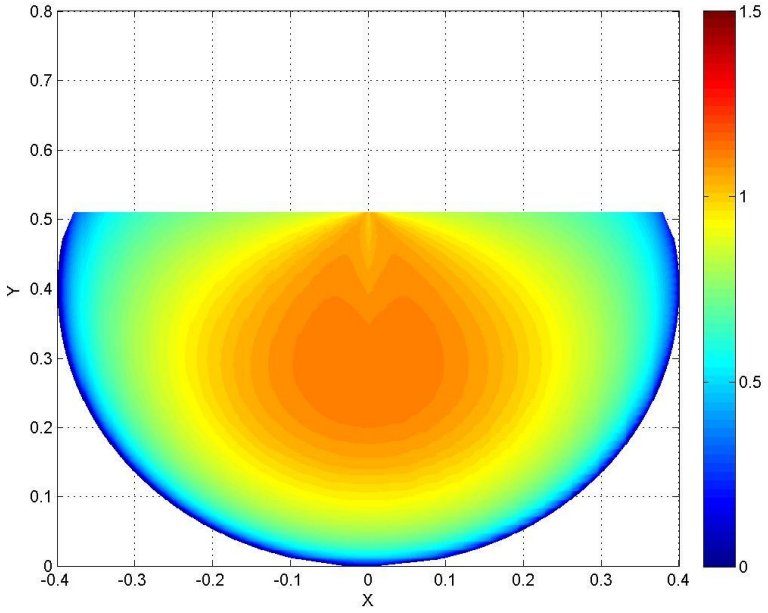

Figure 100: Test 9 - Normalized Empirical Equation predicted velocity (U_{ck}/U_{av})

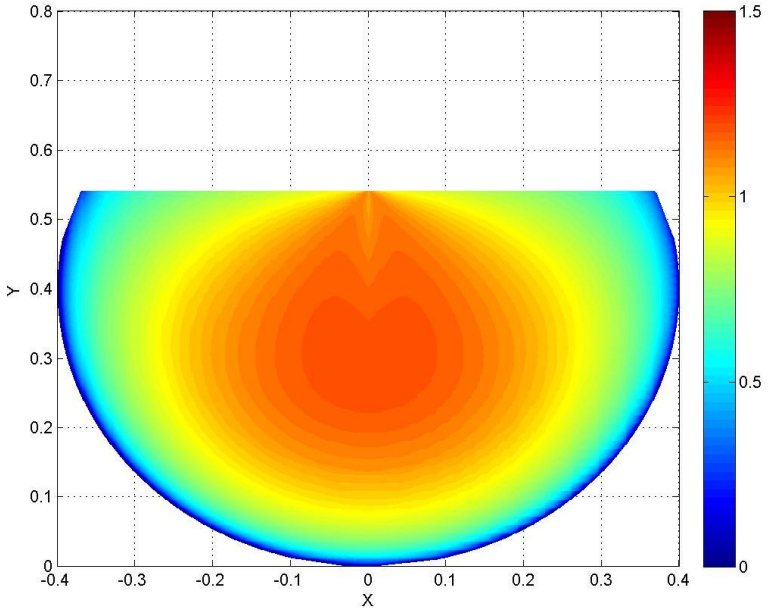

Figure 101: Test 11 - Normalized Empirical Equation predicted velocity (U_{ck}/U_{av})

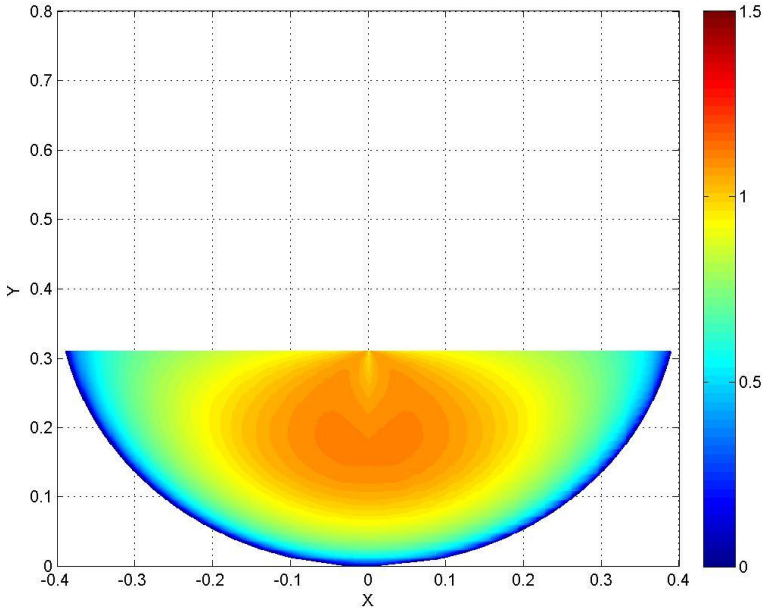

Figure 102: Test 12 - Normalized Empirical Equation predicted velocity (U_{ck}/U_{av})

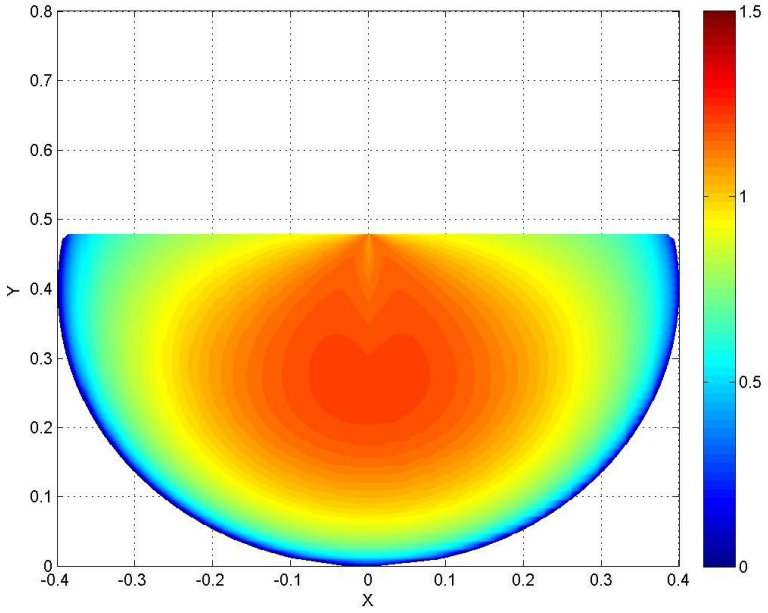

Figure 103: Test 14 - Normalized Empirical Equation predicted velocity (U_{ck}/U_{av})

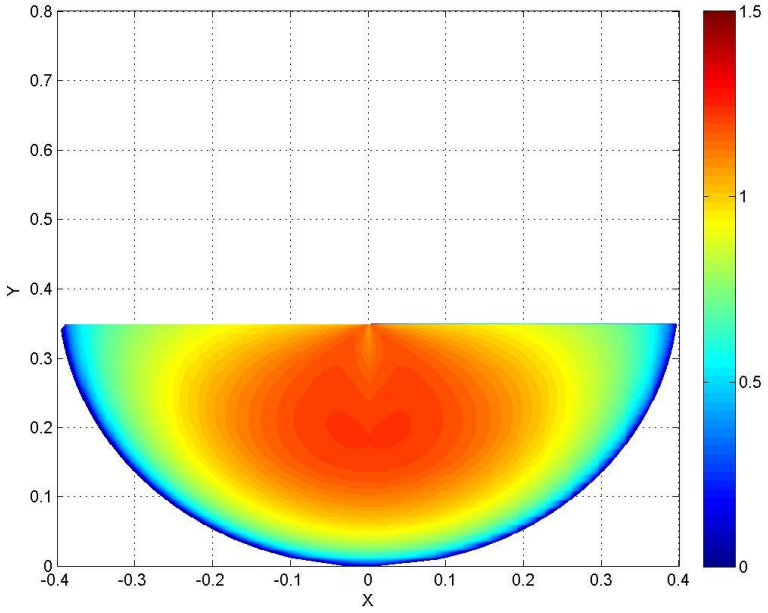

Figure 104: Test 15 - Normalized Empirical Equation predicted velocity (U_{ck}/U_{av})

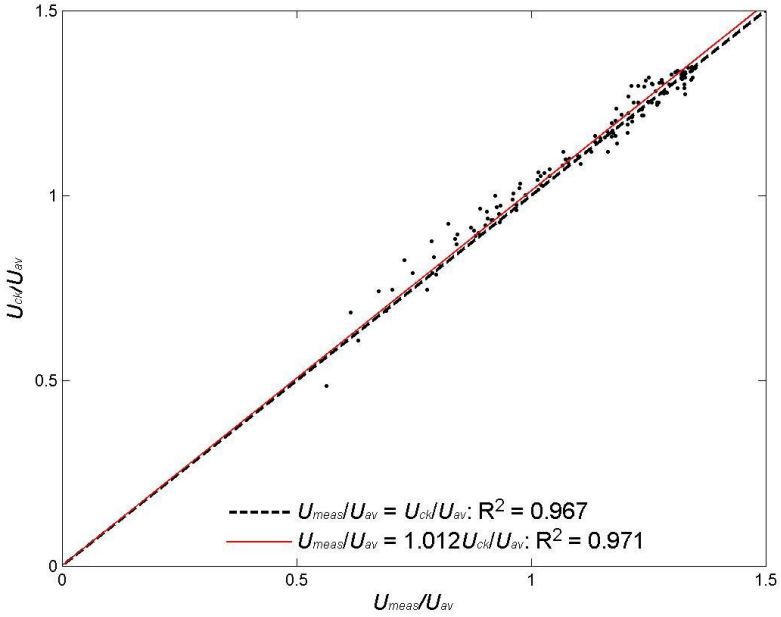

Figure 105: Test 2 - Empirical Equation proportionality plot

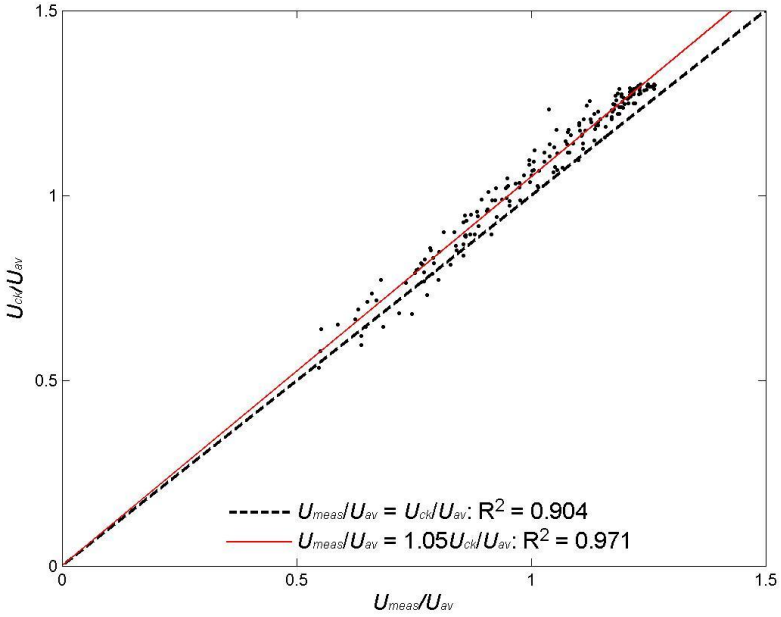

Figure 106: Test 3 - Empirical Equation proportionality plot

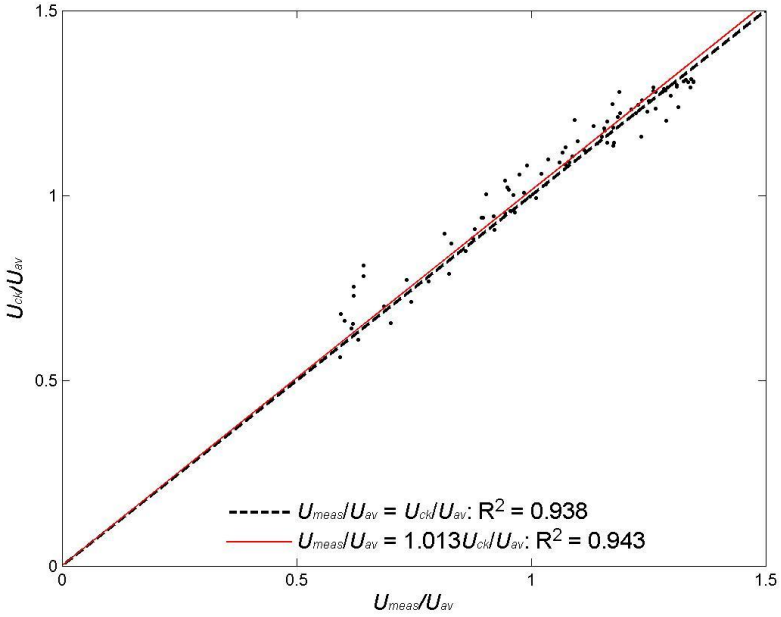

Figure 107: Test 4 - Empirical Equation proportionality plot

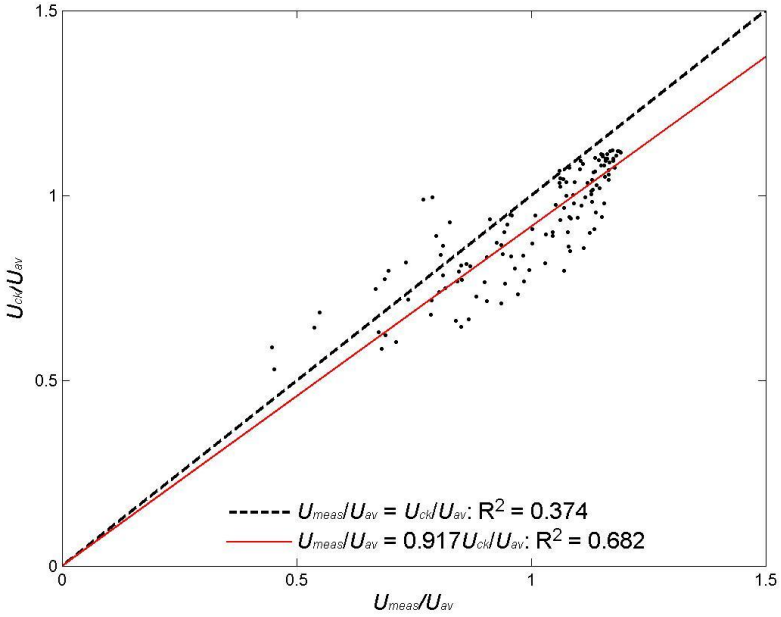

Figure 108: Test 9 - Empirical Equation proportionality plot

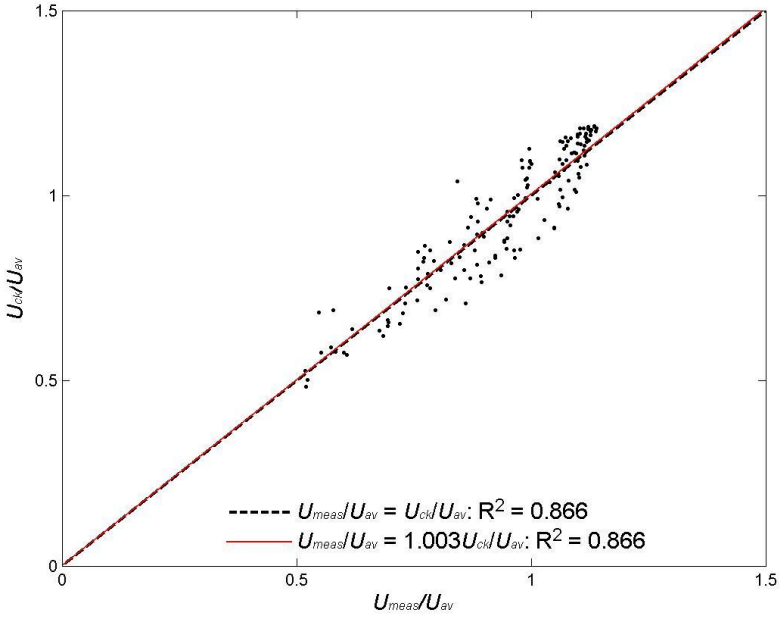

Figure 109: Test 11 - Empirical Equation proportionality plot

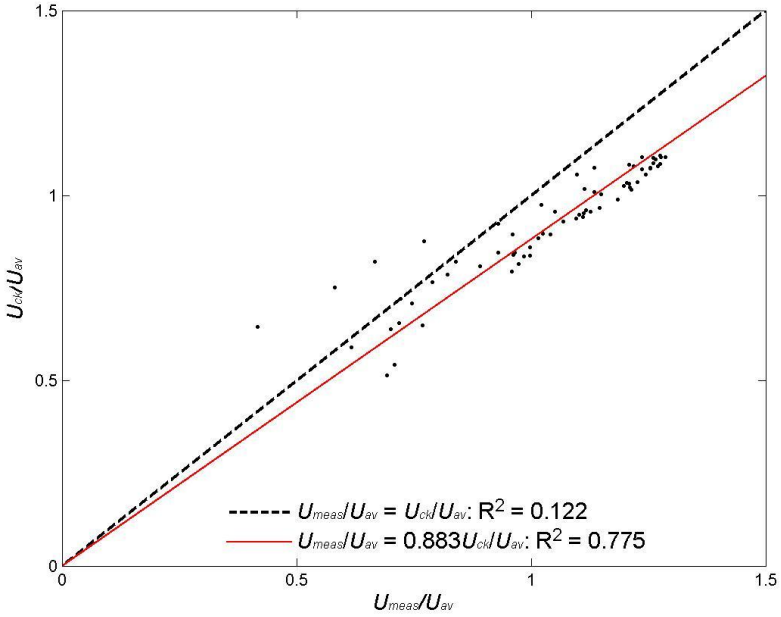

Figure 110: Test 12 - Empirical Equation proportionality plot

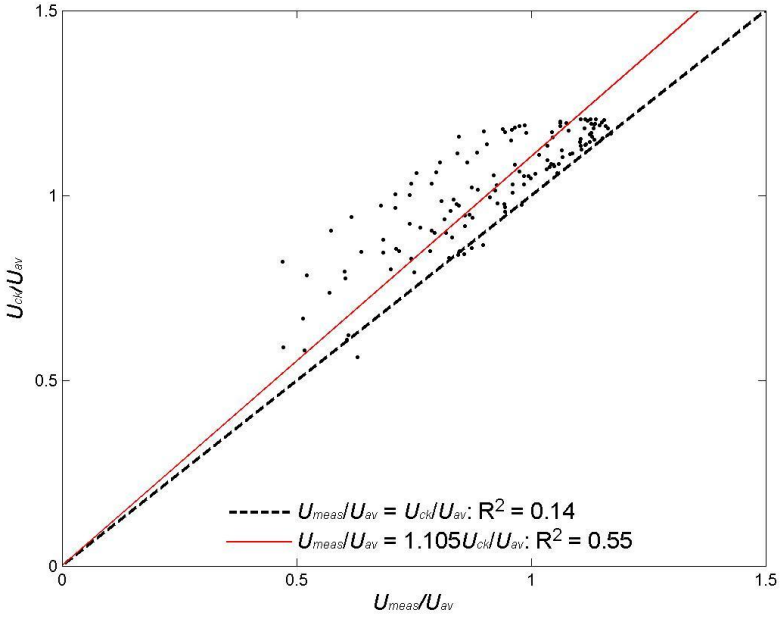

Figure 111: Test 14 - Empirical Equation proportionality plot

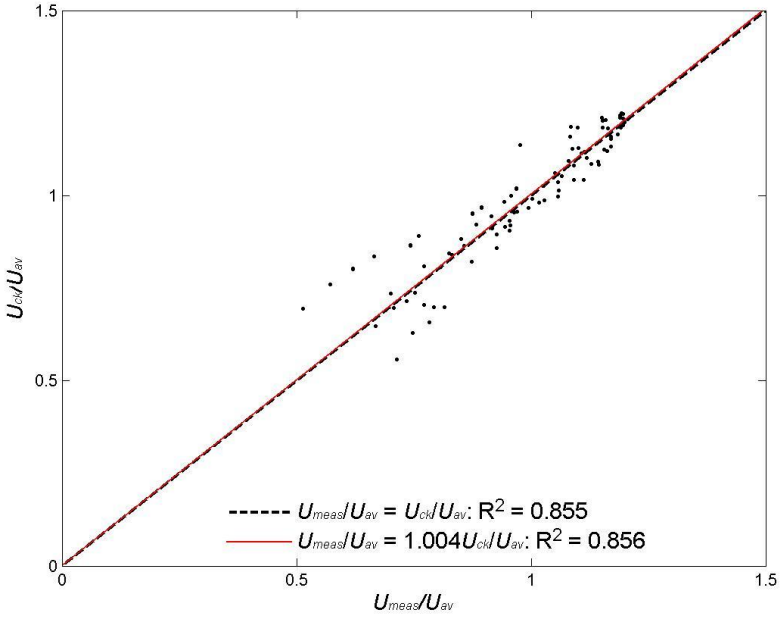

Figure 112: Test 15 - Empirical Equation proportionality plot

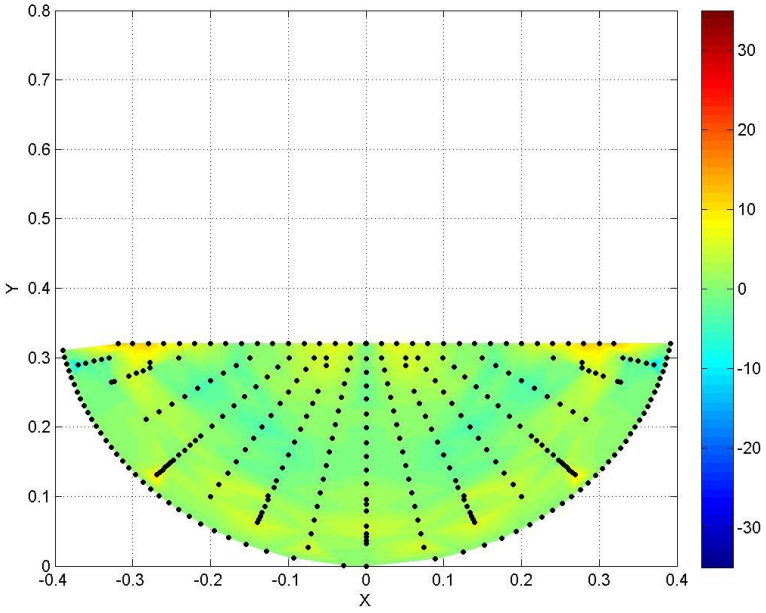

Figure 113: Empirical equation percent difference two-dimensional distribution for Test 2 (%)

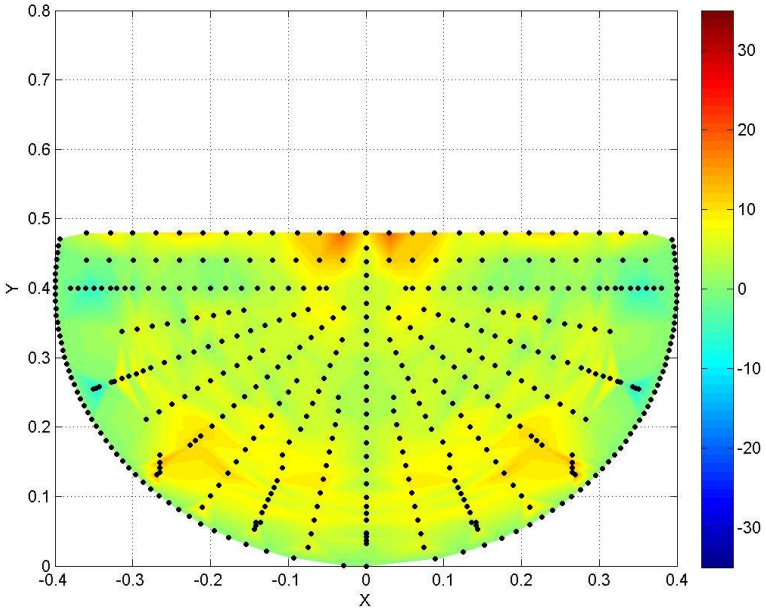

Figure 114: Empirical equation percent difference two-dimensional distribution for Test 3 (%)

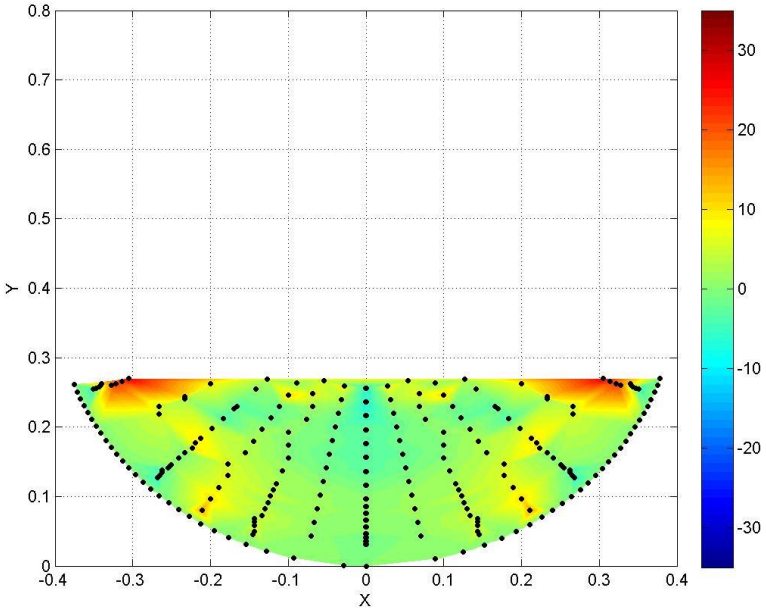

Figure 115: Empirical equation percent difference two-dimensional distribution for Test 4 (%)

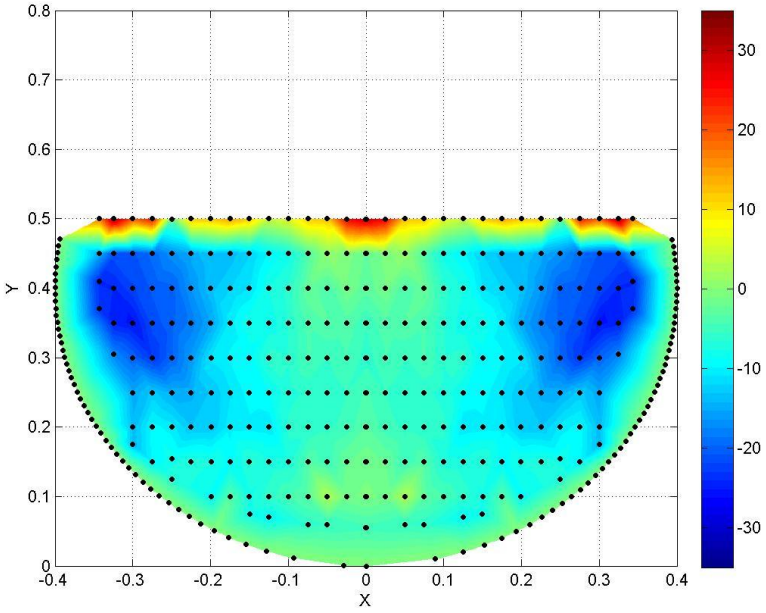

Figure 116: Empirical equation percent difference two-dimensional distribution for Test 9 (%)

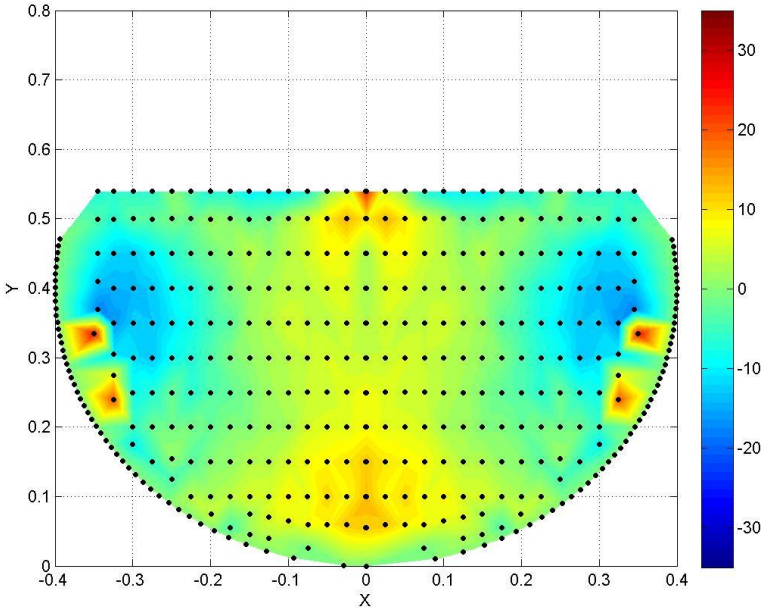

Figure 117: Empirical equation percent difference two-dimensional distribution for Test 11 (%)

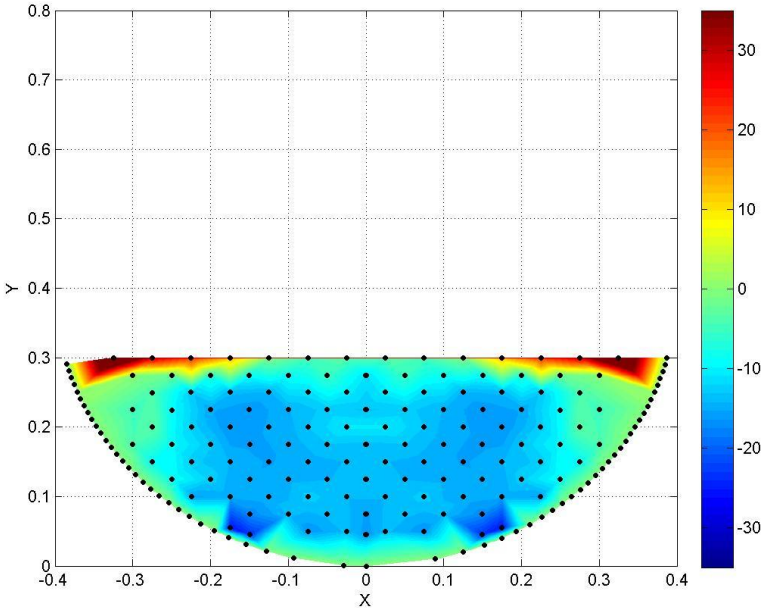

Figure 118: Empirical equation percent difference two-dimensional distribution for Test 12 (%)

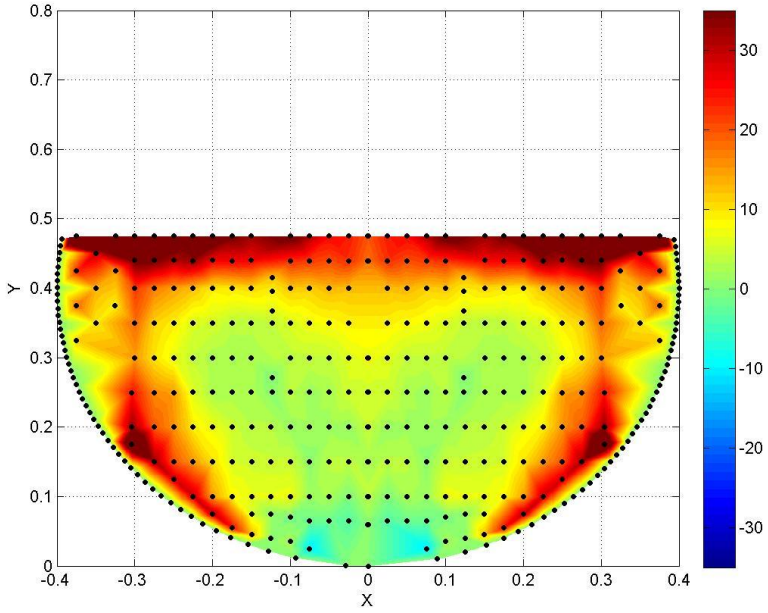

Figure 119: Empirical equation percent difference two-dimensional distribution for Test 14 (%)

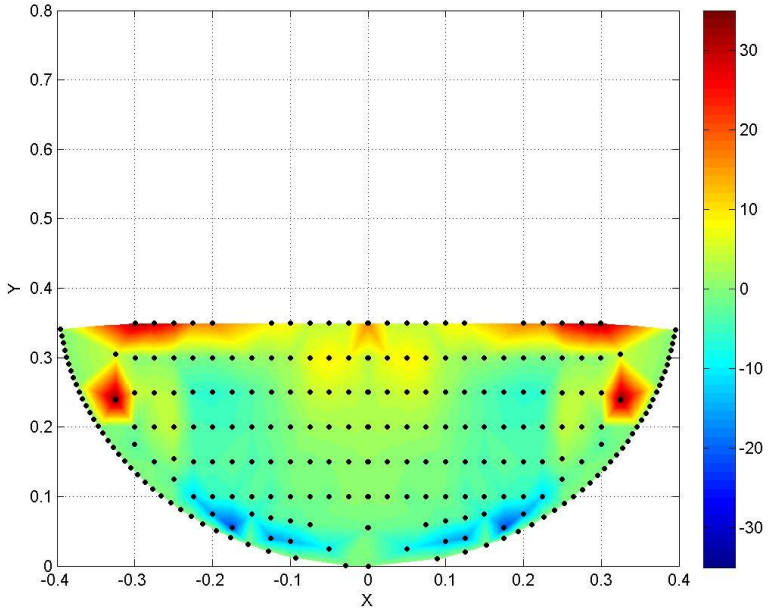

Figure 120: Empirical equation percent difference two-dimensional distribution for Test 15 (%)